Applications of AAA rational approximation

Yuji Nakatsukasa

Mathematical Institute, University of Oxford, Woodstock Road, Oxford, OX2 6GG, UK E-mail: nakatsukasa@maths.ox.ac.uk

Lloyd N. Trefethen

School of Engineering and Applied Sciences, Harvard University, 29 Oxford St., Cambridge, MA 02138, USA E-mail: trefethen@seas.harvard.edu

Draft 17th October 2025

The AAA algorithm for rational approximation is employed to illustrate applications of rational functions all across numerical analysis.

CONTENTS

1	Introduction	2
2	The AAA algorithm	4
3	Approximating functions	10
4	Locating poles and zeros	15
5	Computing derivatives and integrals	22
6	Analysis of branch points	27
7	Inverse functions	30
8	Equispaced interpolation	34
9	Imputing missing data	37
10	Analytic continuation	38
11	Computing the Schwarz function	43
12	Illustrating potential theory	48
13	Solution of ODEs and PDEs	54
14	Extending ODEs and PDEs into $\mathbb C$	58
15	Multivariate analytic continuation	61
16	Computing complex resonances	65
17	Matrix eigenvalue problems	68
18	Nonlinear eigenvalue problems	73
19	Model order reduction	76
20	The Zolotarev sign problem	79
21	The Zolotarev ratio problem	85
22	Quadrature formulas	88
23	Cauchy, Wiener-Hopf, Riemann-Hilbert	94
24	Laplace problems and AAA least-squares	99
25	Conformal mapping	107
26	Helmholtz equation and scattering	112
27	Biharmonic problems and Stokes flow	116
28	The Hilbert transform	118
29	AAA-Lawson for best approximation	121
30	Continuum AAA	126
31	Periodic AAA	128
32	Type (m, n) AAA	131
33	Vector-valued AAA	133
34	Discussion	135
Acknowledgments		137
References		

1. Introduction

Suppose we had an algorithm that could quickly compute a rational function r to approximate almost any function f on almost any real or complex

domain Z to machine precision. What could we do with such a tool? That is the topic of this review.

Such an algorithm, the AAA algorithm, was introduced in 2018 (Nakatsukasa, Sète and Trefethen (2018)). Section 2 describes how it works, with extensions presented in sections 29–33, but our focus will be on applications, not the algorithm itself.

In most areas of numerical analysis, the starting point is polynomials. We see this for example with series expansions (Gregory, Newton, Taylor), interpolation (Harriot, Gregory, Newton, Waring), quadrature (Gregory, Newton, Cotes, Simpson, Gauss, Jacobi), rootfinding (Newton, Raphson, Simpson, Good), splines (Schoenberg, de Casteljau, Bezier, de Boor), matrix iterations (Lanczos, Hestenes, Stiefel, Saad), solution of ODEs (Adams, Runge, Heun, Kutta) and solution of PDEs by finite difference (Richardson, Southwell, Courant, Friedrichs, Lewy), finite element (Courant, Argyris, Clough) and spectral methods (Lanczos, Clenshaw, Elliott, Orszag, Gottlieb). The names listed are some early figures in each area, not a systematic list.

Rational functions, which are quotients of the form r(z) = p(z)/q(z) where p(z) and q(z) are polynomials, are generalisations of polynomials since polynomials correspond to the case q=1. The reason for the power of rational functions is clearer, however, if we think of polynomials as the special case of rational functions whose poles are constrained all to lie at $z=\infty$. For approximating analytic functions far from any singularities, this constraint is mild, and polynomials are useful for all kinds of problems, giving fast exponential convergence. Bulletproof algorithms are available for working with them in many settings, often based on Chebyshev polynomials, Chebyshev points and Chebyshev interpolants (Trefethen (2019a)). Many of these reliable methods are brought together in the Chebfun software system (Driscoll, Hale and Trefethen (2014)). For robust polynomial computation on regions other than intervals and disks, see (Brubeck, Nakatsukasa and Trefethen (2021)).

In other circumstances, however, polynomials lose their power. This is especially true in approximation of functions with singularities on or near the approximation domain, on unbounded domains, or in applications requiring extrapolation off the domain of approximation. Here rational functions, whose poles may go wherever they are needed, have great advantages. Nevertheless, they have not played a large role in numerical analysis, and the biggest reason for this has been the lack of algorithms for working with them easily.

Our aim in this paper is to show how rational functions can change the game in 26 different application areas, the topics of sections 3–28. We present AAA code snippets in MATLAB with many figures to make it easy for readers to adapt rational functions to their own problems. We are equally

interested in outlining the state of theoretical understanding of these methods, and in each section we strive to point to results that are known—or not known—to delineate the possibilities. (Twenty open problems are listed in the Discussion at the end.) We also cite a good deal of related literature on numerical methods involving rational functions, though it is impossible to be exhaustive.

Historically, the AAA algorithm represents a break with the past: what used to be difficult is now usually easy. Two essential features of its success are that it is a greedy descent algorithm rather than aiming to enforce optimality conditions (thereby making it somewhat analogous to gradient descent methods in machine learning) and that it employs a barycentric representation of a rational function rather than the exponentially unstable quotient representation r(z) = p(z)/q(z). However, we do not claim that AAA is the only method that can be effective for numerical rational approximation. Recently, Salazar Celis and Driscoll have shown that similar speed and accuracy can be achieved in many cases by a greedy interpolation algorithm based on an entirely different representation, namely Thiele continued fractions (Salazar Celis (2024), Driscoll and Zhou (2025), Driscoll (submitted)). We do not know if AAA will remain the best approach for these problems in the decades to come, but it seems clear that it has ushered in a new era for rational functions.

Throughout the paper we use this notation:

 $\{\zeta_k\}$: interpolation points, $\{\pi_{k}\}$: poles,

 $\{z_j\}$: sample points, $\{t_k\}$: barycentric support points, $\{f_j\}$: sample values, $\{\beta_k\}$: barycentric weights.

2. The AAA algorithm

We start with a vector $Z \in \mathbb{C}^m$ of m distinct real or complex numbers and a vector $F \in \mathbb{C}^m$ of associated function values. The AAA algorithm aims to find a rational function r such that the maximum error ||r(Z) - F||is small: our standard convergence condition is $||r(Z) - F|| / ||F|| < 10^{-13}$. (Throughout this paper, $\|\cdot\|$ without a subscript is the ∞ -norm for a vector or function, depending on context.) The approximation is represented in barycentric form,

$$r(z) = \frac{N(z)}{D(z)} = \sum_{k=0}^{n} \frac{f_k \beta_k}{z - t_k} / \sum_{k=0}^{n} \frac{\beta_k}{z - t_k} , \qquad (2.1)$$

where N and D stand for numerator and denominator and normally $n \leq$ (m-1)/2. The numbers $\{\beta_k\}$ are barycentric weights, and the numbers $\{t_k\}$, which are n+1 distinct entries of Z, are support points or nodes. If we assume that all the barycentric weights are nonzero, then each t_k is a pole of the numerator in (2.1) (assuming $f_k \neq 0$) and also a pole of the

denominator. The poles cancel out in the quotient, giving the interpolatory property

$$\lim_{z \to t_k} r(z) = f_k. \tag{2.2}$$

Thus t_k is a removable singularity of (2.1), and we define $r(t_k) = f_k$ accordingly. As can be verified by multiplying N(z) and D(z) by $\prod_{k=0}^{n}(z-t_k)$, r belongs to \mathcal{R}_n , the set of rational functions of degree n, i.e., the set of quotients p(z)/q(z) where p and q are polynomials of degree $\leq n$.

The use of a representation of rational functions different from the obvious choice p(z)/q(z) is crucial to the success of AAA. Good rational approximations need to have poles and zeros clustering at singularities, with the consequence that both |p(z)| and |q(z)| in such a representation will have to vary widely with z. Such variation quickly leads to loss of accuracy in floating point arithmetic if p(z) and q(z) are expressed in a global basis, such as monomials or Chebyshev polynomials. In other words, the p(z)/q(z) representation of rational functions is unstable. This is the reason why Varga and his collaborators had to use 200-digit extended precision arithmetic in the 1990s to compute best approximations accurate to 16 digits (Varga, Ruttan and Carpenter (1993)). By contrast, with the help of the barycentric representation, the AAA algorithm reliably achieves close to machine accuracy in standard 16-digit arithmetic.

There remains the problem of how to find good values of $\{t_k\}$ and $\{\beta_k\}$. Before AAA, most methods for rational approximation followed nonlinear optimisation strategies motivated by an attempt to satisfy optimality criteria, often involving an iterative adjustment of poles. The principal methods we are aware of are presented in (Sanathanan and Koerner (1963)), (Osborne and Watson (1969)), (Ellacott and Williams (1976)), (Istace and Thiran (1993)), (Gustavsen and Semlyen (1999)) ("Vector fitting"), (Alpert, Greengard and Hagstrom (2000)), (Gugercin, Antoulas and Beattie (2008)) ("IRKA"), and (Berljafa and Güttel (2017)) ("RKFIT"). Crucially, AAA is not based on optimality criteria, and it does not work with poles. It is a greedy algorithm, which just aims locally for descent. It needs no initial guess to get started, and no specification of the degree of the approximation (though a degree can be specified if desired).

Let the nonlinear approximation problem $F \approx N(Z)/D(Z)$ be linearised to $F \cdot D(Z) \approx N(Z)$, that is,

$$f(z)\sum_{k=0}^{n} \frac{\beta_k}{z - t_k} \approx \sum_{k=0}^{n} \frac{f_k \beta_k}{z - t_k}, \quad z \in Z$$
 (2.3)

together with the normalisation

$$\sum_{k=0}^{n} |\beta_k|^2 = 1. {(2.4)}$$

The AAA algorithm solves a sequence of problems (2.3)–(2.4) with $n=0,1,2,\ldots$ The support points t_0,t_1,\ldots are chosen along the way, one by one, from Z. This means that the least-squares problem at step n actually involves sampling in the remaining m-n-1 points. To be precise, at step n, we compute weights $\{\beta_k\}$ satisfying (2.4) such that

$$\sum_{j=1}^{m} {}' \left[f_j \sum_{k=0}^{n} \frac{\beta_k}{z_j - t_k} - \sum_{k=0}^{n} \frac{f_k \beta_k}{z_j - t_k} \right]^2 = \text{minimum}, \tag{2.5}$$

where the prime on the summation sign indicates that the summation extends over the points $Z\setminus\{t_0,\ldots,t_n\}$. This is a problem of numerical linear algebra involving an $(m-n-1)\times(n+1)$ matrix A with entries

$$a_{jk} = \frac{f_j - f_k}{z_j - t_k},\tag{2.6}$$

known as a *Loewner matrix* (Antoulas, Beattie and Gugercin (2020)). If β denotes the column vector with entries β_0, \ldots, β_n , the problem (2.4)–(2.5) is to find a vector β satisfying

$$||A\beta||_2 = \text{minimum}, \quad ||\beta||_2 = 1,$$
 (2.7)

where $\|\cdot\|_2$ is the vector 2-norm. It is routine matter to solve (2.7) by computing the singular value decomposition (SVD) of A and setting β equal to the right singular vector corresponding to the smallest singular value σ_{n+1} . (In section 20 we will modify (2.7) in certain contexts and also mention an adjustment introduced in 2025 to improve accuracy in cases where A is highly ill-conditioned.)

The other half of the algorithm is the greedy choice of support points. At step n, the next support point t_n is selected as a sample point z_j where the approximation error $|f_j - r(z_j)|$ is maximal, and then the next SVD calculation is carried out. We can write the full algorithm like this:

```
AAA ALGORITHM

Given: m-vectors Z of sample points and F of function values.

r:= the zero function.

for n=0,1,2,\ldots:

t_n:= a sample point z_j where |f_j-r(z_j)| is maximal;

Construct the (m-n-1)\times (n+1) matrix A from (2.6);

Compute the vector \beta of (2.7) from the SVD of A;

Define r by (2.1).
```

Depending on one's purposes, the iteration may be run for a fixed number of steps or until a convergence criterion is met. In the Chebfun code aaa.m, the default condition is that the maximal error should be less than 10^{-13} times the maximal value $|f_k|$. There is no guarantee that this will be achieved in the presence of rounding errors, but the reliability in practice is striking.

The name AAA ("triple-A") comes from "adaptive Antoulas-Anderson." Antoulas and Anderson (Antoulas and Anderson (1986)) proposed the use of the barycentric formula for rational interpolation (see section 11 of (Nakatsukasa et al. (2018)) for a discussion of the history), and the AAA algorithm couples this with its adaptive selection of support points and the linearised least-squares determination of barycentric weights. The original AAA paper includes a basic MATLAB code, which evolved with various checks and extra features into the aaa.m command in Chebfun, which has been used for all the examples in this paper except for the black curves in Figure 10.2. Different MATLAB implementations are available in the MATLAB RF, Control System and System Identification toolboxes (MathWorks Inc. (2020)), and there are also open-source AAA implementations in Julia (Driscoll (submitted), MacMillen (2024)) and Python/SciPy (Virtanen et al. (2020)).

Quite a few modifications to the basic AAA algorithm can be added to introduce useful properties or enhance its reliability. The most important property not imposed by the algorithm as described above is real symmetry. If Z is a complex set with $\bar{Z}=Z$, and if F takes conjugate values at conjugate points, then it is natural to want r to have the property $r(\bar{z})=\overline{r(z)}$. This is not achieved by the basic AAA algorithm, even in the absence of rounding errors. A number of authors, beginning with Hochman even before the original AAA paper appeared in print (Hochman (2017)) and also including the MathWorks RF Toolbox (MathWorks Inc. (2020)), have fixed that by introducing new support points as conjugate pairs when they are complex, rather than one-by-one. (This seems to bring a slight increase in accuracy, too.) Regarding reliability improvements, as mentioned above, one that matters occasionally in practice is to modify the calculation so that the barycentric weights are constructed from several right singular

vectors rather than just the minimal one. Another is to apply column scaling to the matrix A when it is highly ill-conditioned. We shall discuss these modifications in section 20.

The computational cost of the AAA algorithm depends strongly on the degree n. The iteration involves SVD computations of sizes $(m-1)\times 1$, $(m-1)\times 1$ 2) $\times 2, \ldots, (m-n-1) \times (n+1)$, for a total operation count of the order of mn^3 , which amounts to n^4 since m will generally need to scale with n for effective resolution of a function. Most applications we know of involve reasonably small degrees and sample sets, say n < 150 and m < 3000, giving computation times usually under one second on today's laptop and desktop machines. In this regime it is not clear that any good methods are available to speed up the linear algebra significantly, though some proposals have been put forward in (Hochman (2017), Lietaert, Meerbergen, Pérez and Vandereycken (2022)) (based on updating Cholesky factorisations) and (Park and Nakatsukasa (2023)) (based on randomised sketching). (Hochman's work reduces the complexity to $O(n^3)$ in theory, but it is based on the Cholesky factorisation of the Gram matrix, which has stability issues associated with squaring the condition number.) The $O(n^4)$ operation count certainly stands out, however, and we presume that as time passes and larger scale rational approximations become more common, the challenge of speeding up the linear algebra may grow in importance.

One may ask what theory there may be to guarantee the success of AAA. In a certain superficial sense, the answer is easy, as pointed out first in (Hochman (2017)):

Theorem 2.1. In exact arithmetic, AAA always converges to an approximation r satisfying the prescribed accuracy criterion $||r(Z) - F|| / ||F|| \le \text{tol.}$

The proof is merely the observation that in the worst case, a rational function can simply interpolate all the data values. This will happen at the latest at step $n = \lfloor m/2 \rfloor$ if all the barycentric weights are nonzero at that step. If there are zero weights at this step and they keep reappearing at subsequent steps, then one could continue all the way to n = m - 1, at which point all the sample points are support points and the weights can be arbitrarily set to 1 or to any other nonzero values.

This mathematically valid theorem, however, is a "Yogiism" (Trefethen (2016)) in that it misses the actual purpose of most approximations. Convergence on a discrete set Z does not imply convergence on a continuum that E is intended to approximate. Specifically, the convergence theorem does not exclude "bad poles" in the approximant, lying in regions near Z where

With polynomials, this is the familiar lesson of the Runge phenomenon (Trefethen (2019a)): interpolation of all the data does not ensure that anything useful has been achieved.

one doesn't want or expect them. The most familiar instance is the situation in which poles turn up between the sample points in approximation of a real function on a discretised real interval—in odd-degree approximations of |x| on [-1,1], for example, but also in many other problems without such symmetries. This is not just a theoretical problem but a practical one. AAA is at its least reliable for real approximation on real intervals. One way that trouble may arise in AAA approximations is in the form of "spurious poles," typically with residues at the level of machine epsilon or other noise in the data; one also speaks of "Froissart doublets" since these are poles that are paired with zeros at almost but not exactly the same position, cancelling to invisibility further away (Stahl (1998)). Spurious poles or Froissart doublets will be mentioned at various points in this paper, notably near the ends of sections 4, 8 and 12. The code aaa.m has a "cleanup" feature that can sometimes remove spurious poles, first mentioned in Nakatsukasa et al. (2018)—with also a 'cleanup', 2 variant due to Stefano Costa—but we will not discuss cleanup options in this paper, as they are not fully understood and the experiments here do not take advantage of them.

Another case where the choice of Z is an issue is when F has one or more singularities on the continuum E of ultimate interest, so that poles and zeros need to be exponentially clustered near there. In such a situation it is important to make sure that Z likewise contains points exponentially clustered near the singularities. Usually one would also loosen the tolerance, perhaps to 10^{-6} or 10^{-8} , since resolution of a singularity to 13-digit accuracy will usually require rational degrees in the hundreds. Good rational approximations of functions with branch point singularities converge root-exponentially, i.e., at a rate $\exp(-C\sqrt{n})$ for some C>0 as $n\to\infty$ (Newman (1964), Gopal and Trefethen (2019c)). With polynomial approximations, by contrast, since the convergence is only algebraic, one would typically need degrees in the millions to get 6 or 8 digits of accuracy.

To circumvent problems of discretisation of a complex domain by a finite set Z, a continuum version of the AAA algorithm was introduced in (Driscoll, Nakatsukasa and Trefethen (2024)); for software see (Driscoll (submitted)). This applies a priori to intervals, disks, circles, lines and half-planes, or to more general domains via boundary parameterisation. The method appears very promising but has not yet become a standard, no doubt in part because working with a discrete Z is so straightforward and usually successful. In this review all our illustrations are based on the discrete case, except that continuum AAA is discussed and illustrated in section 30.

Returning to the matter of theoretical justification of AAA, suppose we could guarantee that under suitable assumptions AAA (or some modification of AAA) always converged throughout E when applied on a discrete set Z approximating a continuum E sufficiently finely. This would be helpful,

yet such a theorem would still miss the point that usually what is wanted is not just "any old approximant" but one that compresses the data. This could be for the simple purpose of reducing the number of data values needed in a representation, but more often and more interestingly, the point of an approximation $r \approx f$ is to estimate information about f such as its values, or the locations of its poles or other singularities, beyond the data domain. For this to happen, an approximation needs to be near-best, that is, not too far from the optimal approximation of its degree. The true theoretical challenge of AAA approximation is to establish a theorem to ensure that, under appropriate assumptions, AAA finds not just accurate but near-best approximations.

An interesting analogy can be drawn between the AAA algorithm for rational approximation and the QR algorithm for eigenvalues of matrices. (The analogy is mentioned in a footnote in (Driscoll et al. (2024)).) Both algorithms consist of an alternation between an elementary nonlinear step (choice of the next support point for AAA, shifting by a multiple of the identity for QR) and a routine matrix computation (tall-skinny SVD for AAA, QR factorisation and recombination for QR). Both turn problems that were previously troublesome into black-box solvers that almost always get the desired answer fast. In both cases the basic algorithm is extraordinarily simple to describe and highly reliable in practice, but not quite infallible. In both cases fully reliable performance requires a few extra tricks that users are likely to be unaware of (for QR, "balancing" the matrix is in this category), yet rigorous guarantees of success may still be elusive.

The rest of this paper is mostly about AAA applications, not about the algorithm, though some algorithmic details will be discussed in sections 4 (computation of poles and zeros), 5 (computation of derivatives), and 20 (the 'sign' and 'damping' features). Generalisations of AAA to best approximation, approximation on a continuum, periodic functions, type (m, n) approximation, and vector- or matrix-valued functions are discussed in sections 29-33.

3. Approximating functions

Our first application of rational approximation is to the approximation of functions. That may sound tautological, but there are things to be said. A key distinction is between what we might call *offline* or *optimised* approximation and *online* or *on-the-fly* approximation. AAA contributes to both, but it is particularly striking for on-the-fly applications, so we begin there. As in every section of this paper, our aim is to provide ideas and references and illustrations that may be useful for the reader, not to attempt a comprehensive account of all the possibilities.

The key features are speed, reliability and flexibility about sample sets.

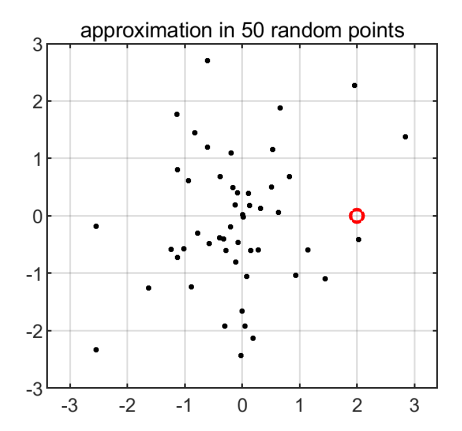


Figure 3.1. Fifty scattered points in the complex plane at which a meromorphic function f(z) is sampled. The aim is to estimate the value at z = 2 (the red circle). For $f(z) = \tan(z)/\tan(2)$, AAA approximation gets a result accurate to 11 digits in a few milliseconds.

For example, suppose the values of a meromorphic function f are known at 50 scattered sample points in \mathbb{C} . (A meromorphic function is one that is analytic apart from poles.) For illustration we take $f(z) = \tan(z)/\tan(2)$ and a set of 50 complex normally distributed random points,

```
rng(2)
Z = randn(50,1) + 1i*randn(50,1);
F = tan(Z)/tan(2);
```

as plotted in Figure 3.1. Suppose we want to evaluate f at an arbitrary point—for example, at z=2, where the exact value is 1. The command

```
r = aaa(F,Z)
```

produces a degree 10 rational approximation $r \approx f$ in a couple of milliseconds on a laptop, and for this choice of f, r(2) matches the true value f(2) = 1 to 11 digits:

```
r(2)
ans =
1.000000000008511 - 0.00000000007166i
```

If the random number seed in this code is set to the values $1, 2, \ldots, 10$ to give an indication of how the results depend on the set of sample points, the numbers of digits of accuracy (rounded values of $-\log_{10}|r(2)-1|$) come out as 12, 11, 10, 13, 10, 13, 14, 10, 14, 11 (mean: 11.8). If the number of sample points is increased to 100, the numbers of digits go up to 14, 15, 13, 15, 15, 13, 14, 12, 15, 13 (mean:13.9).

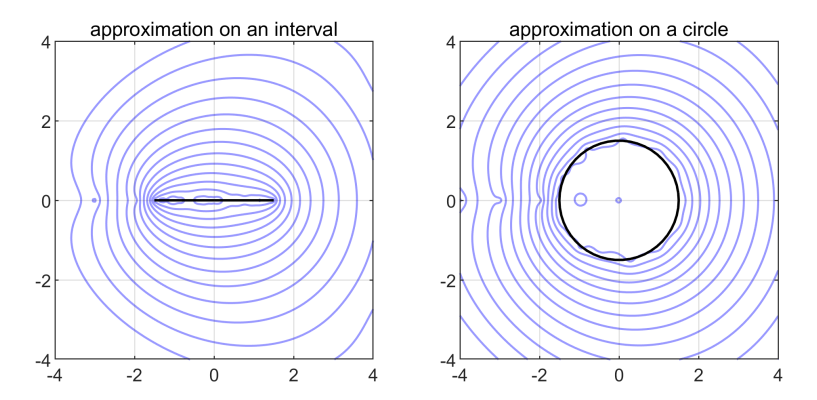


Figure 3.2. AAA approximation of $\Gamma(z)$ based on samples at 50 Chebyshev points in [-1.5, 1.5] (left) and 50 equispaced points on |z| = 1.5 (right). From inside out, the contours represent relative errors $|r(z) - \Gamma(z)|/|\Gamma(z)| = 10^{-13}, 10^{-12}, \ldots, 10^{-1}$.

Rational approximation is not the only way in which one might approximate f, but its simplicity and accuracy are remarkable. The reader might find it interesting to consider the alternatives. What computations could be carried out to obtain an analogous approximation by a polynomial rather than a rational function, say, even if f didn't happen to have any poles? (A well-conditioned basis for the polynomial can be constructed by Vandermonde with Arnoldi orthogonalisation (Brubeck et al. (2021)).) Or perhaps by some other fitting method?

Other on-the-fly function approximation problems may start from data on a continuum, such as an interval or a circle. In Figure 3.2, we suppose that a meromorphic function f(z) is known on the interval [-1.5, 1.5] (left) or the circle |z| = 1.5 and we wish to find a way to evaluate it at other points nearby. For this illustration, we take f to be the gamma function, $f(z) = \Gamma(z)$. The MATLAB gamma command only evaluates $\Gamma(z)$ for real arguments, so the left-hand part of the figure represents a computation that a MATLAB user might find helpful: a quick method for evaluating $\Gamma(z)$ for complex values of z near the origin. Again in a few milliseconds, a call to AAA computes a rational approximation of degree 9 (left) or 12 (right) with a relative error on the approximation domain of less than 10^{-13} . To evaluate $\Gamma(z)$ to full accuracy for complex z for these illustrations, we have used the code of (Godfrey (2025)).

Classically, the best known use of rational functions for approximating functions would be in *offline* mode, notably in the design of a special functions library. Here it may be worthwhile to make greater efforts to obtain an approximation that is truly optimal in some sense. For example, the

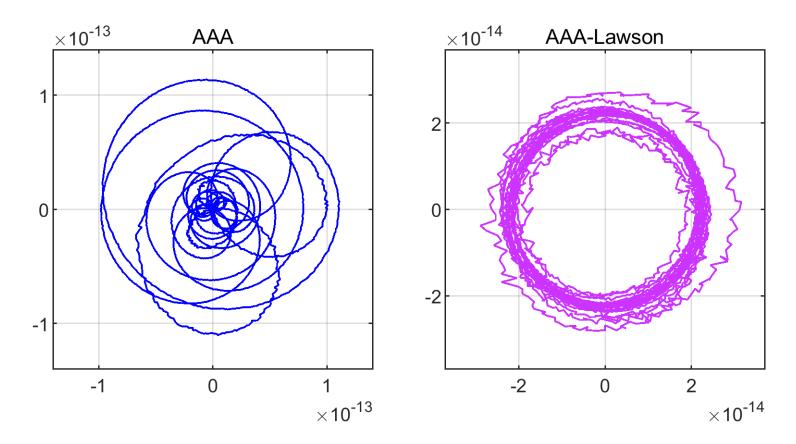


Figure 3.3. Error curves for AAA approximation of $\Gamma(z)$ on the circle |z|=1.5. On the left, straight AAA approximation. On the right, AAA-Lawson approximation with 20 Lawson steps. The error curve has winding number 21 but is ragged because the errors are close to the level of machine precision (compare Figure 29.2). In this paper we use magenta to distinguish error curves from AAA-Lawson best approximation.

FUNPACK (Cody (1975)) and SPECFUN (Cody (1993)) projects of the last century used rational minimax (best ∞ -norm) approximations to evaluate Bessel functions, error functions, gamma functions and exponential integrals. A more recent discussion of such methods can be found in (Muller (2016)).

For a continuous real function on a real interval, a minimax approximation can be obtained with the Remez algorithm based on equioscillation, whose most robust implementation that we are aware of is that of the Chebfun minimax command (Filip, Nakatsukasa, Trefethen and Beckermann (2018)). Though much slower to compute than a AAA approximation, this might typically have accuracy about one digit better, or it might have comparable accuracy but with a rational degree about 10% lower. On domains other than an interval, the Remez algorithm is not applicable. In the last section we cited various published algorithms for minimax rational approximation, but the best available technique in practice may often be the extension of AAA known as the AAA-Lawson algorithm (Nakatsukasa and Trefethen (2020)), to be discussed in section 29. Here, AAA approximation is run as usual (perhaps with a specified degree rather than a specified convergence tolerance) and then the approximation is improved by a subsequent nonlinear iteratively reweighted least-squares iteration.

Figure 3.3 illustrates the use of AAA-Lawson approximation for the problem of approximating $\Gamma(z)$ on |z| = 1.5 as in Figure 3.2. Both images in Figure 3.3 show error curves $e(z) = \Gamma(z) - r(z)$, where z ranges over 5000 equispaced points on the circle of approximation. On the left, with standard AAA approximation, the error curve is irregular and the absolute error is about $1.2 \cdot 10^{-13}$, which corresponds to a relative error less than 10^{-13} since $\Gamma(-1.5) \approx 2.4$. This is not a best approximation of the given degree 12, but a near-best approximation. On the right, 20 iterative Lawson steps have been appended with a call to Chebfun aaa.m of the form

$$r = aaa(F,Z,'lawson',20)$$

and the result is an error curve that is closer to optimal, with the error reduced by a factor of about 4, to $3 \cdot 10^{-14}$. This is a genuine improvement, at least in the ∞ -norm. (The root-mean-square error has roughly halved, from $4.9 \cdot 10^{-14}$ to $2.2 \cdot 10^{-14}$.) We can see that the approximation is nearly optimal from the fact that the error is approximately a circle of winding number 21 (Trefethen (1981)).² The true best approximation would have an error curve circular to plotting accuracy and a maximum error perhaps 10% smaller, but we cannot find it in this case because we are too close to machine precision, as is revealed by the jaggedness of the plot. Section 29 will show examples further from machine precision, hence with cleaner behaviour.

The reason a discussion of AAA-Lawson approximation is deferred to near the end of this article is that we do not recommend it as the method to turn to initially for applications, because it is slower and less reliable than standard AAA. It almost always runs into difficulty at accuracies close to machine precision, and even at accuracies well above that level, it does not achieve the "99% reliability" (not a precise figure) of AAA. Sometimes better performance can be obtained by running the AAA-Lawson algorithm with the "sign" and/or "damping" improvements described in (Trefethen and Wilber (2025)); see sections 20 and 29.

Here at the end of this section on approximating functions, let us give a brief and non-rigorous summary of some theorems about convergence of polynomial vs. rational best approximations to an analytic function f on a compact continuum $E \subset \mathbb{C}$, asymptotically as the degree n approaches ∞ . The convergence rates in these theorems depend on how f can be analytically continued to the rest of \mathbb{C} , and they are proved by arguments of poten-

² Near-optimality follows by an argument related to Rouché's theorem, since the winding number 21 is $\geq 2n+1-2p$, where n=12 is the degree of r and p=2 is the number of poles of Γ within the circle of approximation. To be precise in this case, suppose r=p/q with p and q of degree 12 and there were another approximation $\tilde{r}=\tilde{p}/\tilde{q}$ with $\max_{|z|=1.5}|f(z)-\tilde{r}(z)|<\min_{|z|=1.5}|f(z)-r(z)|$. Then $r-\tilde{r}=p/q-\tilde{p}/\tilde{q}$ would also have winding number 21, so assuming q and \tilde{q} each have 2 zeros with |z|<1.5 corresponding to the poles of $\Gamma(z)$ at z=-1 and z=0, $p\tilde{q}-\tilde{p}q$ would have winding number 25. This means $p\tilde{q}-\tilde{p}q$ would have 25 zeros with |z|<1.5, which is not possible since it is a nonzero polynomial of degree 24.

tial theory to be outlined in section 12. If f is an entire function—analytic throughout C—then both polynomial and rational best approximations converge superexponentially, i.e. with error $O(C^{-n})$ for any C>1, though possibly at very different rates despite that (Figure 12.1). If f is analytic apart from poles, whether finite or countably infinite in number, then polynomials converge exponentially, i.e. at the rate $O(C^{-n})$ for some C > 1, whereas rational functions still converge superexponentially (Figure 12.3). The same applies if there are essential singularities as well as poles—but in this case the superexponential convergence of rational approximations is likely to look just exponential for the ranges of n accessible computationally. If f has one or more branch points, then both polynomial and rational approximations converge only exponentially—though again perhaps at very different rates (Figure 12.4). If E is a nonconvex domain and f has branch points in typical locations (Trefethen (2025a)) in reentrant "inlets" of E, then both polynomials and rational functions converge exponentially, but the convergence constant for the polynomials is exponentially worse as a function of the length-to-width ratio of the inlet—i.e., $O(C^{-n})$ with C exponentially close to 1 (Figure 12.5). These results are mostly due to the Moscow school associated with Gonchar, except the last from (Trefethen (2024)); for surveys, see (Trefethen (2024, 2020c)). Finally, if f is not analytic on the boundary of E but has one or more branch points there, then polynomials converge just algebraically, e.g. at the rate O(C/n), whereas rational functions converge root-exponentially, at the rate $O(C^{-\sqrt{n}})$ for some C>1 (Newman (1964), Gopal and Trefethen (2019c)). This root-exponential convergence is made possible by exponential clustering of poles and zeros near the singularities, a phenomenon investigated in detail in (Trefethen, Nakatsukasa and Weideman (2021)) and visible in this paper in Figures 11.3, 23.2, 24.2, 26.1, 27.2 and 28.1.

4. Locating poles and zeros

One of the long-established applications of rational functions is the determination of poles and other singularities of analytic functions in the complex plane. (By "analytic" here we mean analytic away from those singularities.) The version of this technique that is best known is based on Padé approximation, in which a function f is approximated from knowledge of some of its Taylor coefficients at a point (Baker, Jr. and Graves-Morris (1999), Stahl (1997)). With AAA approximation, we can pursue similar ideas when the data consists of function values rather than Taylor coefficients.

Before considering such applications, we explain how poles and zeros are computed by the AAA algorithm. Poles and zeros play no part in the construction of the AAA approximant, which adjusts barycentric weights, not pole locations. Only at the end, after the approximant has been found,

are they computed if desired. This is done by solving a matrix generalised eigenvalue problem involving the support points and barycentric coefficients. We first note that the zeros of r(z) = n(z)/d(z) are those of

$$n(z) = \sum_{k=0}^{n} \frac{f_k \beta_k}{z - t_k},$$

and the poles are (generically) the zeros of

$$d(z) = \sum_{k=0}^{n} \frac{\beta_k}{z - t_k}.$$

Both of these expressions are in partial fractions form, and their zeros can be found by solving the $(n+2) \times (n+2)$ generalised eigenvalue problem

$$\begin{pmatrix} 0 & \beta_0 & \beta_1 & \cdots & \beta_n \\ 1 & t_0 & & & \\ 1 & & t_1 & & \\ \vdots & & & \ddots & \\ 1 & & & & t_n \end{pmatrix} x = \lambda \begin{pmatrix} 0 & & & \\ & 1 & & & \\ & & 1 & & \\ & & & \ddots & \\ & & & & 1 \end{pmatrix} x \tag{4.1}$$

(Corless (2004), (Lawrence 2013, chap. 2)). Indeed, by setting

$$x = \left(1, \frac{1}{\lambda - t_0}, \frac{1}{\lambda - t_1}, \dots, \frac{1}{\lambda - t_n}\right)^T,$$
 (4.2)

one can verify that (4.1) holds for any zero λ of d. The generalised eigenvalue problem (4.1) has at least two eigenvalues at infinity, and the remaining n are the zeros of d. (An alternative formulation without the eigenvalues at infinity has been proposed in (Deckers, Jonckheere and Meerbergen 2022, sec. 3).) The zeros of n(z) are found analogously, with β_k replaced by $f_k\beta_k$. Computing these eigenvalues using the standard QZ algorithm (Moler and Stewart (1973)) requires $O(n^3)$ operations, and is usually a negligible part of the AAA computation.

Concerning the accuracy of these computations of poles and zeros, one can say that they are backward stable in the usual sense of numerical linear algebra, but we do not know what theoretical guarantees there may be concerning their accuracy as poles and zeros of the rational approximation r(z).³ In no applications that we are aware of has accuracy of computation of AAA poles or zeros appeared to be a concern.

The locations of the AAA poles are interesting in almost every application, as this paper will illustrate, and the ability to calculate them easily

³ Nian Shao (personal communication) has pointed out that the backward stability depends on the poles being not too close to the sample points.

means that with any approximation, one can perform an a posteriori check to make sure there are no "bad poles" in unwanted regions of the complex plane—e.g., no poles in [a, b] if the aim is approximation on that interval. If there are bad poles, the standard fix is to replace the AAA approximation r in its barycentric representation by a new rational function r in partial fractions form, whose poles are the acceptable ones from AAA and whose coefficients are determined by solving a matrix least-squares problem. This may worsen the error, but often it actually improves it, since this least-squares problem involves the errors of the approximation one ultimately cares about rather than the errors of the linearised barycentric form (2.5). See (Costa and Trefethen (2023)) and (Driscoll et al. (2024)).

In ordinary AAA operations, the computation of poles is carried out in this *a posteriori* fashion, at the end of the approximation process. However, in the continuum AAA algorithm mentioned above (Driscoll *et al.* (2024)), poles are calculated at every step of the iteration.

Now we look at applications. To begin, let us return to the example of Figure 3.1, in which the function $f(z) = \tan(z)/\tan(2)$ was approximated from its values at 50 scattered points in the z-plane. Instead of r = aaa(F,Z), we can execute

```
[r,pol,res,zer] = aaa(F,Z)
```

to obtain additionally the poles, residues and zeros of the approximation $r(z) \approx f(z)$. Again the computation takes a few milliseconds on a laptop. Figure 4.1 plots the sample points again, as in Figure 3.1, together with the poles (red circles) and zeros (blue circles) of r and the poles and zeros of f (faint red and blue dots). We see immediately that the poles and zeros of r are approximations to those of $\tan(z)$, which are the odd and even multiples of $\pi/2$, respectively. This rational function r is of degree 10, and in the figure there are 8 poles and 9 zeros. One more pair of poles lies at approximately $z = \pm 35$, and as for the tenth zero, it is at $\approx -800 - 1000i$. We can think of this as an approximation to ∞ , so that r is in some sense approximately a rational function of type (9,10) with a numerator of degree 9 and a denominator of degree 10—a consequence of f being an odd function.

To see how closely the poles and zeros of r match those of f, it is convenient to divide these numbers by $\pi/2$ so that the targets for comparison are integers. Here is what we find for the poles, divided by $\pi/2$. (All these numbers would be purely real if computed with a real-symmetric set of sample points by a version of AAA maintaining real symmetry as discussed in section 2.)

```
1.00000000000033 + 0.000000000000003i
-1.00000000000002 - 0.00000000000027i
3.00000332651624 - 0.00000243518063i
-3.00000327305622 + 0.00000129315010i
```

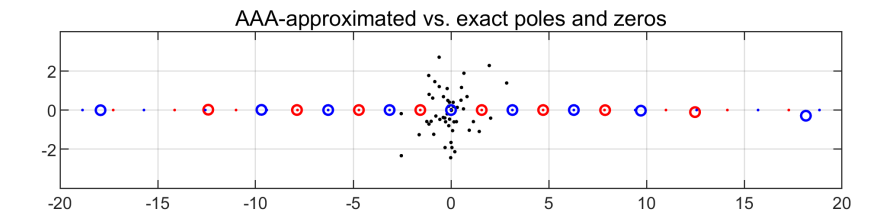


Figure 4.1. Repetition of the experiment of Figure 3.1, now with the poles and zeros of r(z) shown as red and blue circles, respectively. The inner poles and zeros closely match those of the target function $f(z) = \tan(z)/\tan(2)$ (faint red and blue dots).

```
5.01823394381568 - 0.00346572096760i

-5.01704794958420 + 0.00126227829889i

7.94615053339014 - 0.06783633480729i

-7.90540076322207 + 0.01056856361015i

22.84117829937205 - 0.68627425575586i

-22.13232732826279 - 0.22693756275246i
```

Here are the zeros, divided by $\pi/2$:

```
-0.0000000000000
                         0.0000000000000i
  2.0000000074146
                         0.0000000265986i
  -2.00000000080136
                         0.0000000129131i
  4.00058578212117
                         0.00020264321204i
  -4.00054629016288
                         0.00009068387390i
  6.18331670334207
                         0.02050187149938i
  -6.17371491450402
                         0.00563688314931i
  11.55660055153871
                         0.18489790406735i
-11.41334018853083
                         0.00529302069495i
-515.84554454068018
                     - 630.11666599322939i
```

Evidently the poles and zeros within the cloud of data are correct to about 13 digits, which is the tolerance of the AAA approximation. Moving outside the data set, the poles of $f(z)/(\pi/2)$ at ± 3 , ± 5 and ± 7 are captured to about 6, 2 and 1 digits, respectively, and the zeros of $f(z)/(\pi/2)$ at ± 2 , ± 4 and ± 6 are captured to about 9, 4 and 2 digits. This is typical of rational approximations: highly accurate poles and zeros at distances surprisingly far from the data set. One may ask, why do rational approximations locate poles and zeros so well? A rigorous answer is not fully established, though most experts would connect the matter with Hermite integrals and potential theory, to be discussed in section 12. What's clear is that poles and zeros are merely by-products of the approximation process—surprisingly accurate by-products. Similar effects are the basis of numerical methods for computing matrix eigenvalues. The Arnoldi and Lanczos iterations, for example,

minimise a certain vector 2-norm at each iterative step, and when the roots of the polynomials involved approximate eigenvalues of a matrix, that is because placing the roots like that is a good strategy for the minimisation problem (Greenbaum and Trefethen (1994), Kuijlaars (2006)).

When poles are captured accurately, the same will normally be true of residues.⁴ Here for example are the residues of the ten poles of r(z) listed above, all multiplied by tan(2) so that we recognise the target value of -1 corresponding to the residues of tan(z):

```
-1.00000000000249 + 0.000000000000049i

-0.9999999999953 - 0.000000000000229i

-1.00002115229468 + 0.00001322035816i

-1.00002043469684 + 0.0000683956587i

-1.05083731528699 + 0.00770105605601i

-1.04773789789134 + 0.00251606979538i

-2.35467344729027 + 0.07037511036527i

-2.30241052490136 + 0.00113182260999i

-21.40951807722749 - 0.67668458618553i

-22.91889560491100 + 1.25209694878431i
```

These match the target value to about 12, 5 and 2 digits for the first, second and third pairs out from the origin.

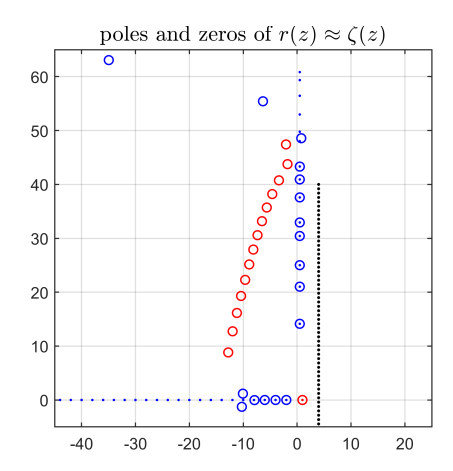
Along with the approximation of $\tan(z)/\tan(2)$ at scattered sample points, the last section considered the approximation of $\Gamma(z)$ at 50 points of the interval [-1.5, 1.5] or the circle |z| = 1.5 (Figure 3.2). The gamma function has poles at $0, -1, -2, -3, -4, \ldots$, and the poles of the rational approximations computed there match these to about $15, 15, 7, 3, 1, \ldots$ digits (for approximation on the interval) and $15, 14, 11, 5, 3, 3, \ldots$ digits (for approximation on the circle).

For another illustration of locating poles and zeros by rational approximation, we turn to the Riemann zeta function $\zeta(z)$, an example presented with a colourful figure in (Trefethen (2023)). The function is defined by the Dirichlet series

$$\zeta(z) = \sum_{k=1}^{\infty} k^{-z},\tag{4.3}$$

which converges just for Re z > 1 even though $\zeta(z)$ is analytic throughout the complex plane apart from a simple pole at z = 1. With Re z = 4, we can evaluate $\zeta(z)$ to 13-digit accuracy quickly by summing 20,000 terms of the series. Suppose we evaluate $\zeta(z)$ in this way at 100 points along the line

⁴ The method for computing residues in Chebfun aaa.m changed in 2025. Previously, residues were computed from (2.1) by an algebraic formula. In the new method, they are obtained by solving a linear least-squares problem to fit the sample values as well as possible by a linear combination of the poles. For applications like those of section 22, this sometimes contributes several digits of improved accuracy.



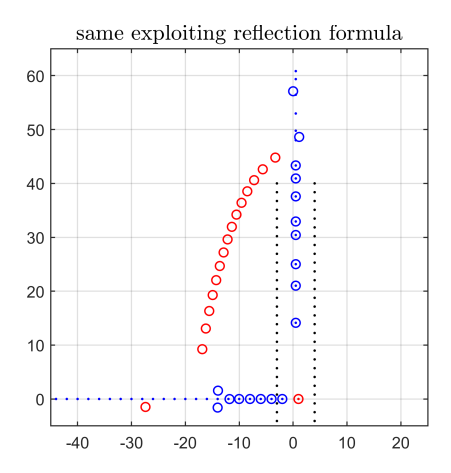


Figure 4.2. On the left, poles (red circles) and zeros (blue circles) of the degree 29 AAA approximation of the Riemann zeta function $\zeta(z)$ based on sample values at 100 points with Rez=4 (black dots). The pole and the zeros of $\zeta(z)$ are marked by red and blue dots, respectively. The pole of $\zeta(z)$ is captured to 11 digits of accuracy, whereas the other poles of r(z) are artifacts of the approximation (red circles). The first few zeros of $\zeta(z)$ on the critical line Rez=1/2 are also highly accurate. This figure shows the upper half of a symmetric configuration in the complex plane. On the right, the same except with 50 sample points in the right half-plane and also their reflections by (4.4) in the left half-plane. The rational approximation is now of degree 32; the accuracy is similar.

segment from 4-40i to 4+40i and then calculate a AAA approximant r(z) to these data values:

```
Z = linspace(4-40i,4+40i).';
zeta = @(z) sum((2e4:-1:1).^(-z),2);
[r,pol,res,zer] = aaa(zeta(Z),Z);
```

The left side of Figure 4.2 shows the resulting poles (red circles) and zeros (blue circles) of r(z). For comparison, the pole and the zeros of $\zeta(z)$ are shown by red and blue dots. The agreements are very good. On the right side of the figure, the experiment is repeated but now with 50 points with Rez = 4 and 50 more points at their reflections in the left half-plane with Rez = -3, where $\zeta(z)$ is evaluated by the reflection formula

$$\zeta(1-z) = 2(2\pi)^{-z} \cos(\pi z/2) \Gamma(z) \zeta(z). \tag{4.4}$$

In both experiments the pole matches the correct value z=1 to 11 digits, and as for the zeros, here are a pair of columns showing the absolute errors in the zeros in the upper half-plane. The reason for the blank in the final

row of the first column of data is that this approximation is of degree 1 less than the other.

	error	error
imag part of zero	100 samples on one side	50 samples on each side
14.135	0.00000000080	0.00000000011
21.022	0.00000000316	0.00000000027
25.011	0.0000000082	0.00000000088
30.425	0.000000074	0.0000000069
32.935	0.00000034	0.000000029
37.586	0.0000030	0.0000040
40.919	0.00089	0.00020
43.327	0.026	0.012
48.005	0.62	0.88
49.774	8.9	7.3
52.970	37.	28.
56.446		164.

The examples of this section so far have dealt with meromorphic functions, which have poles as well as zeros (actually, the gamma function has no zeros). Since rational functions can approximate poles, this is an obvious type of problem to attempt. But the AAA algorithm can be a powerful and exceptionally simple rootfinding tool even for functions that are analytic, when there are no poles. Indeed, AAA may often outperform more complicated bespoke rootfinding methods. To illustrate how simple its use can be, suppose we want to find the roots of the function $f(x) = \sin(5\pi x)$ in [-1,1]. The commands

```
X = chebpts(40);
F = sin(5*pi*X);
[~,~,~,zer] = aaa(F,X);
zeros = sort(zer(imag(zer)==0 & abs(zer)<=1.1))</pre>
```

based on just 40 function values produce this output in a few milliseconds, with all the zeros captured to accuracy better than 10^{-13} :

A general term for this kind of algorithm, introduced by Boyd (Boyd (2014)),

is proxy rootfinding. The idea is to approximate a general function f by a function with simple enough algebraic structure that its roots can be determined easily—typically via a matrix eigenvalue problem. The best-known version of this idea involves polynomial approximation, as suggested first by Good in his paper on "colleague matrices" (Good (1961)), then developed further by Boyd and used as the main rootfinding engine for polynomial approximations in Chebfun (Battles and Trefethen (2004), Driscoll et al. (2014)). Examples like this one illustrate that rational functions can do the job too, and with the AAA algorithm, they can be applied to virtually arbitrary rootfinding problems on arbitrary domains. This method is advocated by Costa in one of the online Chebfun examples (Costa (2022)) and developed more fully in (Bowhay, Nakatsukasa and Zaid (2025)). For rational rootfinding before AAA, see (Austin, Kravanja and Trefethen 2014, section 6).

In this section we have considered how AAA may be used to find both poles and zeros. It is natural to ask, are these two problems symmetric, or might AAA perhaps be more accurate, say, as a polefinder than as a zerofinder? If this were true, then there might be an advantage sometimes in replacing data values F by their reciprocals 1/F.

So far as we are aware, the answer to this question is perhaps surprising, and surprisingly elementary. It seems that polefinding and zerofinding are at bottom essentially equivalent, but that polefinding is sometimes slightly more accurate for the accidental reason that a function tends to be bigger near its poles than near its zeros! Since AAA is designed to approximately minimise the ∞ -norm of the absolute error, this means that in a relative sense, it sometimes gives more weight to approximation near a pole than near a zero. Perhaps the balance would be more even if AAA measured the ∞ -norm of errors via a metric on the Riemann sphere rather than the complex plane, but so far as we know, no AAA codes have tried this.

AAA approximation of poles is the foundation of several of the topics discussed later in this article, notably in sections 13, 16–18 and 22. See the final paragraph of section 12 for an informal classification of computed poles into approximation poles, pole poles, branch cut poles and spurious poles.

5. Computing derivatives and integrals

Differentiation and integration are two of the basic problems of numerical analysis, and rational approximations sometimes lead to good methods for them.

Let us begin with the problem of calculating the derivative of

$$f(x) = \tanh(8x) \tag{5.1}$$

for $x \in [-1,1]$. One approach would be by polynomial approximation.

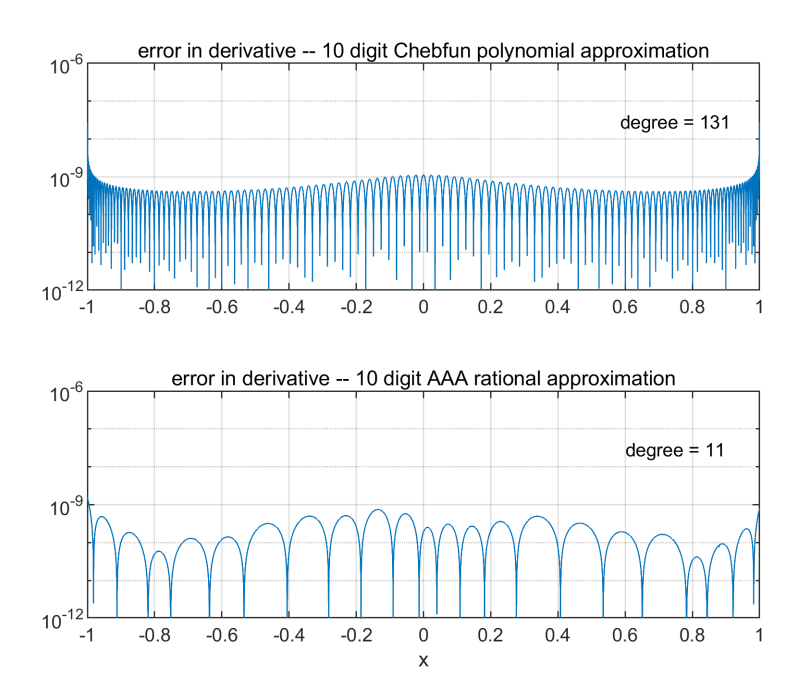


Figure 5.1. Numerical computation of the derivative of $f(x) = \tanh(8x)$ for $x \in [-1, 1]$ based on polynomial and rational approximations of f accurate to 10 digits. For $f(x) = \tanh(80x)$, the degrees increase to 1201 and 22.

We can compute a polynomial approximant to f accurate to 10 digits and differentiate it with the Chebfun commands

```
p = chebfun('tanh(8*x)','eps',1e-10);
dp = diff(p);
```

Executing length(p) reveals that the approximation has degree 131. (This is a polynomial interpolant in an adaptively determined number of Chebyshev points.) As shown in the upper half of Figure 5.1, the accuracy of the derivative is about 10^{-9} (hence a relative error of order 10^{-10}). The plot shows the absolute error |f(x) - p(x)| on a log scale, evaluated on a 10,000-point equispaced grid in [-1,1].

Another approach to differentiating (5.1) would be by rational approximation. We can compute a AAA approximation to 10 digit accuracy and differentiate it with the commands

```
X = linspace(-1,1,200)';
F = tanh(8*X);
[rr,pol] = aaa(F,X,'tol',1e-10,'deriv_deg',1);
r = rr{1}; dr = rr{2};
```

Executing length(pol) reveals that the rational approximation has degree 11. The lower half of Figure 5.1 shows that the accuracy is about the same as for the polynomial approximation, though the degree is ten times lower. For other functions, the ratio can be more extreme.

Computing derivatives is a step toward computing minima and maxima. For example, where does the function f of (5.1) attain its maximum slope, and what is that value? The computation

```
[rr,pol] = aaa(F,X,'tol',1e-10,'deriv_deg',2);
ddr = rr{3};
[r,pol,res,zer] = aaa(ddr(X),X);
pos = zer(imag(zer)==0 & abs(zer)<1)
val = dr(pos)

pos = -9.87e-12
val = 7.9999999981</pre>
```

gives answers accurate to 10 or more digits.

These examples illustrate results of computing a derivative by rational approximation, but not the mechanics of how it is done. Formulas for this were introduced in (Schneider and Werner (1986)), where it was shown that if r(z) is represented in the barycentric representation (2.1),

$$r(z) = \sum_{k=0}^{n} \frac{f_k \beta_k}{z - t_k} / \sum_{k=0}^{n} \frac{\beta_k}{z - t_k} , \qquad (5.2)$$

then the derivative r'(z) can be written in the same way, except with the data f_k replaced by the divided differences $(r(z) - f_k)/(z - t_k)$:

$$r'(z) = \sum_{k=0}^{n} \frac{(r(z) - f_k)\beta_k}{(z - t_k)^2} / \sum_{k=0}^{n} \frac{\beta_k}{z - t_k}.$$
 (5.3)

As usual, these formulas apply when z is not one of the support points; of course z should also not be one of the poles of r. If $z=t_j$ for some j, we have the special formulas

$$r(t_j) = f_j, \quad r'(t_j) = -\frac{1}{\beta_j} \sum_{k \neq j} \frac{\beta_k (f_j - f_k)}{t_j - t_k}.$$
 (5.4)

Equations (5.3)–(5.4) cover the computation of the first derivative, and for higher derivatives, Schneider and Werner present a generalised formula involving higher-order divided differences and show how it can be evaluated by a simple recursion.

Barycentric evaluations of polynomials and rational functions are famously stable even at points z close to the support points $\{t_k\}$, where one comes close to "dividing infinity by infinity", and theorems to this effect for

the polynomial case were presented by (Higham (2004)). Barycentric evaluations of first and higher-order derivatives, however, are another matter. The formula (5.3) fails numerically as z approaches a support point, and for accurate results, other methods are needed such as a second AAA fit to data at support and/or other points defining the derivative rather than the function value itself. At present, such refinements are not included in Chebfun aaa.m, nor so far as we know in other AAA software.

Rational approximations can also be used for numerical integration, also known as quadrature: if $f(x) \approx r(x)$, then $\int f(x) dx \approx \int r(x) dx$. We are unaware of formulas that evaluate $\int r(x) dx$ directly in the barycentric representation, so as an alternative, one can convert a rational approximation to partial fractions and then integrate these term by term. A variation on this theme has been proposed in (Bruno and Santana (2025)) to cope with problems in which one or more singularities lie very close to the integration contour. After finding these singularities and their residues with AAA, one can subtract them off and integrate the smoother integrand that remains by AAA or other methods.

An interesting special case of AAA-based integration has been suggested to us by Dave Darrow, in which one wishes to calculate an integral over the whole real line,

$$I = \int_{-\infty}^{\infty} f(x) \, dx. \tag{5.5}$$

Now there is the prospect of evaluating I entirely by residue calculus applied to an approximation $r \approx f$. Specifically, if r satisfies $r(z) = O(|z|^{-2})$ as $|z| \to \infty$ in the upper half-plane, then the contribution to a contour integral over a semicircle in the upper half-plane with |z| = R will vanish as $R \to \infty$, and by the residue theorem we are left with

$$I_r = \int_{-\infty}^{\infty} r(x) \, dx = 2\pi i \sum_{k=1}^{n} a_k, \tag{5.6}$$

where $\{a_k\}$ are the residues of r in the upper half-plane. (In practice, instead of $r(z) = O(|z|^{-2})$ we are likely to have $|r(z)| \le \varepsilon/|z|$ as $|z| \to \infty$ with $\varepsilon \ll 1$, perturbing the result by at most $2\pi\varepsilon$.) As an example, suppose we want to evaluate numerically

$$\frac{1}{\sqrt{\pi}} \int_{-\infty}^{\infty} e^{-(x-1)^2} dx,$$

whose exact value is 1. We use the tangent function to discretise \mathbb{R} by a grid with points extending to large values and approximate the integrand there by a rational function r, which has degree 30.

```
X = tan(.99*linspace(-pi/2,pi/2,200))';
F = exp(-(X-1).^2)/sqrt(pi);
```

```
[r,pol,res] = aaa(F,X);
```

Approximating the integral of r by residue calculus gives 12 digits of accuracy:

```
ii = find(imag(pol)>0);
I = -2*pi*imag(sum(res(ii)))

I = 1.000000000003281
```

Applying the same method to

$$\int_{-\infty}^{\infty} e^{-(x-1)^2} \sqrt{0.001 + x^2} \, dx$$

gives a rational approximant of degree 52 and an estimated integral matching the exact value 1.863662433495... to 11 digits.

Another application that can be approached by AAA approximation is the computation of complex Cauchy integrals, and a successful example of this kind can be found in (Nethercote, Kisil and Assier (2024)). On the other hand, sometimes there may be better approaches. Cauchy integrals typically arise in applications related to residue calculus, and it may be easier and more accurate to proceed directly from a rational approximation rather than by means of an integral. For example, suppose we want to compute the zeros and poles of the function

$$f(z) = \frac{\sin(z)}{z^2 - \frac{1}{4}} \tag{5.7}$$

in the unit disk. There are methods for such computations based on Cauchy integrals (Austin et al. (2014)), but it is simpler to follow the methods of the last section and execute

The relationship between Cauchy integrals and rational approximations will reappear in sections 16–18 and 22–23, and section 22 will present some surprisingly deep connections between rational approximations (of a Cauchy transform) and quadrature formulas (over an associated contour).

6. Analysis of branch points

It is perhaps not surprising that rational approximations are good at finding poles and zeros, as we saw in section 4. A deeper challenge arises if a function has branch points. Rational functions can be powerful here too, and their role for such computations became well known in condensed matter physics in the use of Padé approximations for the numerical analysis of critical points related to phase transitions (Baker, Jr. (1961), Guttmann (2015)).

For an example of AAA rather than Padé type, suppose f is the function

$$f(z) = (2-z)^{-0.4}. (6.1)$$

This function has a branch point at $z_0 = 2$, which means that not only is it not analytic at z_0 , but it is not analytic in any punctured neighborhood of z_0 . Now suppose we know some function values for f well away from the singularity, say, at 50 points in [-1,1]:

```
f = @(z) (2-z).^(-0.4);
Z = linspace(-1,1,50)';
F = f(Z);
```

We can use these values to approximate f(z) by AAA, and the approximation will be excellent for many values of z. For example, at z=-4, which is well beyond the radius of convergence of 2 of the Taylor series, we get six digits of accuracy:

```
[r,pol,res,zer] = aaa(F,Z);
f(-4), r(-4)
ans = 0.488359342
ans = 0.488359411
```

Suppose, on the other hand, our goal is not just to evaluate f but to determine the location and the nature of its singularity. We find that there are six zeros and poles of r, lining up in interlacing order on the real axis to the right of z_0 , clustering at that point. The configuration is plotted in Figure 6.1, and here are the numbers. In this example the zeros and poles happen to be real, but in general there may also be complex conjugate pairs even in approximation of a real function.

```
zeros
                  poles
                                residues
 2.0929234
                2.0308549
                              -0.1350795
                              -0.1938906
  2.4436865
                2.2630564
 3.2970933
                2.8646639
                              -0.2887175
 5.5180478
                4.3453159
                              -0.5017359
 13.5608306
                8.8550598
                              -1.1596502
100.5398233
               34.7222948
                              -5.3256391
```

It is clear from the figure and the data that there is some kind of singularity near z = 2. It must be a branch point, since it is not approximated

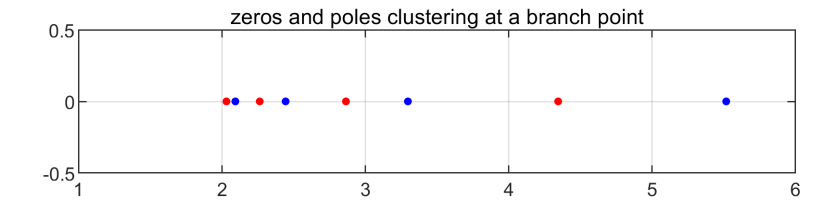


Figure 6.1. Zeros (blue) and poles (red) of a AAA approximation to the function (6.1) with a branch point at $z_0 = 2$. The zeros and poles cluster near the singularity. By rational approximation of the logarithmic derivative (6.2), one can determine the singularity location and exponent to 10 digits of accuracy.

simply by a pole. But how could we determine its location to more than, say, a couple of digits of accuracy? And how could we determine the nature of the singularity?

A powerful method for some such problems is to work with the logarithmic derivative of f,

$$\frac{f'(z)}{f(z)} = (\log f)'. \tag{6.2}$$

Suppose f is a function of the form

$$f(z) = g(z)(z - z_0)^{\alpha},$$
 (6.3)

where z_0 is an unknown complex number, g is an unknown analytic function, and α is an unknown real number that is not an integer. Then we have

$$f'(z) = g'(z)(z - z_0)^{\alpha} + \alpha g(z)(z - z_0)^{\alpha - 1}, \tag{6.4}$$

which implies

$$\frac{f'(z)}{f(z)} = \frac{g'(z)}{g(z)} + \alpha(z - z_0)^{-1}.$$
 (6.5)

The logarithmic derivative has converted the branch point to a simple pole. If we now approximate f'/f by a AAA rational function r, we can expect to find a pole of r very close to z_0 with a residue that is very close to α .

To apply this method we need the derivative f'. Working from function values but not derivatives, we can estimate f' from a preliminary rational approximation as in the last section. Thus the natural AAA method for this problem consists of three steps, applied at a suitable set of sample points Z. So far as we know, this method has not been published previously.

- 1. Approximate f(z) for $z \in Z$ by a rational function $r_1(z)$;
- 2. Approximate $r_1'(z)/r_1(z)$ on $z \in Z$ by another rational function r(z);

3. Estimate z_0 and α by a pole and a residue of r(z).

For step (2), we need to calculate $r'_1(z)$, where r_1 is a AAA rational function in the barycentric representation. In this computation, since one rational approximation is being built from another, 13-digit precision is not achievable. We proceed with the tolerance of the second approximation weakened to 11 digits:

```
rr = aaa(F,Z,'deriv_deg',1);
f2 = @(z) rr{2}(z)./rr{1}(z);
[r,pol,res] = aaa(f2(Z),Z,'tol',1e-11);
```

The computed pole location and exponent come out with about ten correct digits:

```
pol = 2.000000000024

res = -0.40000000012
```

As pointed out in (Bowhay et al. (2025)), this method for analysis of branch points also works for the analysis of poles (or zeros) of order higher than 1: where α in (6.3) is an integer ≤ -2 (or ≥ 2). For example, if AAA is applied to the function $f(z) = e^z/(z-z_0)^3$ with $z_0 = 1+0.5i$, the triple pole is approximated by three poles in a near-circle about z_0 of radius 0.000134, with residues of magnitude about $5.03 \cdot 10^7$. By contrast, a repetition of the logarithmic derivative calculation above finds the triple pole location with accuracy $5 \cdot 10^{-13}$ and its multiplicity (which of course we know to be an integer) with accuracy $4 \cdot 10^{-12}$.

The method we have discussed also works if f has several branch points related multiplicatively. For example, suppose we have the function

$$f(z) = g(z)(z - z_1)^{\alpha}(z - z_2)^{\beta}$$
(6.6)

and we want to find z_1, z_2, α , and β . The logarithmic derivative is

$$\frac{f'(z)}{f(z)} = \frac{g'(z)}{g(z)} + \frac{\alpha}{z - z_1} + \frac{\beta}{z - z_2},\tag{6.7}$$

indicating that a rational approximation can find both branch points and exponents. To illustrate, consider the function

$$f(z) = \frac{e^z (2i - z)^{1/2}}{(1.5 - z)^{3/4}}.$$

If we sample in 50 roots of unity and follow the procedure above, we find these poles and residues also correct to 10 places:

```
pol =
   0.000000000105 + 2.000000000013i
   1.49999999999 + 0.000000000008i
```

```
res = 0.500000000017 - 0.000000000085i -0.74999999996 - 0.000000000024i
```

A greater challenge arises if we have a function with several branch points related additively. For example, the logarithmic derivative of

$$f(z) = (z - z_1)^{\alpha} + (z - z_2)^{\beta}$$
(6.8)

is

$$\frac{f'(z)}{f(z)} = \frac{\alpha(z - z_1)^{\alpha - 1} + \beta(z - z_2)^{\beta - 1}}{(z - z_1)^{\alpha} + (z - z_2)^{\beta}}.$$
(6.9)

Like f itself, this function has branch points at z_1 and z_2 , so looking at the logarithmic derivative will not obviously be helpful. Indeed, the same challenge applies for an additive combination involving just one branch point, such as this seemingly minor modification of (6.1),

$$f(z) = 1 + (2 - z)^{-0.4}, (6.10)$$

with logarithmic derivative

$$\frac{f'(z)}{f(z)} = \frac{0.4(2-z)^{-1.4}}{1+(2-z)^{-0.4}}. (6.11)$$

7. Inverse functions

If $f: z \mapsto w$ is a one-to-one function of a real or complex variable z, then the inverse function f^{-1} is defined by the condition $f^{-1}(f(z)) = z$. (As often in this paper there is a matrix analogue, but our focus is on the scalar case.) Some inverse functions are known analytically, but others must be found numerically, and this can be challenging since f^{-1} may have singularities even though f does not. In this section we show how rational approximations can be used to compute inverse functions numerically.

To start with an easy example, suppose we didn't know about $\log(t)$ and wanted to find an inverse of $f(x) = e^x$ for $x \in [-1, 1]$, which it maps into the interval $[e^{-1}, e]$. The code

```
X = linspace(-1,1)';
f = @(x) exp(x);
[finv,pol] = aaa(X,f(X));
```

returns a function handle **finv** in about 5 ms that matches $\log(t)$ on $[e^{-1}, e]$ with maximum error $1.6 \cdot 10^{-14}$ (on all of the interval, not just at the sample points). The rational approximation is of degree 8, with poles in $(-\infty, 0]$ clustering at 0, where the true inverse function has a logarithmic branch point.

As a more challenging example, again with an exact solution available

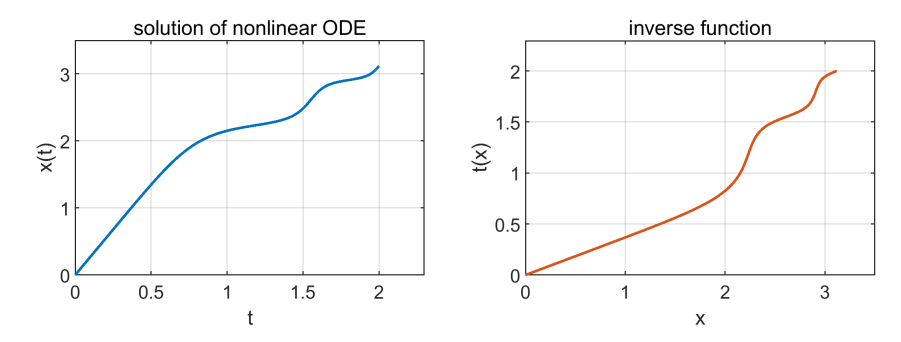


Figure 7.1. Solution of the ODE (7.1) and its inverse function computed with AAA.

for comparison, suppose we want the inverse of $\sin(x)$ for $x \in [-\pi/2, \pi/2]$. Since f(x) has derivative zero at $x = \pm \pi/2$, $f^{-1}(t) = \sin^{-1}(t)$ has square root singularities at $t = \pm 1$. Because of ill-conditioning, we cannot expect a global approximation to $f^{-1}(t)$ on [-1,1] to have accuracy better than about the square root of machine precision. With this in mind we compute a AAA approximant with tolerance 10^{-7} , using a sample grid of 400 points exponentially clustered near $\pi/2$ and $-\pi/2$:

```
X = (pi/2)*tanh(linspace(-14,14,400)');
f = @(x) sin(x);
[finv,pol] = aaa(X,f(X),'tol',1e-7);
```

This time the computation takes about 20 ms, giving a rational function of degree 40, with 20 poles in $(-\infty, -1]$ and 20 in $[1, \infty)$. The maximum error is $1.4 \cdot 10^{-7}$.

Of course, inverses can also be computed of functions that one does not know analytically. For example, the ODE initial-value problem

$$x' = \exp(\cos(t^2 x)), \quad u(0) = 0, \quad t \in [0, 2]$$
 (7.1)

can be solved numerically by the Chebfun commands

```
N = chebop([0 2]);
N.op = @(t,x) diff(x)-exp(cos(t^2*x));
N.lbc = 0;
x = N\0;
```

Figure 7.1 shows the result together with the inverse function (approximated by a rational function of degree 34) computed by the sequence

```
T = linspace(0,2,500)';
[t,pol] = aaa(T,x(T),'tol',1e-10);
```

Our next problem comes from a Chebfun example posted by Kuan Xu

64 equispaced points on a contour

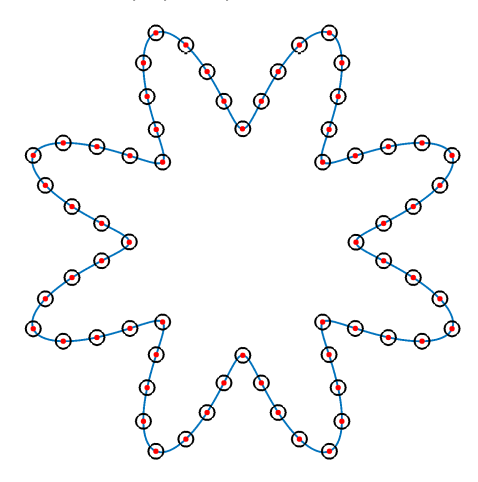


Figure 7.2. 64 equispaced points on a curve determined by a numerical computation of the inverse of an arc length function. Circles come from a polynomial approximation in Chebfun, dots from a rational approximation with AAA.

in 2012 (Xu (2012)). The planar curve shown in Figure 7.2 is parametrised by $x \in [0,1]$ and defined by these Chebfun commands, using complex arithmetic for convenience:

```
x = \text{chebfun('x',[0 1])};

f = \exp(1i*2*pi*x).*(0.5*sin(8*pi*x).^2+0.5);
```

For any open or closed curve like this, one can define a function s(x) representing the arc length over the parameter interval [0, x]:

$$s(x) = \int_0^x |f'(t)| dt.$$
 (7.2)

Chebfun realises this definition in one line:

```
s = cumsum(abs(diff(f)));
```

Now we ask, how can points be placed equidistantly along the curve? This is an inverse problem: we want values of f(x) corresponding to equispaced values of s. In (Xu (2012)), the result is computed by means of the inv command in Chebfun, generating the black circles plotted in the figure:

```
chebfuninv = inv(s);
distances = s(1)*(1:64)/64;
chebfunpts = f(chebfuninv(distances));
```

With AAA, we can obtain the same result by rational approximation. The

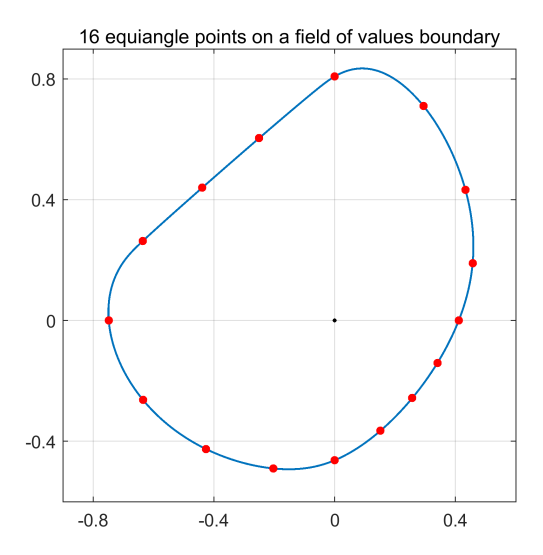


Figure 7.3. Sixteen points on the boundary of the field of values of a 5×5 matrix spaced at equal angles with respect to the origin. AAA approximation of an inverse function simplifies the representation of this curve from a degree 5703 polynomial to a degree 68 rational function.

following computation gives the red dots in the figure, whose maximum difference from the Chebfun circles is $1.5 \cdot 10^{-5}$:

```
T = linspace(0,1,800)';
AAAinv = aaa(T,s(T),'tol',1e-5,'mmax',200);
AAApts = f(AAAinv(distances));
```

The timings for this experiment on our laptop are about 1.9 s for Chebfun and 1.1 s for AAA. This is not much of a speedup, because a function like this, which is smooth and has many points of complexity, does not play to the strengths of rational approximation. It is interesting though how simple the inverse function calculation is conceptually and computationally: just apply AAA in the reverse of the usual direction by means of a command <code>aaa(T,s(T))</code> rather than the more familiar <code>aaa(s(T),T)</code>.

For another example with a similar flavor but a clearer benefit from rational approximation, consider this 5×5 matrix A explored in (Loisel and Maxwell (2018)):

The boundary of the field of values (= numerical range) of A can be computed by the Chebfun command

```
C = fov(A)
```

and is plotted in Figure 7.3. This is a smooth curve, but as discussed in (Trefethen (2019b)), that doesn't mean it is obvious how to find a representation of it with a small number of parameters. In fact, the Chebfun representation is by a polynomial of degree 5703. Large polynomial degrees are typical in Chebfun representations of fields of values, and in this case the behaviour is particularly extreme because a matrix has been chosen whose field of values boundary includes a nearly straight segment (Loisel and Maxwell (2018)).

With a AAA rational approximation of degree just 68, we can convert the curve to a representation as a function of angle with respect to the origin:

```
a = -unwrap(angle(C));
tt = chebpts(2000,[0 2*pi]);
[r,pol] = aaa(tt,a(tt),'tol',1e-12);
```

The commands

```
angles = (1:16)*2*pi/16;
angles2 = mod(angles-a(0),2*pi) + a(0) - 2*pi;
plot(C(r(angles2)),'.')
```

give the red dots shown in the figure, 16 points equally spaced with respect to angle.

The application that first made us aware of the power of rational approximation for computing inverse functions was numerical conformal mapping, to be discussed in section 25.

8. Equispaced interpolation

One of the oldest computational challenges is the interpolation of data in equally spaced points. To illustrate, Figure 8.1 considers samples at 40 equispaced points from -1 to 1 of an analytic function,

$$f(x) = e^x \cos(10x) \tanh(4x). \tag{8.1}$$

From these data, how might we recover f to good accuracy between the samples?

One idea would be polynomial interpolation. This method was discredited by Runge, who showed that degree n-1 polynomial interpolants of data at n equispaced points don't generally converge as $n \to \infty$, even when the underlying function is analytic (Runge (1901)). The second panel of Figure 8.1 shows that for this problem, all accuracy is lost for |x| > 0.8, and in fact, the error near the endpoints for this computation with n=40 is as

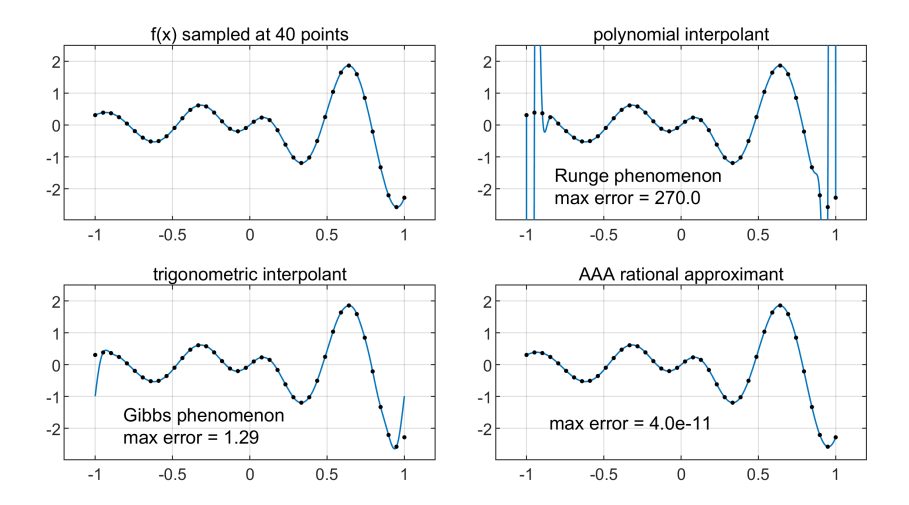


Figure 8.1. For interpolation of nonperiodic equispaced data, polynomials suffer from the Runge phenomenon and trigonometric polynomials from the Gibbs phenomenon. The best general-purpose method appears to be AAA approximation.

large as 270. (With 60 equispaced interpolation points, it would be 6450.) This effect is called the $Runge\ phenomenon\ (Trefethen\ (2019a))$.

Another idea would be Fourier or trigonometric interpolation, i.e., interpolation by a minimal-degree trigonometric polynomial composed of sines and cosines scaled to the given interval. This would be excellent if f were periodic, but in the non-periodic case the idea fails for a reason also going back to around 1900, the Gibbs phenomenon (Trefethen (2019a)). For the variant of trigonometric interpolation shown in the figure, the value interpolated at $x = \pm 1$ is the mean of f(-1) and f(1), leading to an error at that point of $|f(1) - f(-1)|/2 \approx 1.29$. There are large errors also nearby, though this is not so visible in the plot, and even in the middle of the interval, the accuracy is no better than 0.003.

In the face of these long-recognised failures of the two most obvious methods of interpolation, a large literature has grown up of papers with titles like "Defeating the Runge phenomenon" and "On the Gibbs phenomenon and its resolution." Many methods have been proposed, some of them rather complicated, including polynomial least-squares fitting, Fourier extensions, Fourier series with boundary corrections, multi-domain approximations, splines, conformal maps, Gegenbauer reconstruction, regularisation, and Floater-Hormann interpolation of adaptively determined degree. This list comes from (Huybrechs and Trefethen (2023)), where references can be found; see also the earlier review in (Platte, Trefethen and Kuijlaars (2011)). In the latter paper the "impossibility theorem" is proved, which

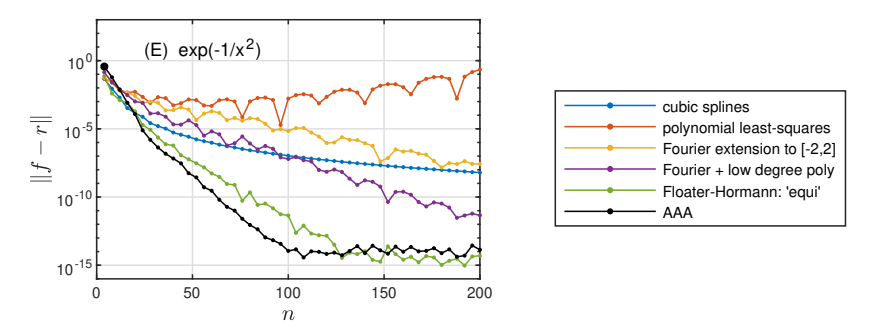


Figure 8.2. Illustration from (Huybrechs and Trefethen (2023)) of six different methods of equispaced interpolation applied to the function $f(x) = \exp(-1/x^2)$ for $x \in [-1, 1]$. AAA approximation shows steady convergence down to accuracy 10^{-13} as the number of sample points n increases. The other methods converge less quickly. Examples vary, but this behaviour is, broadly speaking, typical.

asserts that no method for approximating analytic functions from equispaced samples can be exponentially convergent unless it is exponentially unstable. This establishes in a rigorous sense that a comprehensive defeat of the Runge and Gibbs effects is not possible.

Examples can be found in which almost any of these methods outperforms the others. The best general purpose method for equispaced interpolation, however, appears to be simply to construct a AAA fit to the data. (Strictly speaking the result is then an approximation, not an interpolant.) The final part of Figure 8.1 shows that for this example, the accuracy is ten digits as delivered by the code segment

```
f = @(x) \exp(x).*\cos(10*x).*\tanh(4*x);

X = -1+2*(0:39)'/39;

r = aaa(f(X),X);
```

The degree of the AAA rational approximant is 18. For an extensive discussion with many further examples and comparisons with other methods, see (Huybrechs and Trefethen (2023)). To illustrate one such comparison, Figure 8.2 reproduces an image from (Huybrechs and Trefethen (2023)) showing the behaviour as a function of the number of sample points in approximation of the C^{∞} function $f(x) = \exp(-1/x^2)$ on [-1, 1].

Perhaps this is a good place to emphasise a consideration that applies throughout this article and to AAA approximation generally. AAA can be extremely accurate for smooth data, but in the presence of noise, it typically fails. If data are known to be corrupted by noise at a level ε , one can often do quite well by running AAA with a tolerance set above that level. This is why the default AAA tolerance is as high as 10^{-13} even though IEEE

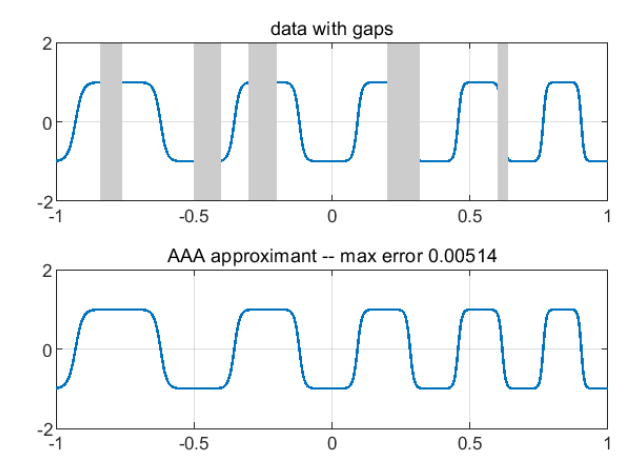


Figure 9.1. Use of AAA approximation to fill in gaps in an analytic function.

machine epsilon is about 10^{-16} . Attempting to fit closer to the noise level is likely to lead to loss of accuracy and spurious poles, and for noisy problems in general, and noisy equispaced interpolation in particular, one may be well advised to rely on methods that are more robust—more linear—even if they will usually be less accurate when the problem is smooth.

9. Imputing missing data

A variation on the last section's theme of interpolation between equispaced data points is the problem of filling in larger stretches of a smooth function that may be absent from a dataset. An example of this kind (for trigonometric as opposed to ordinary rational approximation) appeared in Heather Wilber's 2021 PhD thesis (Wilber (2021)) and was reproduced in (Wilber, Damle and Townsend (2022)).

Figure 9.1 illustrates the process. The function $f(x) = \tanh(4\sin(30e^{x/2}))$ has been sampled in 1000 equally spaced points in [-1,1], and then 275 of the samples, marked by the grey stripes, have been removed. When AAA approximation is applied to the remaining data, f(x) is recovered in about 0.1 s on a laptop by a rational function of degree 90 that matches it with a maximum error of $0.8 \cdot 10^{-5}$ on [-1,1]. For this experiment the standard tolerance of 10^{-13} leads to spurious poles with very small residues on [-1,1], so it was loosened to 10^{-10} . Figure 9.2 shows a similar experiment but with a function that is C^{∞} rather than analytic, $f(x) = \exp(-1/\cos(5x)^2)$. This time the rational approximation has degree 72.

A generalisation of this idea can be applied in multiple dimensions, as illustrated in Figure 9.3. Here we start from the MATLAB "peaks" function,

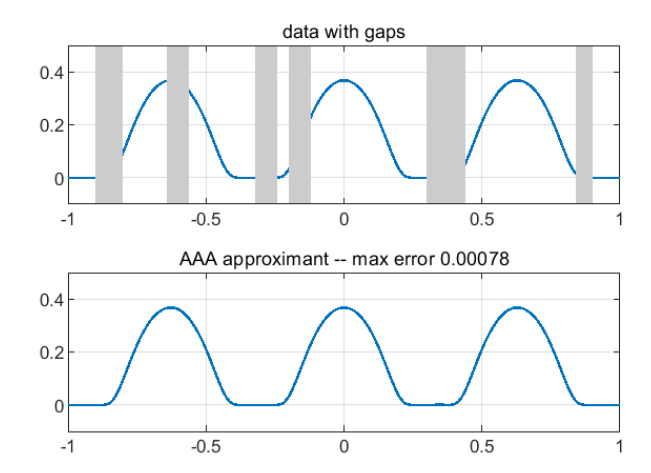


Figure 9.2. A similar experiment to that of Figure 9.1 but now for a C^{∞} function.

which is the bivariate real analytic function

$$f(x,y) = 3(1-x)^{2}e^{-x^{2}-(y+1)^{2}} -10(x/5-x^{3}-y^{5})e^{-x^{2}-y^{2}} - e^{-(x+1)^{2}-y^{2}}/3.$$
 (9.1)

Ideally, we would like to find a near-best approximation of f by a bivariate rational function r(x,y). However, no method for computing multivariate rational approximations is known that has anything like the power of AAA in the univariate case (see section 15). Instead, to fill in the gaps, we can use a sequence of univariate approximations. (This idea originates in (Trefethen (2023)).) In the example, f is sampled on a 100×100 regular grid, and then on each horizontal line, a AAA approximation is computed from the data after eliminating the values in the gaps. In other words, we compute 100 1D approximations like those illustrated in Figures 9.1 and 9.2. The whole computation takes 0.7 s on a laptop and obtains excellent accuracy.

In image analysis, the process of filling in missing data is known as *in-painting*, and this is an area of engineering on which many methods have been brought to bear, including machine learning. The strength of rational approximation is its ability to deal with smooth functions to high accuracy, and we would not claim that this regime is typical of inpainting problems.

10. Analytic continuation

In one way or another, half the applications of rational approximation and half the sections of this paper might be said to have something to do with analytic continuation. This is the process whereby information about an analytic function in some domain of the complex plane is used to infer

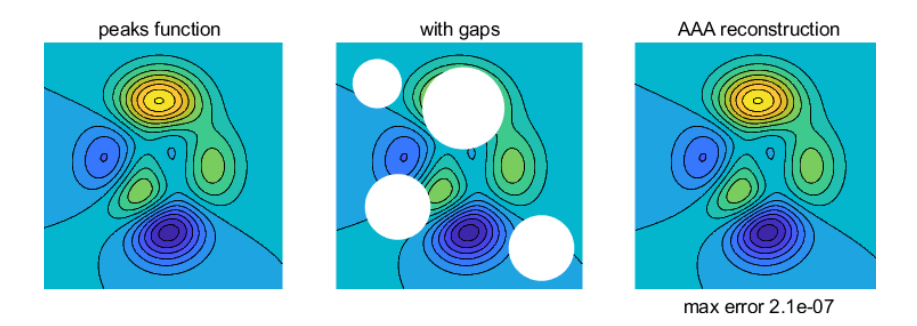


Figure 9.3. Filling in missing data in the bivariate MATLAB "peaks" function (9.1). Here 100 univariate AAA approximations are computed along horizontal slices of the image. The total computing time is still less than a second.

information about it elsewhere. The idea is fundamental in theory, but problematic in practice. For an extended discussion, see (Trefethen (2023)).

In theory, analytic continuation can be carried out by the "chain-of-disks" method of Weierstrass. If f is analytic at a point z_1 , then its Taylor series converges in a disk about z_1 . At any other point z_2 in that disk, f is also analytic, so one can construct a new Taylor series about z_2 . By moving along in this way one can in principle extend an analytic function along an arbitrary path in the complex plane so long as no singularities are encountered. Poles and essential singularities are isolated, and one can analytically continue around them. Branch points are not isolated, and lead to analytic continuations having different values depending on which way you pass around them—"multivalued analytic functions" with different branches, but still analytic. These are the singularities occurring most commonly in practice, but another possibility is that f might have a natural boundary beyond which no analytic continuation at all is possible. For example, a Taylor series with random coefficients from the standard normal distribution will have the unit circle as a natural boundary with probability 1 (Kahane (1985)).

The trouble is that these operations assume one has exact information about a function. If f is only known to accuracy ε , all is lost. Here is how it is put in Theorem 5.1 of (Trefethen (2020c)). An earlier paper that expresses the same result is (Miller (1970)).

Theorem 10.1. Let Ω be a connected open region of $\mathbb C$ and let E be a bounded nonempty continuum in $\overline{\Omega}$ whose closure \overline{E} does not enclose any points of $\Omega \backslash \overline{E}$. Let f be an analytic function in $\Omega \cup E$ satisfying $||f||_E \leq \varepsilon$ for some $\varepsilon > 0$. Then no bounds whatsoever can be inferred on the value of f at any point $z \in \Omega \backslash \overline{E}$.

This theorem would appear to suggest that numerical analytic continuation is impossible, but in fact, much can often be achieved for reasons whose theoretical basis is not always clear. One case that can be analysed mathematically, going back to the Hadamard three-circles theorem of complex analysis, is the situation where it is known that f is bounded in Ω . Here is how it is put in Theorem 5.2 of (Trefethen (2020 c)).

Theorem 10.2. Let Ω , E, ε , and f be as in Theorem 10.1, but now with f additionally satisfying $||f||_{\Omega} \leq 1$, and let z be a point in $\Omega \setminus \overline{E}$. Assume that the boundary of E is piecewise smooth (a finite union of smooth Jordan arcs). Then there is a number $\alpha \in (0,1)$, independent of f though not of f, such that for all f > 0,

$$|f(z)| \le \varepsilon^{\alpha(z)}. (10.1)$$

The fractional power $\alpha(z)$ in this theorem has a simple interpretation. If we know f to d digits of accuracy on E, then it is determined to $\alpha(z)d$ digits of accuracy at $z \in \Omega \setminus \overline{E}$. For a bounded analytic function f in the annulus $r_1 < |z| < r_2$, for example, the case of the three-circles theorem, if d digits are given on the inner circle, then the number of digits falls off smoothly to 0 on the outer circle according to the formula

$$\alpha(z) = 1 - \frac{\log|z/r_1|}{\log(r_2/r_1)}.$$
(10.2)

Results for other domains can be obtained by conformal transplantation, and are generally more adverse. In an infinite half-strip of half-width 1, for example, if one knows f to d digits on the end segment, the number of digits falls off by a factor of 10 with each translation along the strip by a distance $(2/\pi) \log 10 \approx 1.47$. At a distance of 6 into the strip, therefore, which is just three times the width, the number of digits has been divided by more than 10,000. Similarly if one tracks a function like \sqrt{z} known to be bounded and analytic for 0 < |z| < 2 from z = 1 around the origin and back to z = 1 again, the number of accurate digits may be divided by $(\pi/4) \exp(\pi^2) \approx 15,000$. You'd need to start out with 15,000 digits of accuracy to end up with 1—or 225,000,000 digits for two trips around the origin. All these results are discussed in (Trefethen (2020 c)).

It is interesting to note that (10.1) indicates that analytic continuation, under a boundedness assumption, is an example of a problem that is well-posed (continuous dependence on data) but with infinite condition number (not Lipschitz continuous).

In the face of such pessimistic bounds, it is often surprising how successfully analytic continuation can be carried out in practice by various means. A chapter of the textbook (Fornberg and Piret (2022)) describes nine methods that are often useful (several of them analytic or semi-analytic as opposed to strictly numerical): (1) Circle-chain method, (2) Schwarz reflection

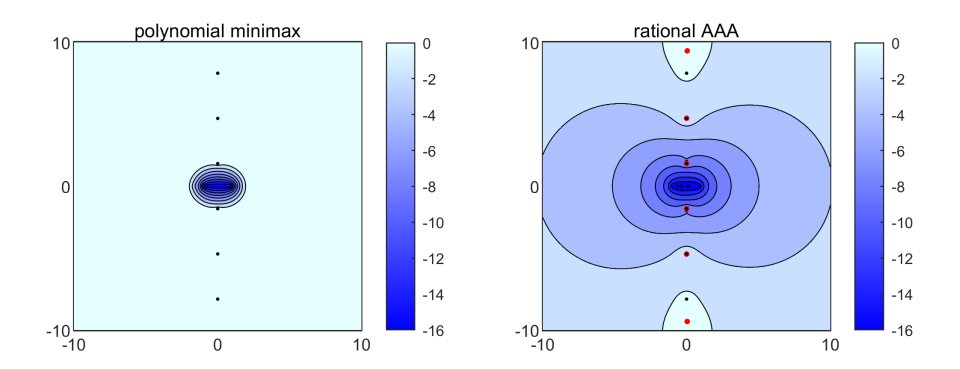


Figure 10.1. Numerical analytic continuation of $\tanh(z)$ from data on [-1,1] by degree 30 polynomial minimax fitting (left) and degree 7 AAA rational fitting (right) (error contours of $\log_{10}|f(z)-r(z)|$). Black dots mark poles of f, and red dots mark poles of the rational approximation r. As is well known, polynomials have no accuracy beyond the first singularity—with "beyond" and "first" for this case of approximation on the interval defined by Bernstein ellipses surrounding [-1,1]. Figure from (Trefethen (2023)).

principle, (3) Use of a functional equation, (4) Partitioning of an integration interval, (5) Replace Taylor coefficients by integrals or sums, (6) Subtraction of a similar series or integral, (7) Borel summation, (8) Ramanujan's formula, and (9) Padé approximations.

Here, we will focus on a tenth approach (or one could regard it as an extension of the ninth), namely rational approximation. So far as we are aware, this is the best method available for general-purpose strictly numerical analytic continuation.

Any experiment in which a AAA approximant is evaluated outside the approximation domain can be taken as an illustration of numerical analytic continuation by rational approximation. Figure 10.1, taken from (Trefethen (2023)), shows one such. Note that polynomial approximation, shown on the left, cannot get past the closest singularity ("closest" as defined in a fashion related to potential theory), whereas rational functions can do much better. We have already seen these effects earlier in the paper. For example, the contour lines of Figure 3.2 show considerable accuracy in analytic continuation of $\Gamma(z)$ from the unit interval or disk out to values of |z| as great as 3 or 4, despite the poles at $x = 0, -1, -2, \ldots$ Similarly, the zeta function example of Figure 4.2, though the images focus on zeros and poles, reflect accurate analytic continuation from the line Re(z) = 4 well across the imaginary axis and into the left half-plane.

Though such experiments are encouraging, it is hard to know what can be said precisely. As discussed at length in (Trefethen (2023)), the main

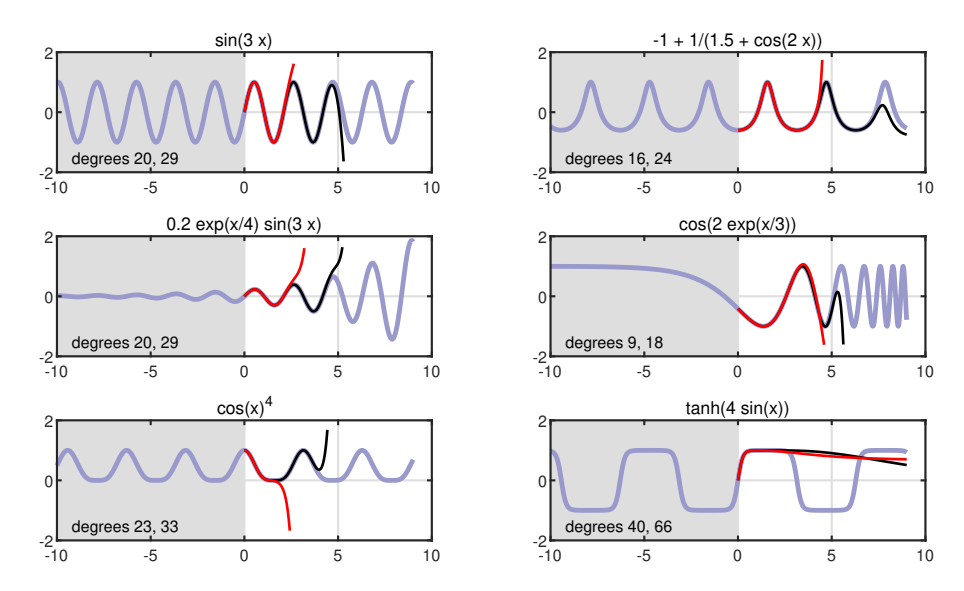


Figure 10.2. Illustration of the "one-wavelength principle" by six examples in which an analytic function f(x) is analytically continued by AAA approximation from data for $x \in [-10,0]$ to x>0. The thick blue-grey curves show f(x), the red curves show approximations r(x) with 13-digit accuracy, and the black curves show approximations r(x) with 29-digit accuracy. Approximately one and two wavelengths of successful continuation, respectively, appear to be achieved at least in the first four cases.

analysis available in this area is derived from potential theory following ideas of Walsh, Gonchar, Stahl and others which we will present here in section 12. Approximately speaking, this theory suggests that numerical analytic continuation by near-best rational approximations will typically achieve accuracies related to a potential function defined by n poles $\{\pi_{k}\}$ of r and 2n+1 interpolation points $\{\zeta_k\}$ where $r(\zeta_k)=f(\zeta_k)$, and that the positions of these poles and interpolation points will be determined by singularities of f. However, we are not aware if arguments of this kind have been carried very far to attempt to quantify convergence rates. There is also the problem that convergence at particular points $z \in \mathbb{C}$ can never be guaranteed because of difficulties related to "Froissart doublets"—poles with near-zero residues at seemingly arbitrary locations in \mathbb{C} that appear spurious from an approximation point of view and yet may be unavoidable even in exact arithmetic (and are almost invariably worse with rounding errors). Such effects have been studied extensively in connection with Padé approximation (Baker, Jr. and Graves-Morris (1999), Stahl (1998)).

Figure 10.2 illustrates an idea introduced in (Trefethen (2023)), the one-

wavelength principle. This is a rule of thumb, not a theorem. The observation is that in many cases in which AAA is applied to a function which has some kind of oscillatory behaviour, about one wavelength of successful analytic continuation beyond the data domain is observed, after which accuracy is lost. One wavelength is not an absolute figure, but is tied to the accuracy of the rational approximation, which by default in the Chebfun AAA code is 13 digits. Figure 10.2 shows that if the AAA accuracy is increased to 29 digits (thanks to Driscoll for 128-bit computations in Julia (Driscoll (submitted))), the number of wavelengths approximately doubles. Continuing such experiments to higher precision, Figure 7 of (Trefethen (2023)), based on data from Daan Huybrechs, shows a roughly linear relationship of the number of wavelengths with the number of digits of accuracy of the rational approximation. Thus about two wavelengths are possible with 26-digit approximations, three wavelengths with 39-digit approximations, and so on.

It is not clear how general the one wavelength principle is, or how it might be formulated precisely. Before (Trefethen (2023)), we have found just one publication that seems to speak to the topic: an article by Henry Landau in 1986 written in the context of sampling theory. See Theorem 2 of (Landau (1986)). Unfortunately, the route this suggests to try to make the principle precise, by restricting attention to band-limited functions of a certain class, has been falsified by a theorem proved by Alex Cohen of MIT (Trefethen (2025c)). So the problem remains open of finding a theorem to explain the one-wavelength effect. We shall discuss the related literature of "function extension" in section 15.

11. Computing the Schwarz function

The last section mentioned a list of nine methods of analytic continuation discussed in the textbook (Fornberg and Piret (2022)), of which the second was the Schwarz reflection principle. This is one of the fundamental results of complex analysis, going back to Schwarz long ago (Schwarz (1870)). The present section on the generalisation known as the Schwarz function is both interesting in its own right and important for the theoretical understanding of the PDE solution techniques to be discussed in sections 24–28.

The simplest version of the reflection principle runs as follows. For a proof and further details, see (Trefethen (2025a)).

As sketched on the left in Figure 11.1, let $\Omega \subseteq \mathbb{C}$ be a connected open set that is symmetric about \mathbb{R} , $\overline{\Omega} = \Omega$, and whose intersection with \mathbb{R} is a finite or infinite open interval Γ . (The symbol $\overline{\Omega}$ denotes the complex conjugate of Ω , in contrast to the last section, where it represented the closure of Ω .) Define $\Omega^+ = \{z \in \Omega : \operatorname{Im}(z) > 0\}$ and $\Omega^- = \{z \in \Omega : \operatorname{Im}(z) < 0\}$.

Theorem 11.1. Schwarz reflection principle. Let Ω , Γ , Ω^+ and Ω^- be as defined above, and let f be analytic in the interior of Ω^+ and continuous

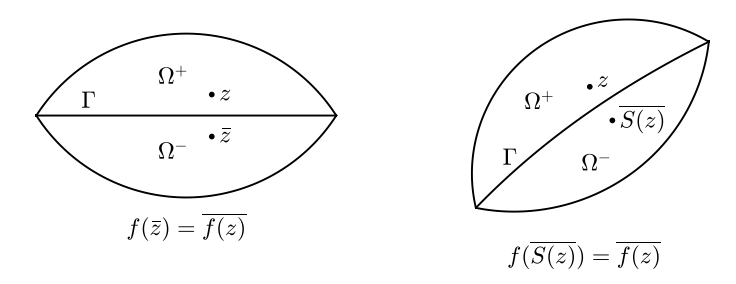


Figure 11.1. On the left, the Schwarz reflection principle (Theorem 11.1) extends an analytic function that takes real values on a real interval across the interval from one half-plane to the other. On the right, the generalisation by the Schwarz function S(z) for reflection of an analytic function across an analytic arc Γ , again assuming it takes real values on Γ . Figure from (Trefethen (2025a)).

on $\Omega^+ \cup \Gamma$, taking real values on Γ . Then the formula

$$f(\bar{z}) = \overline{f(z)} \tag{11.1}$$

defines an analytic continuation of f to all of Ω .

The Schwarz function generalises this result to cases where Γ is not a real segment but an analytic curve, as sketched on the right in Figure 11.1. Let Γ be an analytic Jordan arc or Jordan curve, that is, the image in $\mathbb C$ of the unit circle or an arc of the unit circle under a one-to-one analytic function with nonvanishing derivative. Consider the function

$$S(z) = \bar{z}, \quad z \in \Gamma. \tag{11.2}$$

Like any other analytic function defined on a curve in \mathbb{C} , S can be analytically continued to a complex neighborhood of Γ , and this is the Schwarz function. (It may be startling to read that $z\mapsto \bar{z}$ is an analytic function, and this would not be true on a domain with interior, but here we are dealing with just a curve.) The point of S is that $z\mapsto \overline{S(z)}$ is the generalisation to a general arc Γ of the reflection $z\mapsto \bar{z}$ when Γ is real. As the simplest example, the Schwarz function of the unit circle—or of any arc of the unit circle—is $S(z)=z^{-1}$.

The analytic continuation works as follows. Since S is analytic, it must extend to an analytic function on some neighborhood of Γ . Since $|d\overline{S(z)}/dz| = 1$ on Γ , it follows that in a sufficiently small neighborhood of Γ , $\overline{S(z)}$ maps a point z close to Γ on one side to a point close to Γ on the other side. This function $\overline{S(z)}$ is co-analytic, not analytic, but if we compose it with itself we get an analytic function, the identity:

$$\overline{S(\overline{S(z)})} = z. \tag{11.3}$$

With this property in hand, as sketched on the right side of Figure 11.1, we define a reflection domain for Γ to be an open set $\Omega \subseteq \mathbb{C}$ containing Γ that is divided into two disjoint open sets Ω^- and Ω^+ by Γ and in which a single-valued analytic Schwarz function S for Γ can be defined that satisfies

$$\overline{S(\Omega^+)} = \Omega^-, \quad \overline{S(\Omega^-)} = \Omega^+,$$
 (11.4)

and

$$\overline{S(\overline{S(z)})} = z, \quad z \in \Omega.$$
 (11.5)

With this definition, the generalisation of the reflection principle is as follows. See (Trefethen (2025a)) for a proof.

Theorem 11.2. Reflection across an analytic curve. Let Ω be a reflection domain for an analytic Jordan curve or Jordan arc Γ and let f be analytic in the interior of Ω^+ and continuous on $\Omega^+ \cup \Gamma$, taking real values on Γ . Then the formula

$$f(\overline{S(z)}) = \overline{f(z)} \tag{11.6}$$

defines an analytic continuation of f to all of Ω .

Although some of these ideas go back as far as Schwarz (Schwarz (1870)), the Schwarz function was not defined and named until almost a century later (Davis and Pollak (1958)). Two books have been published about it (Davis (1974), Shapiro (1992)), but they are nonnumerical. So far as we are aware, no numerical method was proposed for computing the Schwarz function before the arrival of AAA, when the paper (Trefethen (2025a)) has appeared in elaboration of earlier experiments presented in (Trefethen (2023, 2024)).

The AAA method for computing the Schwarz function could not be simpler: just calculate a rational approximation of \overline{z} on Γ . To illustrate, Figure 11.2 shows the poles of AAA approximations to the Schwarz functions of two curves defined by:

The AAA approximations and their poles are computed by the command

```
[r,poles] = aaa(conj(Z),Z);
```

with poles plotted inside Γ as blue dots and outside as red dots. To the experienced eye, these poles show a great deal. Evidently the Schwarz function S is well-behaved close to Γ , but has branch points inside concave regions, whether interior or exterior to the curve. One cannot see the whole

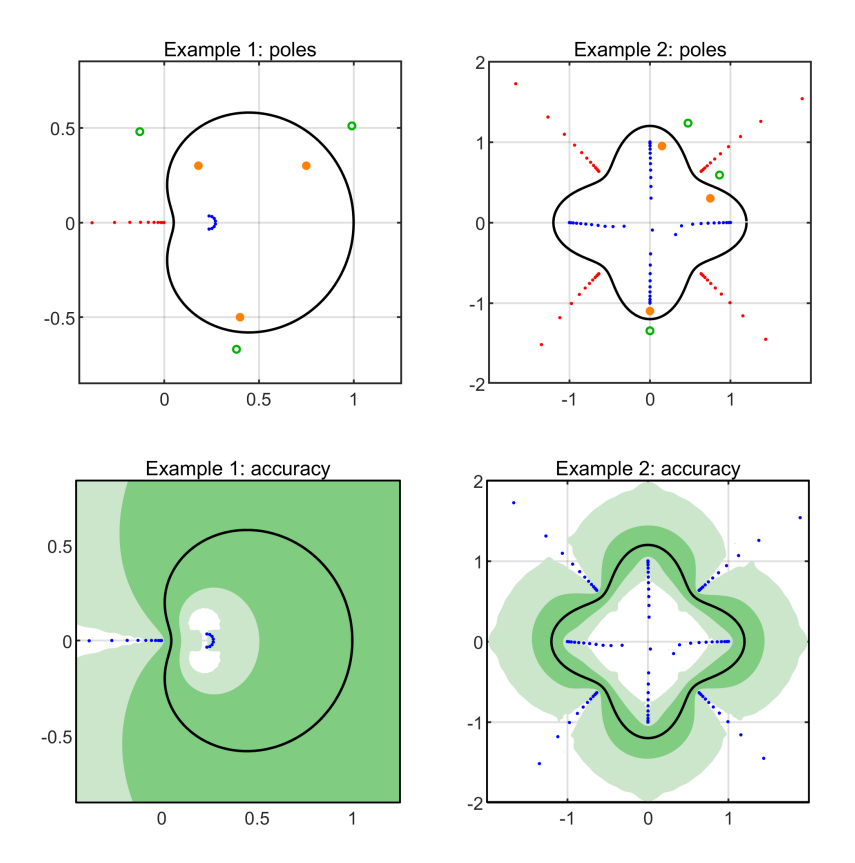
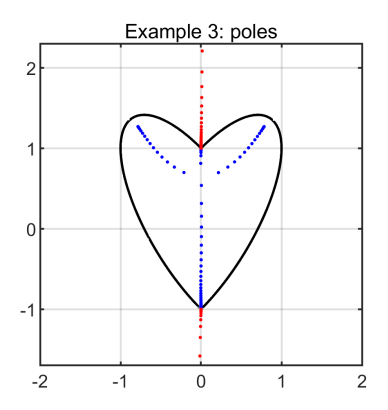


Figure 11.2. Numerically computed Schwarz functions for closed curves Γ obtained as images of the unit circle under maps f. On the left, $f(z) = \exp(1.5(z-1))$, and on the right, $f(z) = z(1+0.2\cos(4\arg(z)))$. In the first row of plots, the dots show poles of the AAA approximants, blue for poles inside Γ and red for poles outside. The orange/green dots illustrate three arbitrary pairs of points mapped to each other by $\overline{S(z)}$. In the second row, as a test of (11.3), dark and light green shading indicates regions where $|\overline{S(\overline{S(z)})} - z|$ is less than 10^{-8} and 10^{-1} , respectively.

Riemann surface of S(z) from such a plot, but one can guess where a reflection domain for each curve appears to lie. Such guesses are supported by the second row of the figure, in which the identity (11.3) for the AAA approximation r to S is verified by plotting level curves of the discrepancy

$$|\overline{r(\overline{r(z)})} - z|.$$
 (11.7)

(We thank Keaton Burns for suggesting this type of plot.) The dark-green region is bounded by the curve where this measure is 10^{-8} , i.e., 8 digits of



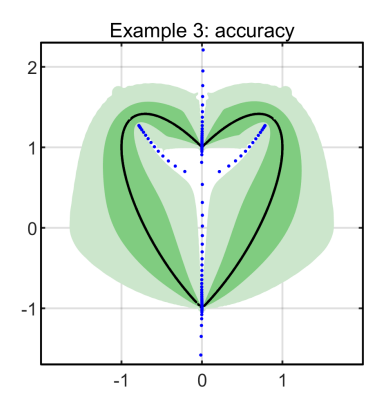


Figure 11.3. Similar plots for a curve Γ consisting of two pieces joined at branch points at $z = \pm i$. Mathematically, we now have a Schwarz function with unrelated branches associated with the left and right halves.

accurate approximation to the Schwarz function in a reflection domain, and the light green region corresponds to 10^{-1} , one digit of accuracy.

The Schwarz function is defined for open arcs Γ as well as closed ones. In fact, if Γ is a closed analytic arc, then in theory any open segment of it defines the full structure of S by analytic continuation, though this will be far from true in numerical practice. See (Trefethen (2025a)) for illustrations of Schwarz functions of open arcs.

It is also interesting to consider what happens with non-smooth contours, as in Figure 11.3. Here Γ is a heart-shaped region consisting of $z + i \operatorname{Re}(z)$ in the right half-plane, where z ranges over the right half of the unit circle, together with its reflection in the left half-plane. Mathematically, Γ is here not a single analytic curve but two unrelated components connected at a pair of branch points at $z = \pm i$. Each of these pieces would have its own Schwarz function, with poles presumably configured approximately like those in the figure that are not along the imaginary axis. The rest of the poles in the figure, along the axis, are from this point of view artifacts of constructing a global rational approximation to data that consists of two unrelated branches (see sections 20 and 22). However, this strict interpretation of the situation misses the deeper reality that the picture would look much the same if, instead of breaks of analyticity at $z = \pm i$, Γ merely had high curvature there. For this reason among others, computing a single Schwarz function for a contour consisting of distinct branches often makes good sense in practice. Examples will appear in sections 24–28, which concern applications of rational approximation to the solution of PDEs in the plane. Here branch points (corners) and nonconvex points (points of high curvature) arise frequently and are precisely the situations where rational

approximation shows its greatest power, since poles can be placed in inlets nearby. The Schwarz function is a fundamental tool for explaining the success of these methods, as discussed in (Barnett and Betcke (2008)) and (Trefethen (2024)).

12. Illustrating potential theory

The theory of rational approximation has developed greatly since Chebyshev first worked on such problems in the 19th century. The central tool is the Hermite integral formula, whose roots go back to Cauchy in the 1820s (at École Polytechnique) and Hermite in 1878 (École Polytechnique, University of Paris). Méray (Dijon) and Runge (Hannover) showed that Hermite's integral could be applied to bound the error of polynomial interpolants, and beginning in the 1920s, Walsh (Harvard) investigated analogous results for rational interpolants. This was the subject of many papers by Walsh in the ensuing forty years and the central topic of his magnum opus Interpolation and Approximation by Rational Functions in the Complex Domain, which appeared in five editions from 1935 to 1969 (Walsh (1969)). Beginning in the 1960s, Gonchar and Rakhmanov (Moscow) and Stahl (Berlin) and others then laid the foundation for analysis of asymptotic rates of best degree n rational approximation as $n \to \infty$. They showed that in this limit, the Hermite integrals lead to equilibrium PDE problems of potential theory.

In its most familiar form as presented in Theorem 8.2 of (Walsh (1969)), the Hermite integral for a rational approximation $r \approx f$ is

$$f(z) - r(z) = \frac{1}{2\pi i} \int_{\Gamma} \frac{\phi(z)}{\phi(t)} \frac{f(t)}{t - z} dt, \qquad (12.1)$$

where $\phi(z)$ is a complex potential function, which measures the product of the distances of a point z from interpolation points where r = f relative to the product of its distances from the poles of r. The standard definition of ϕ is

$$\phi(z) = \prod_{k=0}^{n} (z - \zeta_k) / \prod_{k=1}^{n} (z - \pi_k) , \qquad (12.2)$$

where π_1, \ldots, π_n are the poles of r, assumed at the outset to be simple and finite, and ζ_0, \ldots, ζ_n are any n+1 interpolation points satisfying $r(\zeta_k) = f(\zeta_k)$. The contour Γ must lie in a domain of analyticity of f and enclose the interpolation points and also the point z. Normally we would choose Γ to exclude the poles $\{\pi_k\}$ to get a good estimate from (12.1), but this is not necessary for the validity of the equation. Equations (12.1)–(12.2) also apply if some of the points are confluent (i.e., higher-order poles or interpolation points), and if there are poles at ∞ , these can simply be dropped from the denominator product in (12.2).

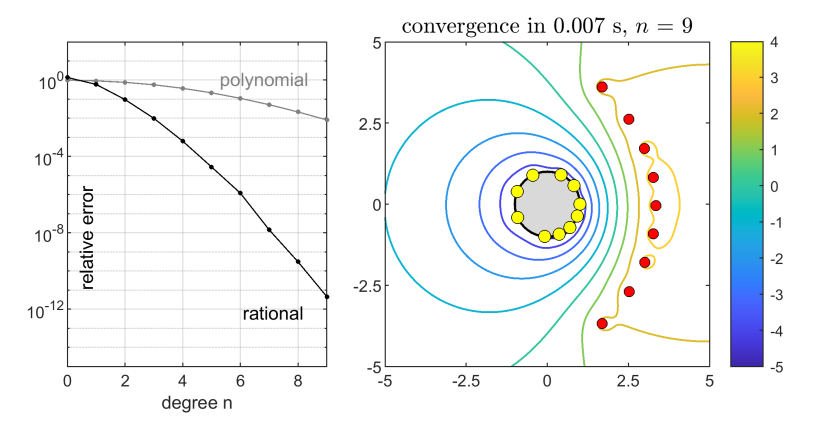


Figure 12.1. Approximation of $f(z) = e^{4z}$ on the unit circle. The plot on the left shows superexponential convergence of AAA approximations as a function of degree n down to tolerance 10^{-10} with n=9, with slower superexponential convergence for polynomials. On the right, level curves of the potential function (12.2) for n=9 based on the n+1 AAA support points (yellow dots) and n poles (red dots). With the Hermite integral (12.1), such plots explain at least in part the high accuracy of rational approximants.

What makes rational approximations so powerful, and (12.1) so effective at revealing their power, is that in many situations, ϕ is much smaller at points z on a set Z where f is to be approximated than at points t on the contour Γ . If f is analytic in a neighborhood of Z, so that Z and Γ can be taken to be disjoint, then suitable choices of $\{\zeta_k\}$ and $\{\pi_k\}$ will make $\phi(z)/\phi(t)$ exponentially small as $n \to \infty$, leading to exponential convergence—and AAA reliably finds such choices. If f is entire or meromorphic, or even if it has essential singularities, one is guaranteed superexponential convergence, as mentioned at the end of section 3. These are among the fundamental results that Gonchar, Stahl and others established in the past 50 years. By contrast, polynomials can never converge superexponentially unless f is entire.

AAA offers a beautiful method of illustrating the mathematics of (12.1)–(12.2). At step n, the algorithm has determined n+1 support points (explicitly) and n poles (implicitly). These can be fed into (12.1) and (12.2) to give plots of a kind first published in (Trefethen (2025b)), which the figures of this section are modeled on. In all the experiments here, the relative error tolerance has been set to 10^{-10} rather than the usual 10^{-13} , because we need a few extra digits to play with for a reason to be explained on p. 52.

Consider Figure 12.1, corresponding to approximation of e^{4z} in 100 roots of unity on the unit circle. Accuracy 10^{-10} is achieved at degree n = 9, as

shown in the convergence curve on the left. The curve bends downward, indicating superexponential convergence. The similar curve for polynomial least-squares fitting on the same plot confirms that for this entire function, polynomial approximants also converge superexponentially, though at a lower rate. In the plot on the right, one sees the poles of the degree 9 rational approximant as red dots in the complex plane, lining up along a curve whose asymptotic shape and position as $n \to \infty$ were analysed by Saff and Varga (Saff and Varga (1978)) (for Padé approximation at the origin rather than best approximation on the disk, but the asymptotics will presumably be the same). The 10 AAA support points are plotted as yellow dots on the unit circle, somewhat denser on the right side than the left. Between the poles and the interpolation points, level curves of $|\phi(z)|$ are plotted, with the numbers indicated on the colourbar corresponding to base 10 logarithms of $|\phi(z)|$. One sees that $|\phi(z)|$ decreases exponentially between the poles and the unit disk, implying by (12.1) that |f(z) - r(z)| will be extremely small for any z there.

Images like Figure 12.1, which are easily produced after any AAA computation, explain how a rational approximation achieves its accuracy. It is remarkable how AAA has detected all this structure in the complex plane, though it is just a greedy descent algorithm working with function values at the sample points. Anyone familiar with potential theory will recognise the flavor of these plots. If we think of the yellow dots as positive point charges generating potentials $\log |z - \zeta_k|$ and the red dots as negative point charges with potentials $-\log|z-\pi_k|$, then the level curves are associated equipotential lines, and it is evident that AAA has distributed the points so that the interpolation points lie approximately on a low equipotential curve and the poles on a high one. In other words, the charges lie in an approximately minimal-energy configuration. This is the effect exploited by Gonchar, Stahl and others in their analysis of convergence of approximations as $n \to \infty$. They showed that the solution of a PDE problem involving continuous distributions of signed charges provides rigorous upper bounds on best rational approximation convergence rates in this limit.

All this may seem like a complete story, but it isn't. If we look at the numbers, we see that Figure 12.1 does not give a quantitative explanation of the ten-digit accuracy of this approximation. The colourbar spans just about eight orders of magnitude, not ten, and moreover, digits will be lost in an estimate of (12.1) since this function $f(z) = e^{4z}$ has magnitude as large as 10^4 near the poles. For these reasons, applying (12.1)–(12.2) based on what we see in Figure 12.1 only explains about five of the ten digits of accuracy. From this point of view one would have to explain the other five as a result of cancellation in the integrand of (12.1) along a contour Γ . But why should there be five orders of magnitude of cancellation? It seems strangely fortuitous.

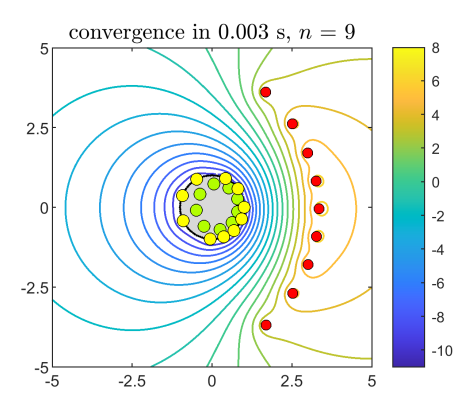


Figure 12.2. Approximation of $f(z) = e^{4z}$ on the unit circle again. Now n more interpolation points have been added to the image, shown as green dots, and the potential function has been approximately squared from (12.2) to (12.3). This roughly doubles the span of amplitudes shown in the colourbar, enabling (12.1) to fully explain the 10-digit accuracy of this approximation.

Happily, there is a modification of (12.1)–(12.2) that changes the figure in such a way as to yield a wider range of contour levels and thereby a quantitative as well as qualitative explanation. We mentioned that the integral (12.1) is valid for any choice of n+1 interpolation points $\{\zeta_k\}$, but in many best and near-best approximations, the total number of such points in the approximation region of interest will actually be 2n+1. (One familiar case of this is in real approximation on an interval, with equioscillation generically between 2n+2 extrema. Another is in degree n Padé approximation, where the approximant interpolates the function generically to order 2n+1.) In this case, (12.1) remains valid with a new and stronger definition of ϕ based on all the interpolation points $\zeta_0, \ldots, \zeta_{2n}$,

$$\phi(z) = \prod_{k=0}^{2n} (z - \zeta_k) / \prod_{k=1}^{n} (z - \pi_k)^2.$$
 (12.3)

Roughly speaking, both the numerator and the denominator of (12.2) have been squared! Figure 12.1 improves to Figure 12.2, with green dots now added to show the n=9 additional points of interpolation of this approximation in the unit disk. Notice how much denser the contour lines are than before. Now the contours span a range of 14 orders of magnitude, enough to explain how the approximation achieved 10 digits of accuracy, not just 5.

We learned of the improvement $(12.2)\rightarrow(12.3)$ from Maxim Yattselev, whose assistance we gratefully acknowledge (private communication, May 2025). We state the result as a theorem, a special case of (Stahl 1989,

Lemma 2). This result has roots in earlier work by Gonchar for approximation of Markov functions (Gonchar (1975), Gonchar and López Lagomasino (1978)).

Theorem 12.1. Hermite integral formula with 2n+1 interpolation points. Let f be analytic in the closure of a Jordan region Ω bounded by a Jordan contour Γ , and let the degree n rational function r(z) interpolate f in 2n+1 points $\zeta_0, \ldots, \zeta_{2n} \in \Omega$. Let r have n finite poles π_1, \ldots, π_n , and define

$$\phi(z) = \prod_{k=0}^{2n} (z - \zeta_k) / \prod_{k=1}^{n} (z - \pi_k)^2.$$
 (12.4)

Then for any $z \in \Omega$,

$$f(z) - r(z) = \frac{1}{2\pi i} \int_{\Gamma} \frac{\phi(z)}{\phi(t)} \frac{f(t)}{t - z} dt.$$
 (12.5)

The poles and interpolation points need not be simple. For simplicity, we have limited the theorem statement to the generic case of greatest interest, but it can be generalised to poles at ∞ and numbers of interpolation points greater than or less than 2n+1. In fact, the denominator of (12.4) does not have to be the square of that of (12.2); it can be the denominator of (12.2) multiplied by any polynomial in z of degree n.

This "factor of 2" improvement from (12.2) to (12.3) was investigated by Stahl in the paper just cited and others and is the subject of what Rakhmanov calls the *Gonchar-Stahl* ρ^2 -theorem; see (Rakhmanov (2016)) and (Trefethen 2023, sec. 7.5). Not all best or near-best rational approximations have the necessary doubling of the number of interpolation points for this to apply, but in practice, many do.

Producing a plot like Figure 12.1 is elementary once one has calculated the support points and poles of a AAA approximation, but how did we find the additional interpolation points—the green dots—needed to produce Figure 12.2? Following the zerofinding ideas of section 4, the method we have used is to invoke AAA a second time to approximate the function f(z) - r(z) by a new rational function q(z), and take the zeros of q as numerically computed interpolation points of f and r. This is where the tolerance 10^{-10} mentioned above comes into play. We compute r with that tolerance, and then q with a tolerance of just 10^{-3} on the theory that f - r will have low relative accuracy since it is smaller by a factor of 10^{10} than f and r individually. This combination seems to reliably give us the desired plots, although we have not investigated the tolerances carefully.

Figures 12.3–12.5 show three more examples, with some associated convergence rate results for various classes of approximations stated in the captions; recall the last paragraph of section 3. An indication of the im-

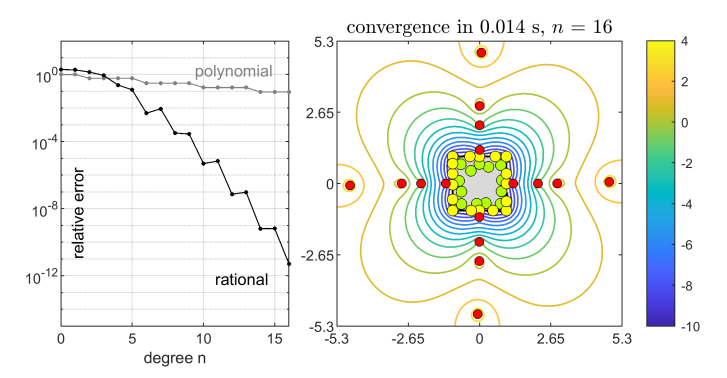


Figure 12.3. Approximation of $f(z) = \tan(z^2)$ on $[-1, 1]^2$. For a meromorphic function like this, polynomial approximations converge exponentially whereas rational approximations converge superexponentially.

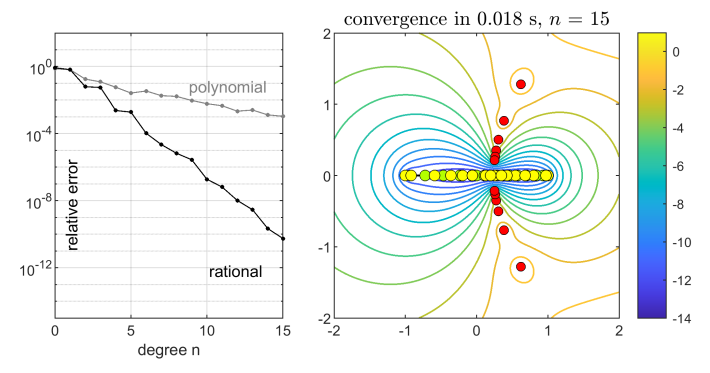


Figure 12.4. Approximation of $f(z) = \sqrt{1 + 25(z - 0.25)^2}$ on [-1, 1]. For any function like this with branch points, both polynomial and rational approximations converge exponentially.

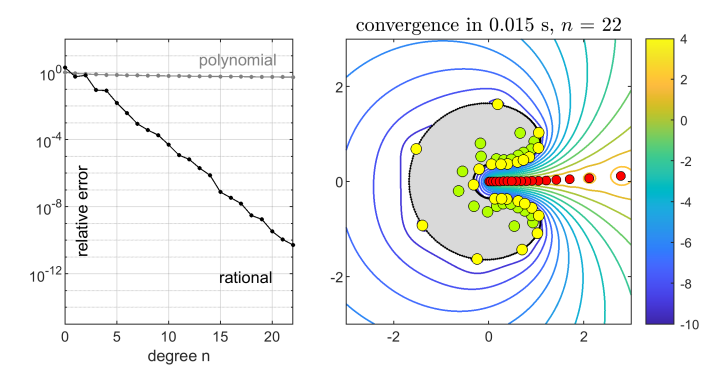


Figure 12.5. Approximation of $f(z) = \log(-z)$ on a nonconvex region. Both polynomial and rational functions converge exponentially, but at vastly different rates (Trefethen (2024)).

Table 12.1. Degrees of the rational approximations in the examples of Figures 12.2–12.5, and for comparison, rough estimates of the degrees that would be needed for polynomial approximations of the same accuracy.

Figure	Rational degree	Polynomial degree
12.2	7	80
12.3	16	200
12.4	15	120
12.5	22	10,000

plications of such results for rational vs. polynomial approximation degrees can be seen in Table 12.1.

We have looked at hundreds of plots of rational approximations in the past few years, perhaps thousands, and we note that it often seems possible to classify the poles loosely into four categories. Sometimes, as in Figure 12.2, poles appear "just" for reasons of approximation—we might call these approximation poles. Sometimes, as in Figure 12.3, they match poles of the function being approximated—pole poles. Sometimes, as in Figures 12.4 and 12.5, they delineate branch cuts—branch cut poles. Finally there are spurious poles (Froissart poles?) with negligible residues, often a result of rounding errors or other noise (Stahl (1998)). We have not attempted to make such distinctions precise, and of course, the boundaries between the cases may be fuzzy.

13. Solution of ODEs and PDEs

We mentioned at the beginning that polynomials are the starting point for algorithms in most areas of numerical analysis, but that rational functions may bring advantages, and the previous sections have shown examples in many areas. Now we turn to the solution of ODEs and PDEs. Our view is that here, too, rational functions should lead to new methods that are more powerful for certain problems, notably those with singularities or near-singularities. For example, Chebfun solves smooth ODE boundary-value problems by means of polynomial and piecewise polynomial spectral approximations. We are often asked, when is "Ratfun" coming along to solve more difficult problems?

So far, there is no Ratfun. Chebfun-style automated rational approximation methods for ODEs and PDEs have not been developed, but we hope that they will be in the next few years. In this section we outline what we think may be possible.

To start with ODEs, the natural terrain of rational approximation methods will be problems with singularities or near-singularities, such as the stiff

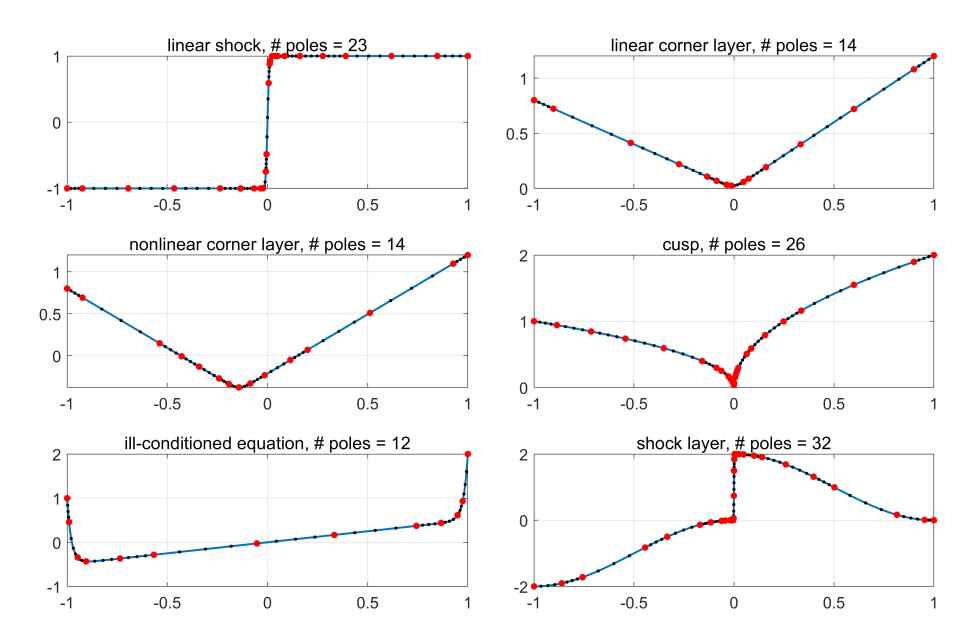


Figure 13.1. Solutions to the six singularly perturbed ODE boundary-value problems from Examples 91–96 of Appendix B of (Trefethen *et al.* (2018)) approximated to 6-digit accuracy by AAA rational approximations computed by the continuum AAA algorithm of section 30. Red dots mark adaptively determined support points, and black dots mark additional sample points. Despite the narrow layers, the fits are of low degrees, suggesting a strong potential for efficient rational function solution of difficult ODEs if a suitable algorithm can be developed.

boundary-value problems treated in (Hemker (1977)) and (Lee and Greengard (1997)). Three examples from each of these sources can be found as Examples 91–96 of Appendix B of (Trefethen, Birkisson and Driscoll (2018)). The solutions to these six BVPs, all involving boundary or interior layers that can be made more challenging by decreasing further a small parameter, are plotted in Figure 13.1.

The computations for Figure 13.1 are as follows. First the BVPs are solved in Chebfun with these commands, which the reader can decode to see the precise specifications of the BVPs:

```
% Example 91: Linear shock
L = chebop([-1 0 1]);
L.op = @(x,y) 1e-4*diff(y,2)+2*x*diff(y);
L.lbc =-1; L.rbc = 1;
y = L\0;
```

```
% Example 92: Linear corner layer
L = chebop(@(x,y) 1e-3*diff(y,2)+x*diff(y)-y);
L.1bc = .8; L.rbc = 1.2;
y = L \setminus 0;
% Example 93: Nonlinear corner layer
N = chebop(@(y) 0.05*diff(y,2)+diff(y)^2-1);
N.lbc = .8; N.rbc = 1.2;
y = N \setminus 1;
% Example 94: Cusp
L = chebop([-1 \ 0 \ 1]);
L.op = @(x,y) 1e-6*diff(y,2)+x*diff(y)-.5*y;
L.lbc = 1; L.rbc = 2;
y = L \setminus 0;
% Example 95: Ill-conditioned equation
L = chebop(-1,1);
L.op = @(x,y) 0.02*diff(y,2)-x*diff(y)+y;
L.lbc = 1; L.rbc = 2;
y = L \setminus 0;
% Example 96: Shock layer
L = chebop([-1 \ 0 \ 1]);
L.op = @(x,y) 1e-6*diff(y,2)+x*diff(y);
L.1bc = -2; L.rbc = 0;
f = chebfun(@(x)-1e-6*pi^2*cos(pi*x)-pi*x*sin(pi*x));
y = L \setminus f;
```

Then each solution is approximated by a rational function using the continuum AAA code aaax to be described in section 30 by executing

```
deg = 150; nlawson = 0; tol = 1e-6; plt = 0;
r = aaax(y,deg,nlawson,tol,plt);
```

Finally, the approximation is plotted with

```
xx = linspace(-1,1,2000)';
plot(xx,r(xx))
```

The support points of the rational approximation are marked by red dots, and the additional sample points, three between each pair of support points, are marked by small black dots.

These computations show that rational functions computed by AAA can represent solutions to certain difficult ODE BVPs very efficiently. The question is, how might AAA be used to actually compute such solutions, rather than just represent them after they have been computed by another tool? Our vision for an algorithm of this kind is inspired by an analogy with

Chebfun. In its early years, Chebfun just approximated given functions by polynomials using the following procedure: interpolate the function on a 17-point Chebyshev grid, then a 33-point grid, then a 65-point grid, and so on until the Chebyshev series of the interpolant goes down to machine precision. Then in (Driscoll, Bornemann and Trefethen (2008)) a method was introduced for generalising this to solve ODE BVPs. Proceed just as before, but instead of sampling a fixed function on each grid, compute a function on each grid by a Chebyshev spectral method. As before, stop when the grid is fine enough that the solution is well resolved and one is happy with the resulting Chebyshev series. This is the basis of all Chebfun solution of ODE BVPs. See Appendix A of (Trefethen et al. (2018)).

We suggest that a similar approach might work for solving ODE BVPs such as those of Figure 13.1 by rational approximation. Instead of Chebyshev grids of growing sizes, one might make use of adaptively growing grids of support points and sample points following the pattern of the continuum AAA algorithm to be described in section 30. Perhaps such a method could be based on finding a way to linearise the barycentric representation at each step so that an appropriate residual could be minimised in a linear least-squares problem. As happened with Chebfun, such an algorithm might be developed first for linear problems and then extended to nonlinear ones via iteration. At the moment, all this is entirely speculative.

Rational functions have been advocated in the past for solving ODEs, for example in (Berrut and Mittelmann (2002, 2004)). What is potentially new now is the availability of the AAA algorithm to make the rational approximations much more flexible and closer to optimal.

Moving from ODEs to PDEs, a setting in which univariate rational approximations might be effective is in problems in one space and one time variable with shocks, blowups, or other singular or nearly-singular behaviour. Previously, rational function methods for such problems have been developed based on various strategies (Baltensperger and Berrut (2001), Berrut and Baltensperger (2001)). In (Tee and Trefethen (2006)) and (Hale and Tee (2009)), conformal maps were used to push singularities in the complex plane further from the computational axis, yielding solutions to difficult problems on grids with just a few points. In this method, positions of singularities are estimated numerically by Padé or Chebyshev-Padé approximation, and then a highly nonuniform grid is established by means of an explicit conformal map, leading to very accurate spectral discretisation despite the singularities. The new vision is to find a way to achieve all this simply by rational approximation, without the need for conformal maps. In terms of Ratfun, we are looking for an analogue of Chebfun pde15s as opposed to Chebfun backslash. Again our view is that something should be possible, but algorithms have not vet been developed.

14. Extending ODEs and PDEs into \mathbb{C}

Often an ODE or PDE or related problem is posed in real variables, yet for one reason or another, there is interest in determining how the solution behaves for complex arguments. In particular, many authors have investigated complex singularities of problems which may be singularity-free for real arguments. This kind of analysis has been pursued for the Lorenz equations (Tabor and Weiss (1981), Viswanath and Sahutoglu (2010)), the Burgers equation (Bessis and Fournier (1990), Sulem, Sulem and Frisch (1983), VandenHeuvel, Lustri, King, Turner and McCue (2023), Weideman (2003, 2022)), the nonlinear Schrödinger equation (Sulem et al. (1983)), the Korteweg-de Vries equation (Kruskal (1974), Weideman (2003, 2022), McCue, Lustri, VandenHeuvel, Zhang, King and Chapman (2025)), water waves (Baker, Jr. and Xie (2011), Crew and Trinh (2016), Lushnikov, Dyachenko and Silantyev (2017), Lustri and Chapman (2013)), vortex sheets and layers (Caffisch, Gargano, Sammartino and Sciacca (2022), Caffisch and Orellana (1989)), Rayleigh-Taylor flow (Tanveer (1993b)), Hele-Shaw flow (Tanveer (1993a)) and the Euler and Navier-Stokes equations (Siegel and Caffisch (2009), Caffisch, Gargano, Sammartino and Sciacca (2015)).

The direct approach to such analysis is simply to extend whatever analytic or numerical method is being used for real variables to complex variables. In this fashion one can explore solutions of problems in complex space and/or time with, typically, comparable accuracy to what one has in the real case. For obtaining particular values at particular points, this can be an excellent strategy. The drawback is that for a more global picture, for example if one simply wants to know where singularities may be located, the work involved may be considerable.

This leads to the alternative idea: use numerical analytic continuation to move from real to complex variables. With AAA approximation this can be remarkably speedy and informative, even if it cannot match the precise information of a true complex calculation. Numerical analytic continuation has also been used in this manner for computational as opposed to analytical purposes, to find nearby singularities of a numerically computed function in order to construct a function-adapted computational grid (Tee and Trefethen (2006), Weideman (2003)).

There are just a handful of publications so far that have used AAA for extending differential equations into the complex plane: see (Deng and Lustri (2023), Trefethen (2023), VandenHeuvel et al. (2023), Weideman (2022)). More will presumably appear in the years to come, as some of the older literature relies on less effective methods such as Fourier series. More recently, some authors have used rational functions in the form of Fourier-Padé approximations (Baker, Jr. and Graves-Morris (1999)) (sometimes called

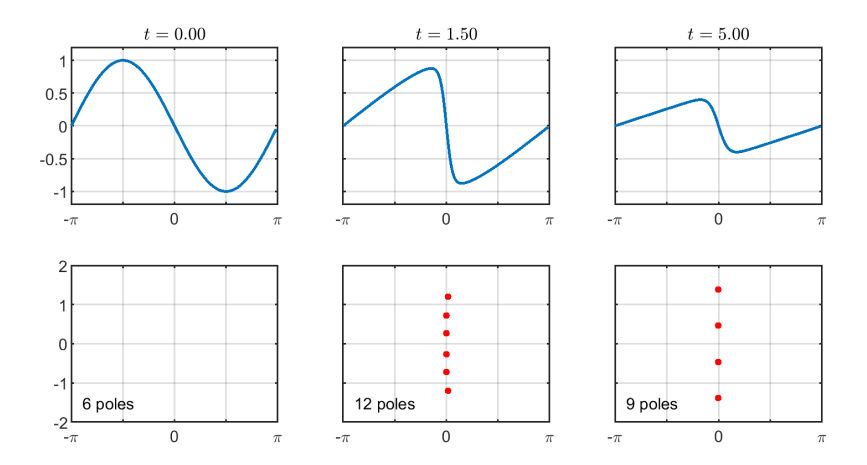


Figure 14.1. Solutions to the periodic Burgers equation (14.1) at three times t together with poles of associated AAA approximations in the complex x-plane. AAA is fast enough that it is feasible to compute poles this way at every time step of a simulation.

just Padé approximations—see section 31), and this can be quite effective (Caflisch *et al.* (2015), Weideman (2003, 2022)).

We will show two examples of AAA computations, both adapted from (Trefethen (2023)), which differ mathematically in an interesting way.

The first example, illustrated in Figure 14.1, concerns the viscous Burgers equation on a periodic domain:

$$u_t + uu_x = \nu u_{xx}, \quad u(-\pi) = u(\pi), \quad u_x(-\pi) = u_x(\pi). \tag{14.1}$$

With $\nu=0.075$ and initial condition $u(x,0)=-\sin(x)$, the upper row of the figure shows the numerically computed solution at times $t=0,\,1.5,\,$ and 5, revealing an approximate shock that steepens up at first and then loses amplitude because of dissipation. Following (Weideman (2022)), the lower row shows poles of a AAA approximation to each solution in a nearby region of the complex plane. (Ordinary AAA approximation was used, though periodic AAA would also be applicable here; see section 31.) It is known that for this problem the exact solution has an infinite train of poles for each t>0 that move toward the real axis at first, and then move out again as the amplitude dissipates. Indeed, this problem has the Painlevé property: the solutions are meromorphic throughout the complex x-plane, so the only singularities are poles (VandenHeuvel et al. (2023)).

The AAA computation of poles in Figure 14.1 is quite accurate for the poles near the real axis and extremely fast, so fast that it is easy to compute poles at every time step in a numerical simulation. The same would be

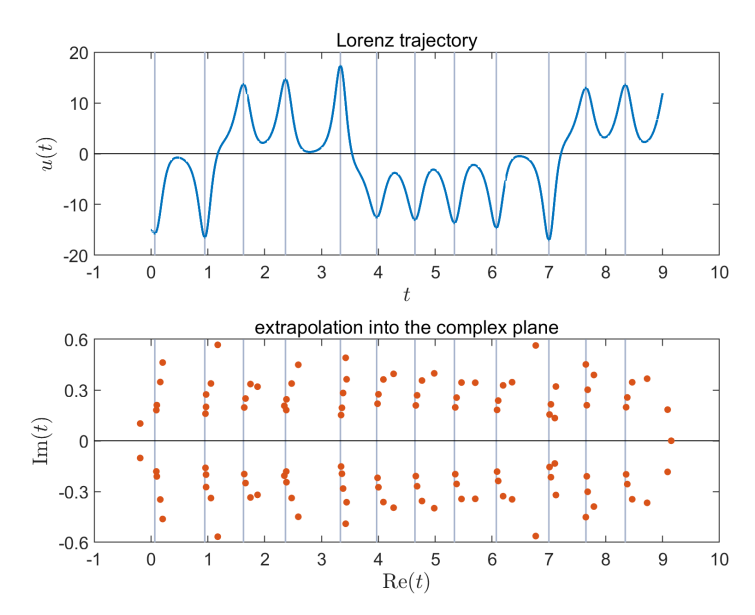


Figure 14.2. A trajectory u(t) of the Lorenz equations together with AAA poles in the complex t-plane. The poles line up along approximate branch cuts.

true for many other problems, indicating the exceptional convenience of estimating complex behaviour by this method.

Our second example, illustrated in Figure 14.2, shows a short stretch of a trajectory u(t) of the Lorenz equations (one of the three components u, v, w in a numerical simulation) together with, again, numerically computed poles in the complex plane (now the complex t-plane rather than x-plane). Once more AAA makes it easy to calculate such estimates, and the vertical gray lines show how the estimated poles match the local extrema of the trajectory. This problem has fundamentally different behaviour from the Burgers example, however. Here, it is known that the analytic singularities are not poles but branch points (Tabor and Weiss (1981), Viswanath and Sahutoglu (2010)), and what Figure 14.2 is displaying are trains of poles that approximate branch cuts near those points, in the fashion we have seen in the figures of sections 11 and 12.

The distinction between poles and branch points, and between resolution of exact singularities and mere function approximation by convenient poles, seems unambiguous in principle but may be difficult in practice. The singularities of a complex function near the x-axis will usually have a strong effect on its behaviour there, but singularities further out may have very little influence. Although mathematically well-defined in the analysis of an exactly specified problem, such distant singularities may change utterly

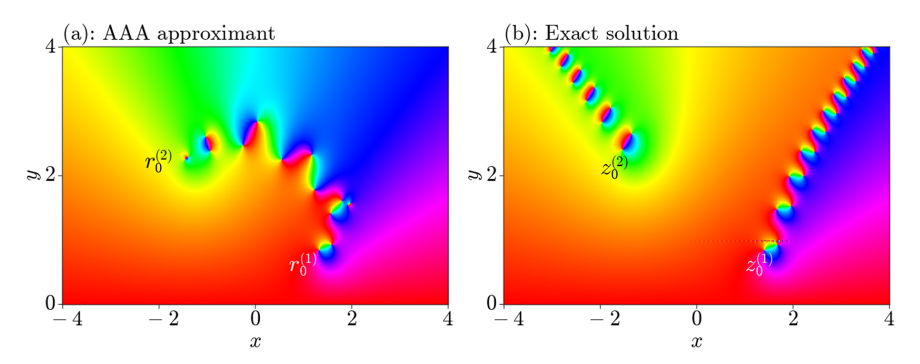


Figure 14.3. A figure from (VandenHeuvel et al. (2023)) comparing the exact pole structure of a Burgers solution with its AAA approximation from data on the real axis. The poles closest to the axis are accurately captured, but not the poles further out. (Note that the real and imaginary axes in these images are not equally scaled.)

when the problem is slightly modified. Their locations may be exponentially sensitive to perturbations, rendering their mathematical significance questionable. We close this section with a beautiful figure from (VandenHeuvel et al. (2023)) showing a pronounced discrepancy between the exactly known poles of a certain Burgers problem and those computed by a AAA approximation. The two sets of poles are very different beyond the pair closest to the real axis, yet they correspond to functions that agree to 10^{-13} on the real axis.

15. Multivariate analytic continuation

Many applications involve functions of more than one variable that one would like to extend beyond the domain where they are known a priori. In a typical case one might have a real analytic bivariate or trivariate function f(x,y) or f(x,y,z) given in a domain in \mathbb{R}^2 or \mathbb{R}^3 , and one might wish to extend it to real arguments outside this domain. "Real analytic" is essentially the same as analytic, being defined by the local convergence of Taylor series (here these would be bivariate or trivariate series, which would necessarily also converge in regions of \mathbb{C}^2 or \mathbb{C}^3). What is distinctive about a function being real as opposed to complex analytic is only that the focus is on real values of the function taken on a real domain.

For multivariate problems, no algorithm is known with the "magic" nearbest approximation behaviour of AAA in the univariate case. At least that is how it appears if we consider the example

$$f(x,y) = \sqrt{x^2 + y^2}, \quad -1 \le x, y \le 1.$$
 (15.1)

This function is real analytic for all $(x,y) \in \mathbb{R}^2$ except for the singularity at

(x,y) = (0,0). There exist good low-degree bivariate rational approximations of it, like

$$r_0(x,y) = 0.707, \quad r_2(x,y) = \frac{0.0618 + 2.257(x^2 + y^2)}{1 + 1.191(x^2 + y^2)},$$
 (15.2)

with maximum errors 0.707 and 0.062 on the given domain, respectively, and

$$r_4(x,y) = \frac{0.0120 + 11.848(x^2 + y^2) + 49.450(x^2 + y^2)^2}{1 + 40.910(x^2 + y^2) + 18.788(x^2 + y^2)^2},$$
 (15.3)

with maximum error 0.012. The first image of Figure 15.1 shows level curves of (15.1), which are equally spaced concentric circles since f is the 2-norm of the vector $(x, y)^T$. The next two images show the corresponding contours for r_2 and r_4 , the latter almost indistinguishable from the contours for f.

The trouble is, no general algorithm is known for finding near-best approximations like these. In particular, no true multivariate AAA algorithm has yet been discovered—seemingly because there is no multivariate barycentric formula applicable with arbitrary support points. (The paper (Rodriguez, Balicki and Gugercin (2023)) introduces a bivariate approximation algorithm called p-AAA with support points restricted to a tensor product grid. For numerical multivariate approximation by other methods, see (Austin, Krishnamoorthy, Leyffer, Mrenna, Müller and Schulz (2021)).) To find the approximations (15.2) and (15.3), we did not use bivariate numerical approximation but exploited the fact that this example can be reduced to a univariate problem of approximation of \sqrt{s} with $s = x^2 + y^2$ for nonnegative values of s. (The reduction is not exact, since the domain $-1 \le x, y \le 1$ is not axisymmetric.) This is Newman's problem (Newman (1964)), for which root-exponential convergence as a function of the degree has been known since 1964. To find the coefficients of r_4 in (15.3), for example, we computed minimax approximations of \sqrt{s} for $s \in [0,2]$ with the Chebfun commands

```
s = chebfun('s',[0 2]);
[p,q,r,err] = minimax(sqrt(s),2,2);
pcoeffs = poly(p)/q(0), qcoeffs = poly(q)/q(0)
```

Is it reasonable to hope for a multivariate algorithm that could find approximations like (15.2) and (15.3) as easily as AAA finds approximations in a single variable? We do not know, and we regard this as an important open problem. A pessimist (or an expert in several complex variables) may note that the singularity of f that is just the point (0,0) for $(x,y) \in \mathbb{R}^2$ becomes the pair of planes $y = \pm ix$ for $(x,y) \in \mathbb{C}^2$ (compare (Boullé, Herremans and Huybrechs (2024))). An optimist may counter that if good approximations exist, there ought to be ways to find them.

In the absence of a true multivariate AAA algorithm, an easy alternative

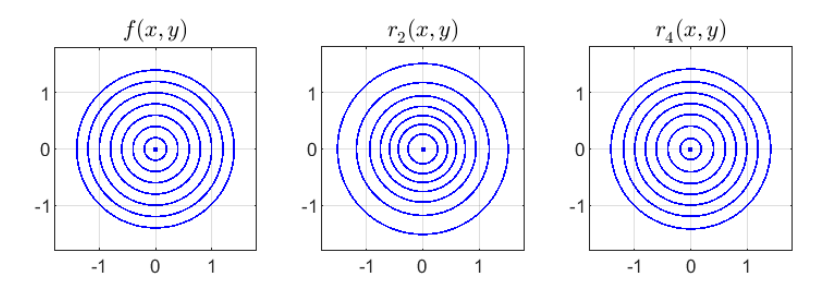


Figure 15.1. At the left, contours $|f(x,y)| = 0, 0.2, 0.4, \dots, 1.4$ of the bivariate function (15.1). The other two images show the same contours for the degree 2 and 4 rational approximations (15.2) and (15.3). No numerical approximation algorithm is known for finding near-best multivariate rational approximations like these.

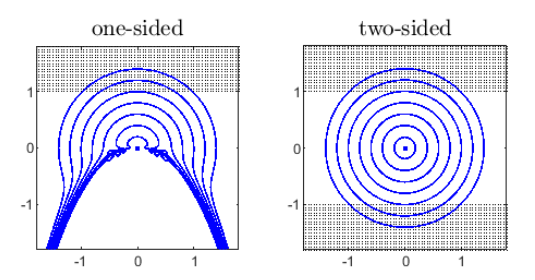


Figure 15.2. Bivariate approximation of (15.1) by AAA approximation along vertical lines. On the left, approximation along vertical lines with data samples just above the singularity, marked by black dots. On the right, approximation along vertical lines with samples on both sides of the singularity.

appears to be the method introduced in (Trefethen (2023)): use a collection of univariate AAA approximations, each applied on a different line or circle or other analytic arc. For example, Figure 15.2 shows the same problem as in Figure 15.1, but now with f(x,y) approximated numerically along vertical lines. There are 73 vertical lines, each with 73 sample points. In the left image, the top 17 sample points of each vertical line (i.e., those with $y \geq 1$) are used to construct a AAA approximant, and the global result is plotted. The computation time for all 73 approximations is small, about 1/3 seconds on our laptop. In the right image a much better result is obtained from AAA sample data both above and below the singularity, the 34 samples with $|y| \geq 1$.

Since the function (15.1) is elementary, one can understand these approximations in detail. Along the vertical line in Figure 15.2 associated with a

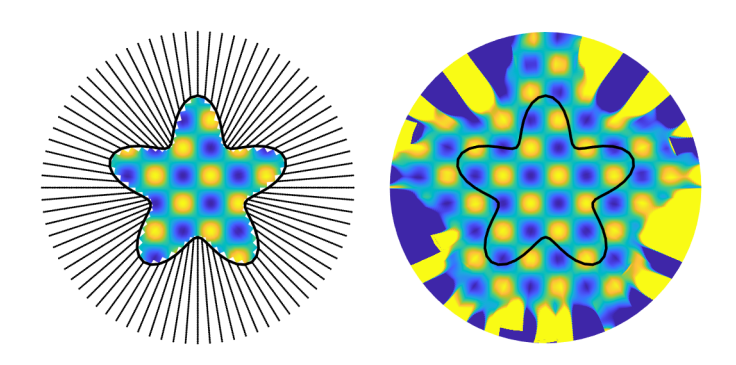


Figure 15.3. Reproduction of a figure from (Trefethen (2023)) showing continuation of a smooth function across a boundary by univariate AAA approximation on 60 radial lines. As in section 10, about one wavelength of accurate extension is achieved.

particular value $x = x_0$, the function being approximated is

$$f_{x_0}(y) = \sqrt{x_0^2 + y^2}.$$

For $x_0 = 0$ this becomes simply $f_0(y) = |y|$, whose rational approximants are easy to understand—it will be r(y) = y exactly in the one-sided case and a good approximation $r(y) \approx |y|$ in the two-sided case (an approximation of sign(x) flavor with a branch cut, to be discussed in section 20).

In the literature of computational methods for PDEs, multivariate analytic continuation is considered in the context of what is called *function extension*. Here, for various algorithmic reasons, it is desired to numerically continue a multivariate function smoothly across a boundary. Accuracy of analytic continuation may not be the goal so much as smoothness. Some contributions in this area include (Adcock and Huybrechs (2019), Boyd (2002), Bruno and Paul (2022), Epstein, Fryklund and Jiang (2025), Fryklund, Lehto and Tornberg (2018), Larsson, Shcherbakov and Heryudono (2017)).

Figure 15.3, which reproduces part of a figure from (Trefethen (2023)), illustrates a computation of this kind. Here AAA approximations have been computed along each of 80 radial lines, and the resulting data on a polar grid has then been fed to the MATLAB contour plotter. As discussed in section 10, about one wavelength of successful extension is evidently achieved, with the number of accurate digits diminishing from 13 on the inner boundary to 0 at the edge.

So far as we are aware, the other methods for function extension proposed in the literature are not as accurate as the AAA approach. For example, figures in (Fryklund *et al.* (2018)) and (Epstein *et al.* (2025)) suggest about

half a wavelength of continuation rather than one wavelength. On the other hand, these methods have advantages of speed, simplicity and robustness related to their lack of dependence on a process as nonlinear as rational approximation. For example, the method of (Epstein et al. (2025)) involves an explicit formula that is the same "in all directions" and therefore produces approximations that are continuous, indeed analytic under appropriate hypotheses, with respect to the direction tangential to the boundary. The AAA approach, by contrast, computes a different approximation along each line and does not guarantee even tangential continuity, let alone smoothness, though it often gives numerical continuity to many digits of accuracy.

16. Computing complex resonances

This section presents an application of AAA approximation that was introduced in (Bruno, Santana and Trefethen (submitted)); a similar method was proposed in (Betz, Hammerschmidt, Zschiedrich, Burger and Binkowski (2024)) and (Binkowski, Betz, Hammerschmidt, Zschiedrich and Burger (2025)). One can regard this as a special case of the linear and nonlinear eigenvalue problems to be discussed in the next two sections.

The physical problem is oscillation in a 2D or 3D cavity; in the 2D case one often speaks of a "drum." In the standard and most familiar setting, the cavity is a closed planar domain bounded by a curve Γ or a closed spatial domain bounded by a surface Γ , and we seek eigenvalues and eigenfunctions for Laplace oscillations in this domain:

$$\Delta u + \kappa^2 u = 0, \quad u = 0 \text{ on } \Gamma.$$
 (16.1)

This is a self-adjoint problem, with negative real eigenvalues $-\kappa^2$ corresponding to real frequencies κ .

AAA can be applied to this well-known problem, as is shown in section 26 and in Figures 2 and 6 of (Bruno et al. (submitted)), but this section is devoted to a variation where AAA comes especially into its own: when the boundary Γ is not fully closed and the eigenvalues become slightly complex. Various terms are in use for such problems, including complex resonances, scattering resonances and scattering poles; see (Dyatlov and Zworski (2019)) for the mathematical foundations. Figure 16.1 shows the simplest possible example, a cavity bounded by a curve Γ consisting of the unit circle with a gap in it, here a gap of angle $\pi/8$. As suggested in the figure, we can imagine that this resonator will have approximate eigenfunctions that oscillate like those of a closed circular cavity but lose amplitude at a slow exponential rate as energy is radiated out through the gap and away to infinity.

Equation (16.1) is still an eigenvalue problem, but no longer self-adjoint, since energy is absorbed at ∞ . One way to interpret it as a scattering problem might be as follows. For each κ , let $G(\kappa)$ be the linear operator that maps an incident wave at frequency κ that hits Γ to the corresponding

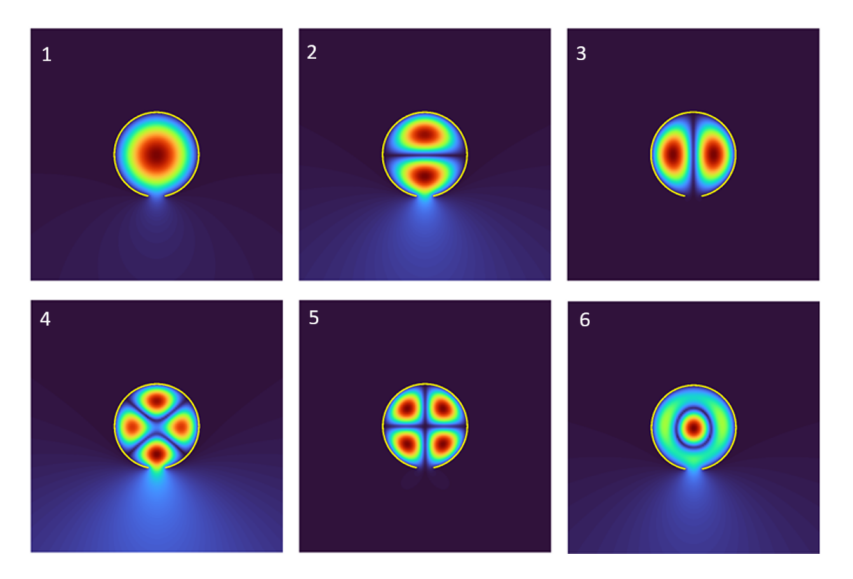


Figure 16.1. Images from (Bruno *et al.* (submitted)) of the first six complex resonances in the unit disk with a gap in the boundary of angle $\pi/8$. Images 2–3 and 4–5 are near-degenerate pairs that become exactly degenerate in the limit of zero gap size.

wave at frequency κ scattered by Γ . If κ is near a resonant frequency, $G(\kappa)$ will be large in norm, mapping incident waves at this frequency to large scattered responses. There will be no real values of κ at which the size of $G(\kappa)$ is infinite, for that would correspond to nonzero radiation with zero incident energy. However, there can be complex eigenvalues. A complex value of κ with a small imaginary part will correspond to an oscillation at the frequency $\text{Re}(\kappa)$ with exponential decay rate $\text{Im}(\kappa)$. If $\text{Im}(\kappa)$ matches the decay rate associated with radiation of energy, then $G(\kappa)$ will be infinite, mapping an incident wave of amplitude zero to a finite response, oscillating and decaying with time.

AAA works with scalar functions, not operators. To turn the concept just described into a scalar problem, we could make the input a scalar amplitude by fixing the shape of the incident wave in some arbitrary fashion: say, a plane wave of frequency κ hitting Γ from a prescribed angle. Likewise, we could make the output a scalar by sampling the scattered wave at an arbitrary point $\vec{x}_0 = (x_0, y_0)$. The complex eigenvalue problem becomes: find a complex frequency κ at which the scattered amplitude at \vec{x}_0 is infinitely larger than the incident amplitude. We might be unlucky, if \vec{x}_0 is situated at a point where the scattered wave has amplitude zero, but if \vec{x}_0 is chosen at random, the probability of this will be zero, and under reasonable assump-

tions the probability of losing d digits of accuracy to a near-zero sampling point can be expected to be of order 10^{-d} .

This is the idea of the method presented in (Bruno et al. (submitted)), though the details are different. The scattering problem is formulated in terms of an integral operator F(k) that maps a distribution on Γ of singular Hankel functions for frequency κ to the outgoing wave field on Γ generated by these Hankel functions. If the wave field can be zero on Γ with a nonzero distribution of Hankel functions, then κ is a complex eigenvalue. So we are looking for values of κ for which $F(\kappa)$ is singular, or equivalently, for which $(F(\kappa))^{-1}$ is unbounded. We scalarise the problem for AAA by considering

$$f(\kappa) = u^*(F(\kappa))^{-1}v, \tag{16.2}$$

where u and v are a pair of nonzero functions fixed at random (independently of κ). We speak of (16.2) as a randomly scalarised integral operator.

What's needed is to find poles of $f(\kappa)$, and AAA does this just as in section 4, by computing approximations $r(\kappa) \approx f(\kappa)$. The most straightforward way to proceed is to sample $f(\kappa)$ at a number of real frequencies κ . Each sample evaluation will require the numerical solution of an integral equation. Then we construct the approximation $r(\kappa)$ and consider poles of $r(\kappa)$ near the sample set, which can be expected to be good approximations to poles of $f(\kappa)$. Details of the integral equation are given in (Bruno et al. (submitted)), and its numerical discretisation comes from (Bruno and Lintner (2012)). The method is fast and accurate, giving eigenvalues reported in (Bruno et al. (submitted)) accurate to 13 digits. Refinements of the method are discussed there involving adaptive sampling of values of κ to zero in on approximate poles as they are identified.

Note that although Figure 16.1 shows a 2D example, nothing in this method is restricted to 2D. For a 3D cavity the discretisation of the integral equation is more complicated, but the AAA approximation is the same.

To eight digits, the complex frequencies associated with Figure 16.1 are as follows. The third column shows the corresponding roots of Bessel functions that are the eigenvalues for the closed unit circle.

Mode	Circle with gap pi/8	Closed circle
1	2.3918509 - 0.0008668i	2.4048256
2 3	3.7858514 - 0.0075513i 3.8315198 - 0.0000008i	3.8317060 same
4 5	5.0664101 - 0.0227539i 5.1345996 - 0.0000118i	5.1356223 same
6	5.4867988 - 0.0108397i	5.5200781

There is some fascinating physics in these numbers, as discussed in (Bruno et al. (submitted)). Note that they are grouped as a singleton, two pairs and another singleton. Figure 16.1 shows that these are associated with a lowest mode that would be radially symmetric if there were no gap, a pair of modes that would be degenerate if there were no gap, a second such near-degenerate pair and then another singleton. The gap in the boundary has broken the degeneracies, and in each pair, we see that the lower-frequency eigenfunction is nonzero near the gap and radiates significantly outside (modes 2 and 4), whereas the higher-frequency eigenfunction is near-zero near the gap and radiates so little that the background appears a uniform deep blue (modes 3 and 5). This is reflected in the eigenvalue imaginary parts being much smaller and the real parts being much closer to the Bessel roots. It is shown numerically in (Bruno et al. (submitted)) based on further AAA computations that if θ is the gap size, the real and imaginary parts of the eigenvalues converge as $\theta \to 0$ at the rates $O(\theta^2)$ and $O(\theta^4)$ for the modes that are nonzero near the gaps, and at the rates $O(\theta^4)$ and $O(\theta^8)$ for the modes that are near zero there. Thus if the gap size in Figure 16.1 were reduced from $\pi/8$ to $\pi/16$, the decay rates for modes 2 and 3 would reduce from $8 \cdot 10^{-3}$ to $5 \cdot 10^{-4}$ and from $8 \cdot 10^{-7}$ to $3 \cdot 10^{-9}$, respectively. Jon Chapman of the University of Oxford (private communication, May 2025) has derived asymptotic formulas for modes 2 and 3 in the table above that match the data beautifully. Chapman finds

$$\frac{\kappa}{\kappa_0} \sim 1 - \frac{\theta^2}{16} - \frac{\theta^4 C}{128\pi} i \pmod{2} \tag{16.3}$$

and

$$\frac{\kappa}{\kappa_0} \sim 1 - \frac{\theta^4}{512} - \frac{\theta^8 C}{2^{17} \pi} i \pmod{3},$$
 (16.4)

where $\kappa_0 \approx 3.8317060$ is the first zero of J_1 and

$$C = \sum_{n=0}^{\infty} \frac{n^2}{|H_n^{(1)}(\kappa_0)|^2},\tag{16.5}$$

with J_1 and $H_n^{(1)}$ denoting the usual Bessel and Hankel functions. All these observations and details have been stimulated by the accurate calculations made possible by AAA.

See (Betz et al. (2024), Binkowski et al. (2025), Bruno et al. (submitted)) for further examples of the use of AAA to calculate complex resonances.

17. Matrix eigenvalue problems

Let A be an $N \times N$ matrix and let I be the $N \times N$ identity. Then

$$R(z) = (zI - A)^{-1}, (17.1)$$

known as the *resolvent* of A (or more properly the negative of the resolvent), is a matrix function of z defined for all $z \in \mathbb{C}$ except the eigenvalues of A, where it is, informally speaking, infinite.

One can consider R(z) as a matrix rational function, but instead let us scalarise it as in (16.2) by multiplying on the left and right by nonzero row and column vectors u^* and v:

$$R(z) = u^* (zI - A)^{-1} v. (17.2)$$

Here u^* and v are fixed, independent of z. This scalarised resolvent is a rational function of degree N. This does not mean that its degree is exactly N; it will be lower if A has any eigenvalues with geometric multiplicity greater than 1, or if u^* or v happen to be orthogonal to one or more left or right eigenvectors of A, respectively. For simplicity, let us suppose that A has distinct eigenvalues and that u^* and v are random vectors with independent entries chosen from a continuous distribution such as the normal distribution. Then with probability 1, R is a rational function of degree exactly N having N simple poles which are the eigenvalues of A. This leads to the possibility that we can find the eigenvalues by calculating a AAA approximation $r \approx R$ based on samples of R(z) at some points z and then calculating the poles of r, as described in section 4.

For example, suppose A is the 20×20 diagonal matrix with diagonal entries $0, 1, \ldots, 19$, which are accordingly its eigenvalues. (The fact that A is diagonal will have little effect on the results, since u and v are random.) Here is a computation of the kind just described based on samples of R at 100 equispaced points on the circle |z|=1.05 in the complex plane. Alternatively, for a real symmetric problem like this, one could use real samples (Austin and Trefethen (2015)).

```
Z = 1.05*exp(2i*pi*(1:100)/100);
N = 20; A = diag(0:N-1); I = eye(N);
rng(1), u = randn(N,1)+1i*randn(N,1);
       v = randn(N,1)+1i*randn(N,1);
R = Q(z) u'*((z*I-A)\v);
for i = 1:length(Z), F(i) = R(Z(i)); end
[",pol] = aaa(F,Z); pol = sort(pol)
pol =
 0.000000000000025 - 0.000000000000008i
 1.99999995063250 - 0.000000443219559i
 3.000344539241449 + 0.000522614895484i
 4.037538715031964 + 0.004841722473988i
 5.079074587752028 + 1.453783302951845i
 8.343483853643621 + 0.565153761906265i
 15.975301039683405 + 0.020589938026920i
```

The two eigenvalues 0 and 1 enclosed by the sample points have been found to 13 digits or more, and the eigenvalues 2, 3, and 4 have been found to about 9, 4 and 2 digits, respectively. After this there are three further poles with less connection to individual eigenvalues. (The nonzero imaginary parts in these numbers result from the fact that aaa.m does not maintain real symmetry, as discussed on p. 7.) The results are similar, just slightly less accurate, if A is made non-normal by the addition of random samples from N(0,1) to its strictly upper-triangular part. If the diagonal matrix experiment is repeated but with dimension 100 or 1000, the results are again not much different, with the number of computed poles increasing in both cases from 8 to 9.

The fact that not all the eigenvalues of A are computed is the very reason why this method may be useful: it can treat matrices of dimensions too large for standard methods such as the QR algorithm. Often A will be a discretisation of a linear operator of infinite dimension. In such cases, a crucial feature of eigenvalue calculation via rational approximation is that attention is concentrated on a particular region of the real line or complex plane. An operator might be discretised by a matrix of dimension 10^6 with eigenvalues widely distributed in $[0, \infty)$, for example. If only the eigenvalues in a subinterval [a, b] are of interest, then it may be possible to determine these at the cost of a few dozen matrix solves, one for each sample point over a set surrounding or approximating [a, b]. These solves are trivially parallelisable.

Figure 17.1 shows an example like the one just displayed, except that A is now the 40401×40401 diagonal matrix whose diagonal entries are the complex integers j + ik, $-100 \le j, k \le 100$. The scalarised resolvent is evaluated at 100 equally spaced points on the circle |z| = 1.75 (easy because of the diagonal structure), and AAA is applied as usual. The rational approximation r(z) has degree 42, and one sees that its poles approximate a number of eigenvalues of A within and near the sample circle, with the approximations inside the circle being accurate to 11 digits or more.

The idea of computing matrix eigenvalues via poles of rational approximations seems to have been first proposed in (Austin et al. (2014)), before the development of AAA. However, there were important contributions in the preceding decade on the related method of computing eigenvalues via discretised contour integrals. This was mainly the work of two schools: Sakurai and his collaborators in Japan (Sakurai and Sugiura (2003)) and Polizzi and his collaborators in Massachusetts, who call their method FEAST (Polizzi (2009), Tang and Polizzi (2014)). An earlier paper by Goedecker preceded both of these contributions (Goedecker (1999)).

To compute eigenvalues by discretised contour integrals, one again starts from the idea of looking for poles of the scalarised resolvent. Mathematically, it turns out that these can be represented in terms of Cauchy integrals

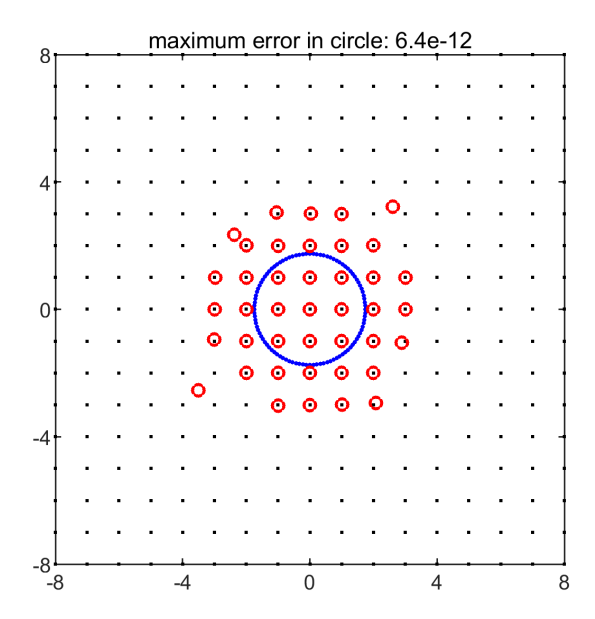


Figure 17.1. AAA calculation of the eigenvalues inside the circle |z| = 1.75 of a 40401×40401 diagonal matrix A with diagonal entries on the integer grid j + ik, $-100 \le j, k \le 100$. Black dots mark the eigenvalues of A in the plotting region and red circles show the poles of the approximation r to the scalarised resolvent. The 100 AAA sample points are marked by blue dots.

of R(z) and related functions over a curve enclosing the desired poles; for details see (Austin *et al.* (2014)) and (Güttel and Tisseur (2017)). When the integrals are discretised, for example by the equispaced trapezoidal rule in the case of a circular contour (Trefethen and Weideman (2014)), one obtains numerical approximations to the poles. The contributions of Sakurai et al. and Polizzi et al. are both of this kind, and have been shown to be effective for large-scale problems. These methods have been used a good deal in computational chemistry and physics.

Although discretised contour integrals and rational approximations may sound quite different, they are related. As we will discuss in section 22, every discrete quadrature formula is equivalent to a rational approximation, with the nodes and weights of the quadrature formula corresponding to the poles and residues of the rational function (Horning and Trefethen (submitted)). So discretised Cauchy integrals give rational approximations too, the difference being that they are constructed by an a priori formula rather than by AAA. AAA approximation is more flexible than contour integration, since the sample points can be distributed arbitrarily rather than having to fit a prescribed configuration, and it will often be more accurate since the approximations are near-best. Discretised Cauchy integrals have the

advantage of a stronger theoretical foundation, since they are built on long-established theorems of complex analysis, but difficulties may arise from the discretisation, especially if there are eigenvalues near the contour. For an analysis of the speed advantage of approximation over discretised Cauchy integrals in a polynomial setting, see Theorem 2.1 and Figure 3 of (Austin et al. (2014)). For a method of eliminating rounding error difficulties in evaluations near poles, see (Horning and Nakatsukasa (2022)).

All these methods tend to lose accuracy when there are multiple eigenvalues in the region of interest. For example, here is what happens when five additional diagonal entries $0.1, 0.2, \ldots, 0.5$ are inserted in the matrix A from the beginning of this section, increasing the dimension from 20 to 25. The accuracy of the inner eigenvalues falls to just 8 or 9 digits.

Similarly, if the 100 sample points of Figure 17.1 with |z| = 1.75 are replaced by 200 sample points with |z| = 2.75, so that there are 21 rather than 9 eigenvalues within the circle, the maximum error deteriorates to $4.4 \cdot 10^{-6}$.

To improve the accuracy in cases like this, three approaches have been considered:

- 1. Zoom in near individual eigenvalues,
- 2. Sketch the resolvent with k > 1 row and column vectors,
- 3. Iterate an approximation or integral as a "filter".

The first method, zooming closer to individual eigenvalues, can be done in many ways and was employed in (Bruno et al. (submitted)) for the resonance calculations described in the last section. The second method amounts to compressing the resolvent (17.1) to a $k \times k$ matrix function instead of a scalar function. This function can then be approximated by the set-valued AAA algorithm to be discussed in section 33, with considerable improvement in accuracy though at the price of working with matrices with k^2 times as

many rows (our experiments, not yet published). The third idea of filtering springs original from the work of Polizzi and his collaborators (Austin and Trefethen (2015), Brennan, Embree and Gugercin (2023), Güttel, Polizzi, Tang and Viaud (2015), Tang and Polizzi (2014), Van Barel and Kravanja (2016)). An investigation of the properties and relative merits of these three possibilities in the context of algorithms based on rational approximation has yet to be carried out.

The discussion continues in the next section.

18. Nonlinear eigenvalue problems

In a nonlinear (matrix) eigenvalue problem the resolvent $(zI-A)^{-1}$ of (17.1) is generalised to $A(z)^{-1}$, where A(z) is an arbitrary (usually meromorphic) $N \times N$ function of z. If $A(\lambda)v = 0$ for some $\lambda \in \mathbb{C}$ and nonzero $v \in \mathbb{C}^N$, then λ is an eigenvalue of the function A(z) and v is a corresponding right eigenvector. Reviews of such problems can be found in (Mehrmann and Voss (2004), Güttel and Tisseur (2017), Brennan *et al.* (2023)), and there is an established test collection of nonlinear eigenvalue problems known as the NLEVP collection (Betcke, Higham, Mehrmann, Schröder and Tisseur (2013)).

Historically, linear and nonlinear eigenvalue problems were discussed separately, with linear cases founded in classical tools of numerical linear algebra such as the QR algorithm. Before the 21st century, there was not very much literature on nonlinear generalisations. When more literature began to appear, the emphasis at first was on tools to approximate nonlinear problems by linear ones. For example, the approach known as linearisation can reduce a nonlinear eigenvalue problem defined by a polynomial $A(z) = A_0 + zA_1 + \cdots + z^kA_k$ to an $N(k+1) \times N(k+1)$ linear eigenvalue problem with block companion matrix structure (Mackey, Mackey, Mehl and Mehrmann (2006)). The special case of quadratic polynomials, k=2, finds many applications (Tisseur and Meerbergen (2001)). More generally, one approach to solving nonlinear eigenvalue problems is to approximate the entries of A(z) by rational functions with shared poles, and then solve a rational eigenvalue problem by a linearisation Lietaert et al. (2022), Güttel, Negri Porzio and Tisseur (2022).

In the era of contour integrals and rational approximations for large-scale computations, however, the distinction between linear and nonlinear has become less important. Early nonlinear contributions based on contour integrals were (Beyn (2012)) and (Asakura, Sakurai, Tadano, Ikegami and Kimura (2009)). Our view is that rational approximation methods for nonlinear eigenvalue problems are essentially the same as for linear ones, since both involve a meromorphic function $A(z)^{-1}$ whose poles one would like to locate. For example, the resonance calculation of section 16 involved

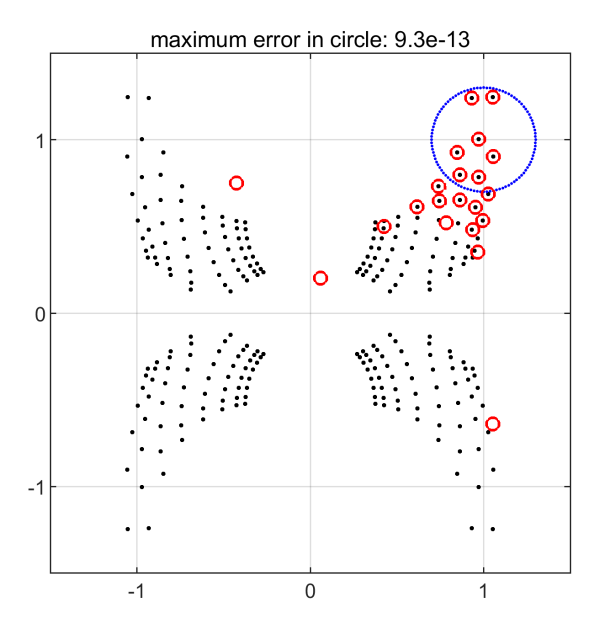


Figure 18.1. Calculation of 7 nonlinear eigenvalues of the "butterfly" problem from the NLEVP collection (Betcke *et al.* (2013)). AAA approximation is based on 100 samples on the circle |z - (1 + i)| = 0.3, shown in blue. Black dots mark all the eigenvalues for this problem, and red circles show the AAA poles.

a matrix A(z) derived by numerical discretisation of an integral equation (Bruno *et al.* (submitted)). Note that A(z) is a linear operator for each z; the nonlinearity lies in the dependence of A(z) on z.

As in the last two sections, a powerful approach to finding the poles of $A(z)^{-1}$ is to work with a scalarised or "sketched" resolvent

$$R(z) = u^* A(z)^{-1} v, (18.1)$$

where $u, v \in \mathbb{C}^N$ are (typically) random vectors; compare (16.2) and (17.2). The scalar function R(z) has the same poles as $A(z)^{-1}$, under the genericity condition that u, v are not orthogonal to the left and right eigenvectors of $A(z)^{-1}$. One can then find the poles of R using AAA. As in the last two sections, it is again straightforward to focus on the eigenvalues in a given domain $\Omega \subseteq \mathbb{C}$ by taking sample points on the boundary of Ω .

As a small-scale example of nonlinear eigenvalue calculation by AAA approximation, Figure 18.1 shows the "butterfly" example from the NLEVP collection, which serves as the logo of that project (Betcke *et al.* (2013)), generated by this code calling the NLEVP software:

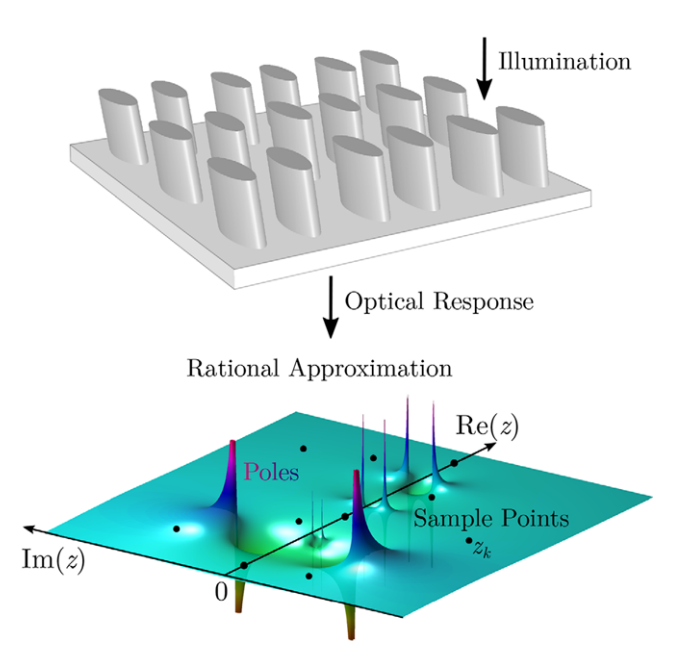


Figure 18.2. Image reproduced from (Betz et al. (2024)) suggesting the use of AAA approximation to calculate nonlinear eigenvalues in photonics applications.

```
e = polyeig(c{:});
plot(e,'.k'), axis equal, hold on
Z = 1+1i + 0.3*exp(2i*pi*(1:300)/300); plot(Z,'.b')
u = randn(64,1); v = randn(64,1);
f = @(z) u'*(A(z)\v);
for k = 1:length(Z), F(k) = f(Z(k)); end
[r,pol] = aaa(F,Z); plot(pol,'or')
```

At the time of this writing, there is not much experience with using AAA to solve nonlinear eigenvalue problems via the poles of the resolvent: the papers available are (Bruno et al. (submitted)), which was highlighted in section 16, and (Betz et al. (2024)) and (Binkowski et al. (2025)), which concern applications in photonics. Figure 18.2 reproduces a figure from (Betz et al. (2024)) suggesting how rational approximation can be used in an application of this kind. In this image, in contrast to the application of section 16, one sees that the eigenvalues and poles lie in complex conjugate pairs. For a recent review of nonhermitian photonics and wave physics, see (Kim, Krasnok and Alù (2025)).

19. Model order reduction

One of the fundamental problems of model order reduction (MOR) is to approximate a transfer function of the form

$$H(s) = C(sE - A)^{-1}B + D, (19.1)$$

usually for s on the imaginary axis. Here A and E are large-scale $N \times N$ real matrices, and $C \in \mathbb{R}^{p \times N}$ and $B \in \mathbb{R}^{N \times m}$ with typically $p, m \ll N$. This results from a linear dynamical system

$$E\dot{x}(t) = Ax(t) + Bu(t),$$

$$y(t) = Cx(t) + Du(t)$$

and taking the Laplace transform (Antoulas et al. 2020, chap. 2).

Here we mainly focus on the Single Input Single Output (SISO) case p = m = 1. The goal of MOR is to approximate H by a simpler function, typically one involving smaller matrices, i.e.,

$$H(s) \approx \hat{H}(s) = \hat{C}(s\hat{E} - \hat{A})^{-1}\hat{B} + \hat{D},$$
 (19.2)

where $\hat{A}, \hat{E} \in \mathbb{R}^{n \times n}$, $\hat{C} \in \mathbb{R}^{p \times n}$ and $\hat{B} \in \mathbb{R}^{n \times m}$, with $n \ll N$. One is usually interested in approximating $H(s) \approx \hat{H}(s)$ on the imaginary axis $s \in i\mathbb{R}$. Since the matrices are real, there is the real symmetry $H(\bar{s}) = \overline{H(s)}$. As discussed in section 2, this symmetry can be imposed exactly in a AAA code, but Chebfun aaa.m does not do this, so we work on a grid of imaginary points symmetric with respect to the real axis, and the resulting approximation is nearly real-symmetric but not exactly.

We have spoken as if the matrices A, B, C, D, E are all known, and this is the classical setting of MOR, but often this is not the case. Often one has an unknown system whose outputs H(s) can be sampled for various values of s, typically on the imaginary axis, and the aim is to extract information about the system from this limited information. In this context the alternative expressions data-driven modelling and Reduced Order Modelling (ROM) are often used. For our purposes in this section, the distinctions between MOR and ROM will not be important.

The transfer function H in (19.1) has pm entries, which are rational functions of degree N sharing the same poles, equal to the eigenvalues of the generalised eigenvalue problem $Ax = \lambda Ex$. The approximation \hat{H} has entries that are rational functions of degree n. Thus approximating H by \hat{H} is an instance of a rational approximation problem, where the original function is also rational (and matrix-valued), but of higher degree.

When p = m = 1, the problem reduces to a scalar rational approximation problem, which AAA is well able to handle. One can sample H at points

on the imaginary axis and find an approximation

$$H(s) \approx \hat{H}(s) = \sum_{k=0}^{n} \frac{f_k \beta_k}{s - t_k} / \sum_{k=0}^{n} \frac{\beta_k}{s - t_k}$$
 (19.3)

as in (2.1). One could take this to be the reduced transfer function. Alternatively, one can use the poles and residues to convert $\hat{H}(s)$ to transfer function form. The matrices involved will be diagonal in the most obvious realisation, but an interesting alternative is

$$\hat{H}(s) = [f_0 \beta_0, \ f_1 \beta_1, \ \dots, \ f_n \beta_n] A^{-1} \begin{bmatrix} 1 \\ 0 \\ 0 \\ \vdots \\ 0 \end{bmatrix}$$
(19.4)

with

$$A = \begin{bmatrix} \beta_0 & \beta_1 & \dots & \beta_{n-1} & \beta_n \\ s - t_0 & t_1 - s & & & \\ & s - t_1 & t_2 - s & & & \\ & & \ddots & \ddots & & \\ & & s - t_{n-1} & t_n - s \end{bmatrix},$$
(19.5)

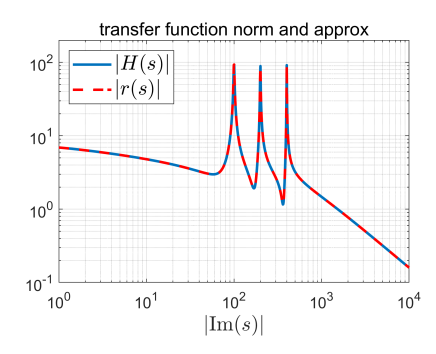
as proposed in (Lietaert et al. 2022, Prop. 2).

To illustrate, we take Penzl's FOM model from the SLICOT Benchmark examples collection (Chahlaoui and Van Dooren (2002)), where $A \in \mathbb{R}^{1006 \times 1006}$ and p=m=1, so H is a rational function of degree 1006. We sample H(s) at 100 logarithmically spaced points in the interval $[i,10^4i]$ and their complex conjugates and compute its AAA approximation with the usual 13-digit relative accuracy, which has degree 29. Figure 19.1 shows |H(s)| and |r(s)| and the convergence of r to H as the AAA iterations proceed. The two functions match to 10 digits of absolute accuracy on the whole imaginary axis.

In the Multiple Input Multiple Output (MIMO) case, with p, m > 1, one can use the blockAAA or setAAA algorithms to find approximations to all pm entries simultaneously (Gosea and Güttel (2021), Lietaert $et\ al.\ (2022)$); see section 33.

Classically, vector fitting (Gustavsen and Semlyen (1999)) was for many years among the most popular methods for finding a rational approximation to a transfer function H. Unlike AAA, in vector fitting the degree of \hat{H} needs to be specified in advance. The convergence of vector fitting is not fully understood.

So far as we are aware, compared with other MOR/ROM approaches,



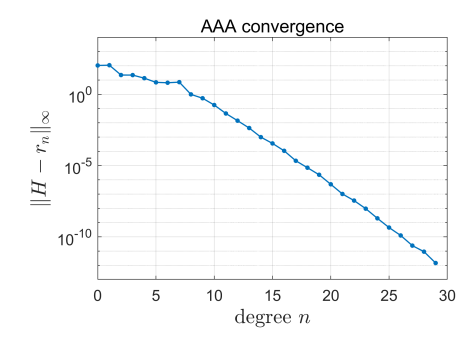


Figure 19.1. On the left, absolute values of the degree 1006 transfer function H(s) and its degree 29 AAA approximant r(s) for the FOM example from SLICOT (Chahlaoui and Van Dooren (2002)). On the right, AAA convergence for this example. Rapid convergence begins at degree n = 6, after the six poles at $-1 \pm 100i$, $-1 \pm 200i$, and $-1 \pm 400i$ are captured.

AAA is often as efficient as any method for scalar problems with p=m=1, and perhaps similarly for setAAA when p,m are small. AAA has been applied in a variety of contexts in the scalar case, including (Gosea and Güğercin (2022)) (higher-degree problems) and (Rodriguez et al. (2023)) (parameterised problems). When p and/or m are large, however, the situation can be different, and AAA-based methods in MOR/ROM are less mature. Studies in this direction include (Aumann, Benner, Gosea, Saak and Vettermann (2023), Gosea and Güttel (2021), Jonas and Bamieh (2024)).

An important class of methods in MOR/ROM is the so-called Loewner framework. In this method (as in AAA), one only requires evaluations of the transfer function H(s), sometimes only tangentially, e.g. evaluations of $H(s_i)b_i$ and $c_j^TH(s_j)$ for vectors b_i and c_j . Then one can use the sampled data to form matrices related to the Loewner matrix (2.6) to obtain a reduced model \hat{H} that satisfies tangential interpolation, i.e., $H(s_i)b_i = \hat{H}(s_i)b_i$, $c_j^TH(s_j) = c_j^T\hat{H}(s_j)$.

Again, for scalar problems p = m = 1, AAA tends to be more efficient

Again, for scalar problems p = m = 1, AAA tends to be more efficient than Loewner, and it benefits from the robustness brought by the least-squares part of AAA. By contrast, Loewner can be better for $p, m \gg 1$. For example, with p = m = n and D = 0, the Loewner framework is able to recover the system to obtain $\hat{H} = H$ by computing H(s) at just two points, $H(s_1)$ and $H(s_2)^5$. AAA or setAAA would not be able to do this.

When the matrices A, B, C, D, E are known explicitly, a common approach in MOR for finding \hat{H} from H is projection: one finds orthonormal

⁵ This may seem surprising at first, but one can note that $H = C(sE - A)^{-1}B$ essentially contains $2n^2$ degrees of freedom, which are provided by $H(s_1)$ and $H(s_2)$.

(tall-skinny) matrices V, W and sets $\hat{E} = W^T E V$, $\hat{A} = W^T E V$, $\hat{B} = W^T B$, $\hat{C} = C V$ and $\hat{D} = D$. Remarkably, tangential interpolation ensues (Antoulas *et al.* 2020, chap. 3). For example, for any fixed $b \in \mathbb{R}^m$, $H(s_i)b = \hat{H}(s_i)b$ holds if Range(V) includes the vector $(s_i E - A)^{-1} B b$.

AAA (and AAA-Lawson) attempt to minimise the L_{∞} -norm of the error $H - \hat{H}$. In the scalar case, this is equivalent to the so-called \mathcal{H}_{∞} norm, defined by $\|H\|_{\mathcal{H}_{\infty}} = \sup_{s \in \mathbb{R}} \|H(\mathrm{i}s)\|_2$. It is unclear how to do the same when p, m > 1. In MOR, attention has also been paid to minimising the \mathcal{H}_2 norm of the error. Extensive theory and optimality conditions have been developed, and in particular IRKA (the Iterative Rational Krylov Algorithm) (Gugercin et al. (2008)) iteratively updates the tangential interpolation points and directions to find the best approximation \hat{H} to H in \mathcal{H}_2 . IRKA is applicable to MIMO systems with p, m > 1 and converges rapidly for most problems, although a full convergence proof is not available. For ROM as opposed to MOR, there is TF-IRKA ("transfer function IRKA") (Beattie and Gugercin (2012)).

Approximating A(z) can be more efficient than working with the resolvent for problems where solving linear systems with respect to $A(z_i)$ is expensive. On the other hand, working with the resolvent has the advantage of simplicity and having no distinction between linear and nonlinear problems.

For more details on MOR/ROM, we refer to (Antoulas et al. (2020), Benner, Güğercin and Willcox (2015)) and the references therein. For practical information about AAA applied to ROM problems, see the code rational in the MathWorks RF Toolbox (MathWorks Inc. (2020)), which can handle multiple outputs as well as scalars. It should be noted that applications such as those targeted by the Toolbox often have significant amounts of noise, an issue discussed here at the end of section 8. In such cases an engineer may be pleased with two digits of accuracy, far less than the ten digits of the SLICOT example we showed. More recently, MathWorks has also introduced AAA fitting in its Control System and System Identification toolboxes (version R2025a). The applications here are closer to MOR as opposed to ROM.

20. The Zolotarev sign problem

Yegor Zolotarev was a student of Chebyshev who visited Berlin in 1872 and learned about elliptic functions from Weierstrass. He brought these ideas back to St. Petersburg, where he published a paper in 1877 on the theme of polynomial and rational approximations on disjoint intervals (Zolotarev (1877)). His work still resonates today, and there is no knowing what more Zolotarev might have done had he not been killed in a train accident in St. Petersburg in 1878, at age 31.

Let E and F be disjoint closed sets in the complex plane, and let $n \geq 0$

be an integer. The Zolotarev sign problem (also known as Zolotarev's 4th problem) is to find a rational function \hat{r}_n of degree n that approximates -1 on E and +1 on F as closely as possible. We denote this target function by $\operatorname{sign}_{E/F}(z)$ (not defined for values of z outside E and F), so the problem can be stated as finding an optimal approximation $\hat{r}_n(z) \approx \operatorname{sign}_{E/F}(z)$ on $E \cup F$. The minimum approximation error is denoted by τ_n :

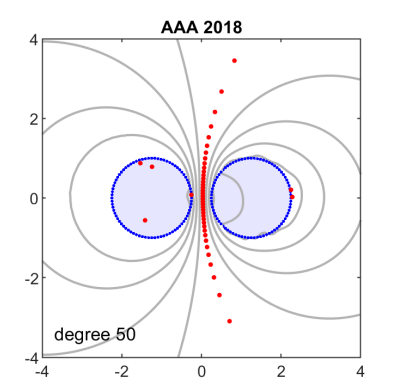
$$\tau_n = \|\hat{r}_n - \text{sign}_{E/F}\|_{E \cup F} = \min_{r \in \mathcal{R}_n} \|r - \text{sign}_{E/F}\|_{E \cup F},$$
(20.1)

where $\|\cdot\|_{E \cup F}$ denotes the ∞ -norm on $E \cup F$. A function \hat{r}_n achieving this minimum is an example of a rational function whose poles and zeros will delineate an approximate branch cut, because no single analytic function can take values -1 on E and +1 on F. (We assume that E and F are continua with no isolated points, though they need not be connected.)

From the beginning of our AAA-related work, we tried experiments with approximating sign functions, and the results appeared adequate but not excellent. The left image of Figure 20.1 gives an illustration for a case where E and F are the circles of radius 1 about z=-1.25 and z=+1.25. (This problem has an analytic solution given below in (21.7)–(21.8).) Two features of this plot fall short of ideal. One is the six spurious poles near the boundary circles, but these can be argued away as artifacts (Froissart doublets) since their residues are negligible, and they can be removed numerically by a least-squares fit of $\operatorname{sign}_{E/F}(z)$ in the space spanned by the remaining poles. The other is the fact that the remaining poles lie on a curve that bends away from the imaginary axis, where by symmetry, the optimal poles should lie. We interpreted this effect in the spirit of backward error analysis. Many different pole configurations will give almost equally good approximations on E and F, we reasoned, so the pole locations are exponentially ill-conditioned and can be expected to show some oddities in a numerical computation.

Then, in the summer of 2024, together with Heather Wilber, we investigated the situation more closely in order to pursue applications to be described in the next section (Trefethen and Wilber (2025)). We found that the difficulties of our "adequate" sign function calculations were more fundamental than we had realised. In fact, approximation of sign functions using the AAA algorithm as described in section 2 almost invariably runs into trouble. The initial iterations tend to show no progress at all, completely failing to find good approximations even though these must exist even for low degrees like 1 or 3.

The details are not fully understood, but it became clear that a source of the problem is that in approximating $\operatorname{sign}_{E/F}(z)$, AAA works with a Loewner matrix A half of whose entries (2.6) are zero. This happens because f_j and f_k are equal when j and k correspond both to E or both to F, and it



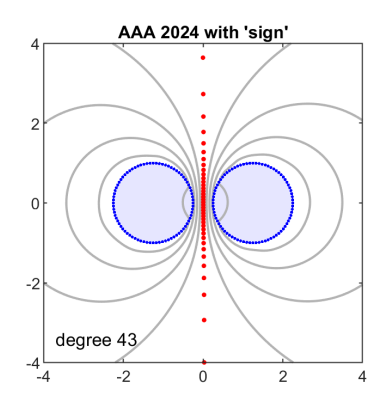


Figure 20.1. Approximation of $\operatorname{sign}_{E/F}(z)$ for a pair of disks discretised by 80 equispaced points on each boundary. Standard AAA does poorly on such problems (left), whereas AAA with the 'sign' modification introduced in 2024 and described in (Trefethen and Wilber (2025)) does much better (right). The grey contours mark deviations 10^{-12} , 10^{-9} , 10^{-6} and 10^{-3} of r(z) at each point z from +1 or -1, whichever is closer.

makes A a rectangular matrix with block 2×2 diagonal structure.⁶ When AAA then computes a minimal singular vector of A to obtain barycentric weights, as described in section 2, the blocks decouple and one obtains a weight vector that more or less randomly attends to approximation on one of E and F while ignoring the other. Convergence is disrupted.

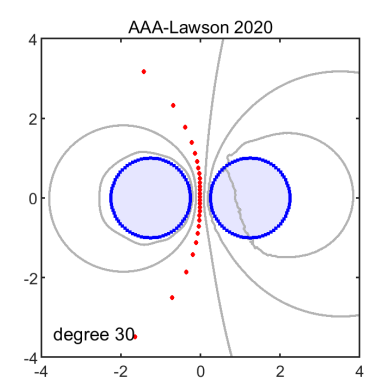
A modification to AAA was proposed in (Trefethen and Wilber (2025)) that goes a good way toward fixing this problem. For calculating a new vector wj of barycentric weights at each step, we changed the MATLAB lines in aaa.m

```
[~,S,V] = svd(A(J,:),0);
wj = V(:,end);
to

[~,S,V] = svd(A(J,:),0);
s = diag(S); wj = V*(1./s.^2); wj = wj/norm(wj);
```

This ensures that wj is a blend of all the singular vectors rather than just one of them. For most AAA computations, the change has little effect, but for approximating sign functions, the difference is considerable, as one sees in the right image of Figure 20.1. As of this writing, the Chebfun code aaa.m offers 'sign' as an option (not turned on by default).

⁶ We are grateful to Sam Hocking for some analysis of this effect.



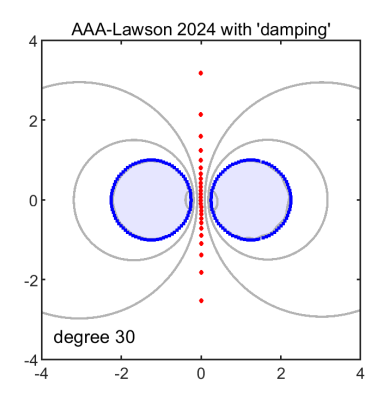


Figure 20.2. Repetition of Figure 20.1 but now for degree 30 approximations with Lawson iteration turned on to attempt an improvement from near-best to best approximation. The contours mark accuracies 10^{-9} , 10^{-6} and 10^{-3} . The plot on the right shows the improvement both the 'sign' and the 'damping' modifications introduced in 2024 (Trefethen and Wilber (2025)).

Another similar modification of AAA has been proposed in (Mitchell (2025)).

Fixing one problem in AAA sign function approximations unexpectedly revealed another, illustrated in the left image of Figure 20.2. For the applications of the next section, it was important for us to be able to improve our Zolotarev approximations from near-best to best. The standard algorithm for this is the AAA-Lawson method (Nakatsukasa and Trefethen (2020)), which is a nonlinear iteratively reweighted least-squares iteration in which at each step, the weights of a least-squares problem are updated by the formula

$$w_j^{\text{(new)}} = w_j |e_j|, \tag{20.2}$$

where w_j denotes the current least-squares weight at sample point z_j and e_j is the current rational approximation error $e_j = r(z_j) - f_j$. When the iteration is working well, the weights converge steadily (linearly) to a configuration corresponding to the best L^{∞} approximant, but we had long known that it sometimes fails to converge, usually then exhibiting period-2 oscillations. To our surprise, it emerged that $\operatorname{sign}_{E/F}$ problems are a case where these failures are exceptionally likely to occur.

And so we introduced a modification in the AAA-Lawson algorithm, which usually (not always) fixes this second problem. When the 'damping' flag is specified, (20.2) is changed to

$$w_j^{\text{(new)}} = \left((1 - \delta) + \frac{\delta |e_j|}{\max_j |e_j|} \right) w_j, \tag{20.3}$$

where $\delta \in (0, 1]$ is a user-supplied damping factor. With $\delta = 1$ we have standard AAA-Lawson, whereas for smaller values it is a more robust iteration that converges more reliably, if more slowly. For details, see (Trefethen and Wilber (2025)).

As a typical example, the approximation plotted in the right image of Figure 20.2 can be generated by the code

```
Z = exp(2i*pi*(1:80)'/80); Z = [1.25+Z; -1.25+Z];
F = sign(real(Z));
[r,pol] = aaa(F,Z,'degree',30,'sign',1,'damping',.95);
```

Since the emphasis of this paper is on applications more than algorithms, we will not say more about the 'sign' and 'damping' modifications. In both cases, there is a clear improvement, but the modifications are not bulletproof, and theoretical justifications are entirely lacking. We hope that these aspects of AAA will be made more solid by further research.

Instead, in the rest of this section we will show four more examples and then comment on applications.

The examples appear in Figure 20.3 and illustrate, among other things, that the sets E and F need not be connected. It is interesting to take note of the grey contours in this figure and also in Figures 20.1 and 20.2. In all of these plots, the red dots mark the approximate branch cut selected by AAA, and the grey contours closest to the dots show accuracies 10^{-3} on two sides. In each case we see that r(z) matches +1 or -1 to three digits in large regions in the left and right half-planes, even though a priori, it was only tasked with approximation on E and F. This is the phenomenon that Walsh called overconvergence (Walsh (1969)), which appears widely in both polynomial and rational approximation and can be seen in several of the figures of this review.

The Zolotarev sign problem arises in a number of applications where one wants to separate one part of a system computationally from another. For example, classic Infinite Impulse Response digital filters start from a rational function that is nearly constant on one part of the real axis and nearly zero on another, and computing coefficients for such filters is essentially a Zolotarev sign problem (Oppenheim and Schafer (2001)). Generalisations arise in numerical linear algebra and computational science, for example in the computation of functions of matrices and operators (Bai and Demmel (1998), Higham (2008), Kenney and Laub (2002)). Divide and conquer methods for computing eigenvalues of large matrices work by suppressing one part of the spectrum relative to another recursively (Bai, Demmel and Gu (1997), Banks, Garza-Vargas, Kulkarni and Srivastava (2023)). This too leads to Zolotarev sign problems, typically starting from the case where E and F are approximations to the left and right complex half-planes (Nakatsukasa and Freund (2016)). In the real case, which goes back to Zolotarev

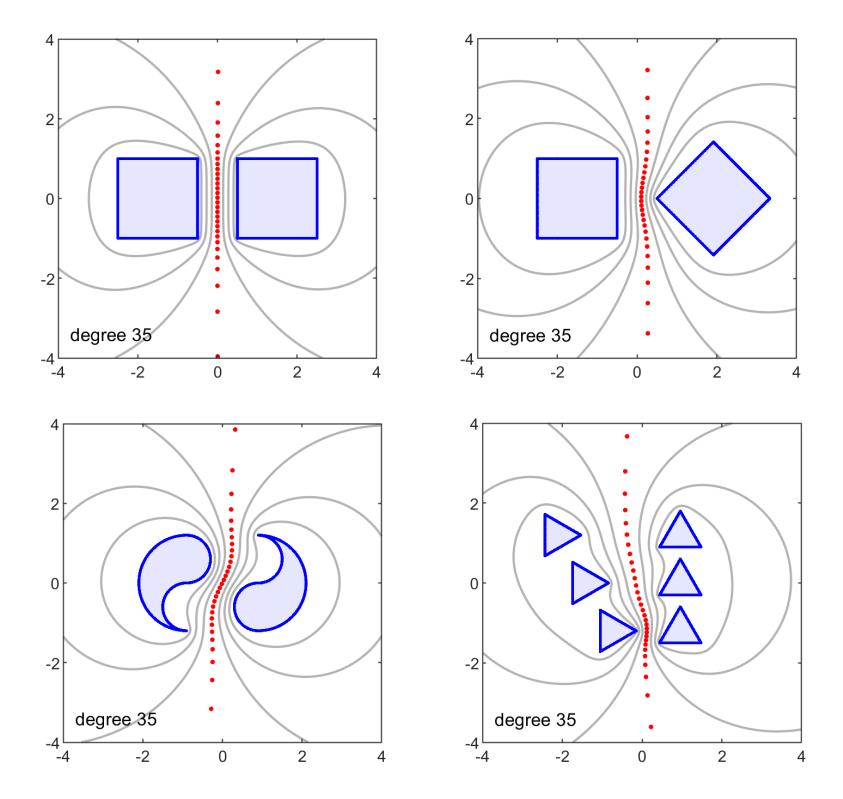


Figure 20.3. Four more examples of AAA-Lawson minimax solutions of the Zolotarev sign problem, all for fixed degree 35. The 'sign' and 'damping' options have been used with a damping factor $\delta = 0.95$. The contours mark accuracies 10^{-9} , 10^{-6} and 10^{-3} .

himself, they may be intervals such as $[-a, -\varepsilon]$ and $[\varepsilon, a]$. "Spectral slicing" ideas of this kind have found generalisation through algorithms such as FEAST, which was discussed in section 17 (Güttel *et al.* (2015)).

We just mentioned the possibility of recursion in algorithms related to $\operatorname{sign}_{E/F}$ approximations, and this is an important aspect of this subject both mathematically and philosophically. In classical rational approximation theory, one seeks a rational function of a specified degree n with certain properties. (Everything we say here also applies to polynomials.) For example, the approximations of Figure 20.3 are rational functions of degree 35. Another possibility in many applications, however, is to compose rational functions in structures like this:

$$r(z) = r_k(\cdots r_3(r_2(r_1(z)))\cdots).$$
 (20.4)

If each element has degree 2, for example, then this *composite rational approximation* has degree 2^k , which may be far beyond the range that numeri-

cal approximation theorists are used to imagining they can deal with (Nakatsukasa and Freund (2016), Gawlik and Nakatsukasa (2021)). Though we don't generally notice, such composite rational approximations are exploited implicitly all the time when Newton's method is applied (Trefethen (March 2022b)). In the case of $\operatorname{sign}_{E/F}$ approximations where E and F are disjoint, even a two-level approximation may be powerful, for a single rational function may produce sets r(E) and r(F) that are small neighborhoods of -1 and +1, respectively, hence well separated from each other, and applying one further polynomial or rational function can then add many more digits of accuracy at minimal cost.

21. The Zolotarev ratio problem

The Zolotarev ratio problem (also known as Zolotarev's 3rd problem) is another problem involving rational functions on a pair of sets E and F in the complex plane. This time the question is, how small can r be on E relative to its size on F? Specifically, the aim is to find a degree n rational function r_n^* that minimises the ratio

$$\frac{\max_{z \in E} |r(z)|}{\min_{z \in F} |r(z)|},\tag{21.1}$$

and we denote the minimum ratio, the *Zolotarev number* of E and F, by σ_n :

$$\sigma_n = \min_{r \in \mathcal{R}_n} \frac{\max_{z \in E} |r(z)|}{\min_{z \in F} |r(z)|}.$$
 (21.2)

To normalise the problem in a symmetric fashion we specify

$$\min_{z \in F} |r(z)| = \frac{1}{\max_{z \in E} |r(z)|}.$$
 (21.3)

(This is different from the normalisation of (Istace and Thiran (1995)) and (Trefethen and Wilber (2025)).) Like the Zolotarev sign problem of the last section, the Zolotarev ratio problem has a number of applications, which we shall mention at the end of the section.

Like the sign problem, the ratio problem was introduced (for real intervals E and F) by Zolotarev (Zolotarev (1877)), and Gonchar generalised it to the complex plane (Gonchar (1969)). As it happens, the two problems are equivalent, but it is not clear if Zolotarev knew this. The equivalence was shown by Achieser for real intervals and by Istace and Thiran for more general sets (Istace and Thiran (1995)), and it runs as follows. Let E, F and n be given, and let \hat{r}_n be a degree n best rational approximation of the sign $_{E/F}$ function with error τ_n as in (20.1). We state the theorem of Istace and Thiran essentially in their words:

Theorem 21.1. Every solution r_n^* , σ_n of the Zolotarev ratio problem with the normalisation (21.3) is related to the solution \hat{r}_n , τ_n in (20.1) of the Zolotarev sign problem by

$$\hat{r}_n(z) = \gamma_n \frac{r_n^*(z) - \sigma_n}{r_n^*(z) + \sigma_n}, \quad r_n^*(z) = \sqrt{\sigma_n} \frac{\gamma_n + \hat{r}_n(z)}{\gamma_n - \hat{r}_n(z)}$$
 (21.4)

with $\gamma_n = (1 - \sigma_n)/(1 + \sigma_n) \approx 1$. The minimal values of the two problems satisfy

$$\tau_n = \frac{2\sqrt{\sigma_n}}{1 + \sigma_n}, \quad \sigma_n = \left(\frac{\tau_n}{1 + \sqrt{1 - \tau_n^2}}\right)^2, \tag{21.5}$$

and the set of extremal points

$$M = \{ z \in E \cup F, \ |\hat{r}_n(z) - \operatorname{sign}_{E/F}(z)| = \tau_n \}$$
 (21.6)

is the union of $M_1 = \{z \in E, |r_n^*(z)| = \sigma_n\}$ and $M_2 = \{z \in F, |r_n^*(z)| = 1\}.$

Thanks to this theorem, once the Zolotarev sign problem has been solved, one has in principle also solved the Zolotarev ratio problem. Until 2024, this was true only in principle (except for a small collection of analytic solutions), since no method was available to compute solutions to the sign problem accurately enough. Now that such a method is available, the ratio problem can be handled as follows:

- (1) Solve the sign problem by AAA-Lawson as in the last section;
- (2) Convert to a solution of the ratio problem by (21.4) and (21.5).

Details are presented in (Trefethen and Wilber (2025)).

For example, the following code computes the solution to the degree 30 Zolotarev ratio problem for the geometry of Figures 20.1 and 20.2, where E and F are disks of radius 1 about $z=\pm 1.25$. This formulation calls the Chebfun code prz (which is also included in aaa.m) to find the zeros and poles of r_n^* .

```
Z = exp(2i*pi*(1:80)'/80); Z = [1.25+Z; -1.25+Z];
F = sign(real(Z));
[rhat,~,~,~,zj,fj,wj] = ...
    aaa(F,Z,'degree',30,'sign',1,'lawson',200,'damping',0.95);
tau = norm(F-rhat(Z),inf);
sigma = (tau/(1+sqrt(1-tau^2)))^2;
gamma = (1-sigma)/(1+sigma);
rstar = @(z) (gamma+rhat(z))./(gamma-rhat(z));
[~,~,zeros] = prz(zj,fj+gamma,wj);
[~,~,poles] = prz(zj,fj-gamma,wj);
```

The result is shown in Figure 21.1. This problem is one of those that can

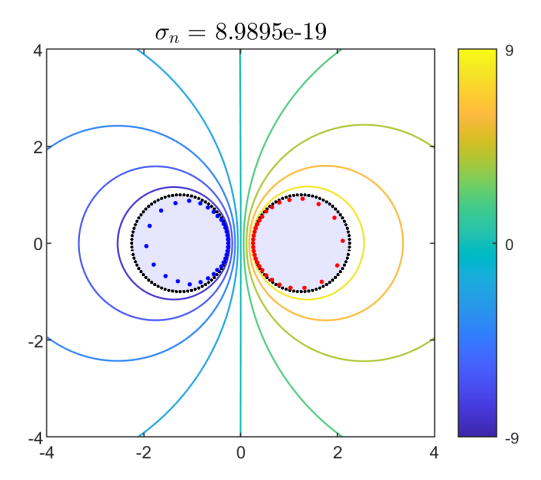


Figure 21.1. Approximation to the degree n=30 solution r_n^* of the Zolotarev ratio problem for the two-disks configuration of Figures 20.1 and 20.2. This is a transformation of the function \hat{r}_n of the right image of Figure 20.2 by the formula (21.4). Blue and red dots mark zeros and poles of the computed r_n^* (the exact results would coalesce at two points), and the contours mark level curves of $\log_{10}|r_n^*(z)|$.

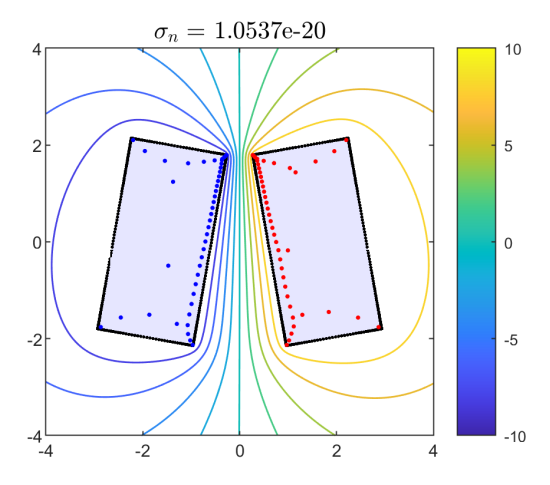


Figure 21.2. Degree 44 solution of the Zolotarev ratio problem for a pair of 2×1 rectangles centred at $z = \pm 1.6$ and tilted by 10 degrees. This computation took 1.5 s on a laptop.

be solved analytically (Starke (1992)):⁷

$$r_n^* = \left(\frac{z + \frac{3}{4}}{z - \frac{3}{4}}\right)^{30}, \quad \sigma_n = 2^{-60} \approx 8.67 \cdot 10^{-19},$$
 (21.7)

$$\tau_n = \frac{2^{-29}}{1 + 2^{-60}} \approx 1.86 \cdot 10^{-9}.$$
 (21.8)

In the numerical solution shown in the figure, $\log(\sigma_n)$ has come out within 0.1% of the analytically known optimal value. The zeros and poles are distributed along circles close to the boundaries of E and F rather than coalescing at $z = \pm 3/4$, an instance of balayage (Gustafsson (2001)) that evidently has had little effect on the accuracy.

More complicated regions E and F can also be successfully treated. For example, Figure 21.3 shows a geometry proposed to us by Levent Batakci of the University of Washington. Here, E and F are a pair of interlocking spirals, each winding $1\frac{1}{2}$ times around the origin. A minimal-ratio rational function r_n^* of degree n=80 has been computed, differing by about ten orders of magnitude on E and F. Our current algorithms are at their limits for domains like this, however. For this computation we used 'sign', 1 and 'damping', 0.75 with 600 AAA-Lawson iterations, but the convergence is only approximate.

Zolotarev, Achieser and Gonchar were motivated by approximation theory, which in Gonchar's case was strongly allied with potential theory, but the practical applications of the Zolotarev ratio problem are in numerical linear algebra. Such applications go back to the Alternating Direction Implicit (ADI) method introduced by Peaceman and Rachford in 1955 for rapid solution of algebraic equations arising from multidimensional finite difference discretisations of PDEs. Later this was generalised to methods for the solution of Lyapunov equations and Sylvester equations, and a summary can be found in (Simoncini (2016)). The PhD thesis of Heather Wilber was largely about numerical solution and application of the Zolotarev problems (Wilber (2021)).

22. Quadrature formulas

A quadrature formula is a discrete formula

$$I_n = \sum_{k=1}^{n} w_k f(z_k)$$
 (22.1)

⁷ The main known cases with analytic solutions involve disks and intervals that can be reduced by elementary maps to a symmetric pair of disks.

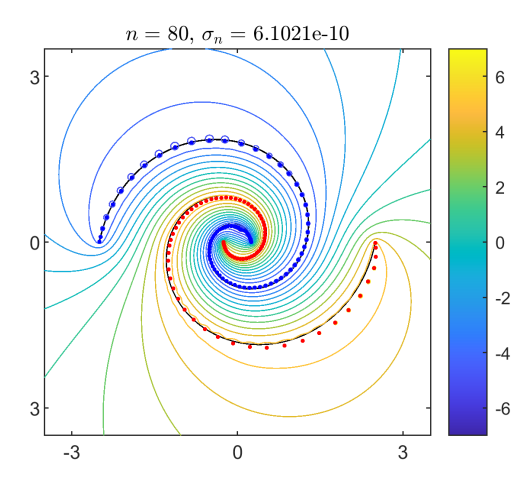


Figure 21.3. The Batakci lollipop. The image shows a degree 80 Zolotarev minimal ratio rational function for a pair of interlocking spirals proposed by Levent Batakci of the University of Washington. The sets E and F are marked by black lines, and the colourbar marks levels of $\log_{10}|r_n^*(z)|$. Zeros and poles are marked by blue and red dots. The value of σ_n is only approximately correct, as the computation is not fully converged.

whose purpose is to approximate an integral

$$I = \int_{\gamma} w(z)f(z)dz, \tag{22.2}$$

where γ is an integration interval or contour, w(z) is an integrable weight function, f is an integrand, and $\{z_k\}$ and $\{w_k\}$ are the quadrature nodes and weights. In the case $\gamma = [-1,1]$ and w(z) = 1 we have the context for well-known formulas such as Gauss, Clenshaw-Curtis and Newton-Cotes (Gautschi (2004)). If γ is the unit circle in $\mathbb C$ and the nodes are roots of unity and the weights are all equal, we have a version of the exponentially convergent periodic trapezoidal rule (Trefethen and Weideman (2014)).

In any of these quadrature rules, the nodes form a string of points on a real or complex contour. In this review, we have seen a number of strings of poles of rational functions that delineate approximate branch cuts: see Figures 11.2–3, 12.4–5, 13.2–3 and 20.1–3. One might speculate, is there a connection here? The answer is strikingly yes, as explained in (Horning and Trefethen (submitted)). Quadrature nodes are poles of rational approximations of a Cauchy transform, delineating approximate branch cuts of that Cauchy transform. The Cauchy transform (eq. (22.6) below) is that of the weight function w(z) in (22.2): an analytic function in $\mathbb{C} \cup \{\infty\}$ except for a jump by w(z) across the contour.

Figure 22.1 illustrates this effect in the familiar case of Gauss (-Legendre)

quadrature on [-1,1]. In the upper-left are the nodes of the 20-point Gauss formula in [-1,1], plotted in the complex plane. Below this is a phase portrait of the associated rational function

$$r(z) = \sum_{k=1}^{n} \frac{w_k}{z - z_k},\tag{22.3}$$

where $\{z_k\}$ and $\{w_k\}$ are the Gauss nodes and weights. On the right is the same pair of plots for a different rational function r: the degree 20 AAA rational approximation to $\log((z+1)/(z-1))$ on the Bernstein ellipse plotted as a black or white curve, with parameter chosen so that it passes through the points $z=\pm i/\sqrt{20}$. (A Bernstein ellipse is an ellipse in $\mathbb C$ with foci ± 1 .) Apart from the presence of the ellipse, there is no visible difference in the plots. This exemplifies the general principle that any quadrature formula (22.1) can be associated with a rational function r as in (22.3), whose approximation properties will have much to do with the accuracy of the formula. To see how close Gauss and AAA are in this example, if we integrate the test function $f(z)=1/(1+20z^2)$, the 20-point Gauss and AAA formulas give essentially identical errors $1.575 \cdot 10^{-4}$ and $1.560 \cdot 10^{-4}$, respectively. The bottom plot in the figure shows that this close agreement is maintained for all n down to the usual AAA tolerance of 10^{-13} .

The association of quadrature formulas with rational functions goes back to Gauss in 1814, who derived his formula (as we would now say) by Padé approximation of $\log((z+1)/(z-1))$ at $z=\infty$.⁸ Many connections between rational functions and quadrature formulas have been exploited in the ensuing two centuries. However, before (Horning and Trefethen (submitted)) there was little discussion of the link with rational approximation per se. The main example we know is (Trefethen, Weideman and Schmelzer (2006)).

Following (Horning and Trefethen (submitted)), here is a summary of the mathematics of these approximations. Assume the integrand f of (22.2) is analytic in the closure of a Jordan region containing γ bounded by a Jordan curve Γ . By the Cauchy integral formula, we have

$$I = \int_{\gamma} \frac{1}{2\pi i} \left[\int_{\Gamma} \frac{f(s)ds}{s-z} \right] w(z)dz, \tag{22.4}$$

hence by exchanging orders of integration,

$$I = \int_{\Gamma} f(s) \, \mathcal{C}(s) \, ds, \tag{22.5}$$

⁸ Potential theorists would explain the close agreement in Figure 22.1 of the rational approximations at ∞ and on a Bernstein ellipse as an example of balayage (Gustafsson (2001)).

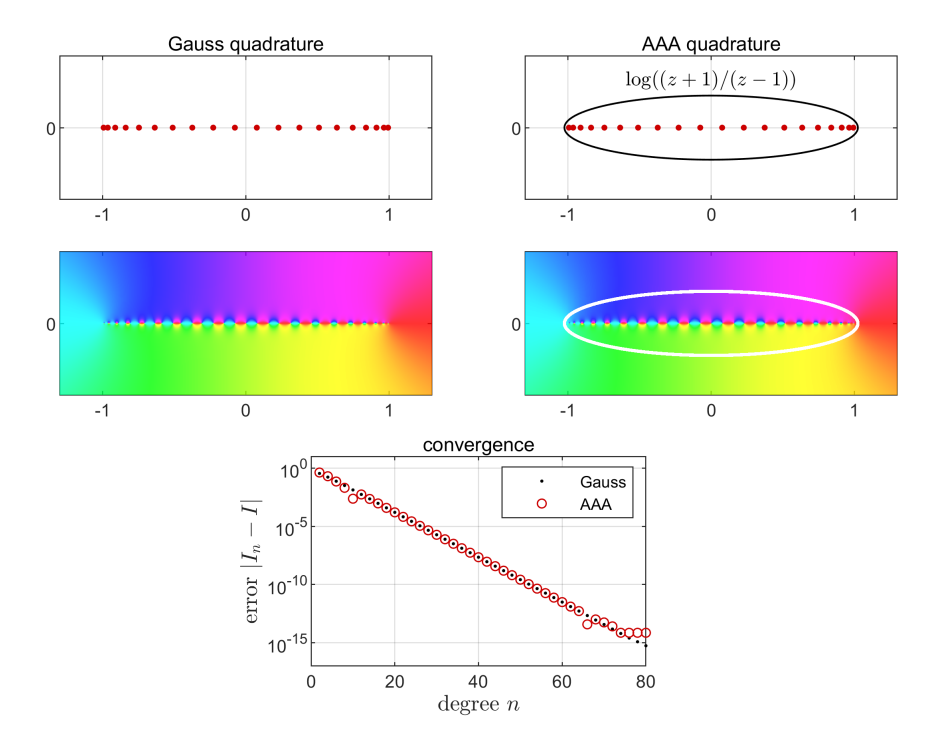


Figure 22.1. On the left, nodes for the 20-point Gauss quadrature formula and a phase portrait of the associated rational function (22.3). On the right, looking virtually identical, the same plots for a degree 20 AAA rational approximation of $\log((z+1)/(z-1))$ on a Bernstein ellipse. Below, convergence of the two quadrature formulas for the test integrand $f(x) = 1/(1+20x^2)$.

where C(s) is the Cauchy transform of w,

$$C(s) = \frac{1}{2\pi i} \int_{\gamma} \frac{w(z) dz}{s - z}.$$
 (22.6)

This function is analytic throughout $\mathbb{C} \cup \{\infty\} \setminus \gamma$ and jumps by w(z) across γ . For the Gauss-Legendre case $\gamma = [-1, 1]$ with w(z) = 1, the value is $\mathcal{C}(s) = (2\pi i)^{-1} \log((s+1)/(s-1))$. Suppose that r is a rational function of degree n that approximates \mathcal{C} on Γ . Then (22.5) suggests approximating I by

$$I_n = \int_{\Gamma} f(s) r(s) ds. \tag{22.7}$$

Assume the poles of r are n distinct finite numbers z_1, \ldots, z_n , so r can be written

$$r(s) = C + \sum_{k=1}^{n} \frac{w_k}{s - z_k},$$
(22.8)

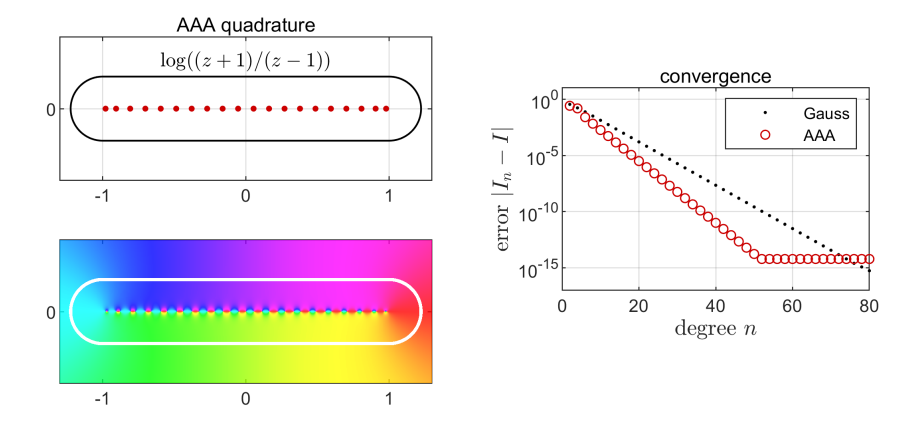


Figure 22.2. Like Figure 22.1, but now the quadrature formulas are based on approximation of $\log((z+1)/(z-1))$ over the boundary of an ε -neighborhood of [-1,1]. For the same test integrand $f(z) = 1/(1+20z^2)$ as before, the convergence is about $\pi/2$ times faster than with Gauss quadrature, and the quadrature nodes are much more evenly spaced.

where $C = r(\infty)$ and w_k is the residue of r at z_k . Then, assuming all the poles are enclosed by Γ , residue calculus converts (22.7) to

$$I_n = 2\pi i \sum_{k=1}^n w_k f(z_k).$$
 (22.9)

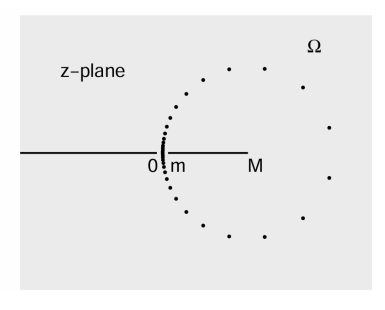
If $\|\mathcal{C} - r\|_{\Gamma} \leq \varepsilon$, where $\|\cdot\|_{\Gamma}$ is the ∞ -norm on Γ , then by (22.5) and (22.7),

$$|I - I_n| \le \varepsilon |\Gamma| \|f\|_{\Gamma}, \tag{22.10}$$

where $|\Gamma|$ is the arc length of Γ .

These relationships enable us to construct quadrature formulas targeted to all kinds of applications by means of rational approximation. For example, it is known that although Gauss quadrature is optimal from the point of view of integrating polynomials of maximal degree, it is suboptimal for dealing, say, with functions analytic in an ε -neighboorhood of [-1,1] rather than in a Bernstein ellipse. Methods for deriving formulas adapted to such situations have been proposed based on conformal mapping (Hale and Trefethen (2008)) and prolate spheroidal wave functions (Trefethen (2022a)), but rational approximation gives us a simpler new possibility, as illustrated in Figure 22.2.

Many further examples of quadrature formulas derived from rational approximations can be found in (Horning and Trefethen (submitted)); we will report just one of these, shown in Figure 22.3. In the "three Nicks" paper published by the second author with Nick Hale and Nick Higham (Hale,



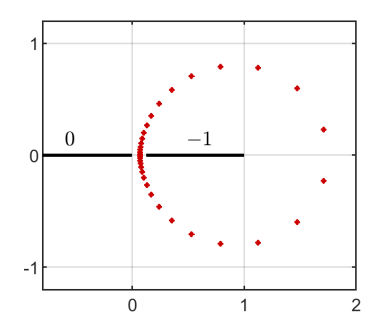


Figure 22.3. On the left, a figure from (Hale *et al.* (2008)) showing quadrature nodes derived by conformal mapping for a problem of computing functions of matrices with eigenvalues in [m, M]. On the right, a figure adapted from (Horning and Trefethen (submitted)) showing nodes derived by a rational approximation of the Zolotarev sign type. The accuracy of the two formulas is comparable.

Higham and Trefethen (2008)), the problem is considered of computing matrix functions like A^{α} or $\log(A)$, where A is a symmetric positive definite matrix with eigenvalues in [m,M] for some $0 < m < M < \infty$. As suggested in the figure, this can be reduced mathematically to a contour integral over a closed curve enclosing [m,M] and passing through the gap between 0 and M. From the matrix point of view, this means the matrix function is reduced to a collection of linear systems of equations of the form $(A-z_kI)x=b$ —the mathematics is close to that of sections 17 and 18. If a simple formula like the equispaced trapezoidal rule is used, the number of such systems is prohibitive: O(M/m) for each digit of required accuracy. By a conformal map of $\mathbb{C}\setminus((-\infty,0]\cup[m,M])$ to a circular annulus, however, this number can be reduced hugely to $O(\log(M/m))$. For a problem with M/m=8, for example, one gets 6-digit accuracy from as few as 10 matrix solves (exploiting real symmetry).

As suggested in the right image of Figure 22.3, the same specialised quadrature form can alternatively be derived by rational approximation without the need for conformal mapping. The Cauchy transform for a closed curve surrounding [m, M] is simply the jump function taking the values -1 inside the curve and 0 outside, so we have an approximation of exactly the Zolotarev sign form discussed in section 20. This is readily solved numerically, and the figure shows the agreement with the result of conformal mapping. Convergence is exponential, as predicted (not shown). In this example the convergence just goes down to about the level of 10^{-8} for reasons related to rounding errors that have not yet been investigated.

We should emphasise an aspect of the mathematics of this section that

is particularly distinctive. Normally we think of an integral (22.2) as associated with a fixed contour γ , and the same is true of a Cauchy transform (22.6). In the analytic functions context of this section, however, any choice of γ that connects the same endpoints in (22.2) and lies in the region of analyticity of f and inside the outer contour Γ in (22.5) will give the same integral I in (22.2) and the same Cauchy transform C(s) along Γ in (22.5). When we find a rational approximation $r(s) \approx C(s)$ along Γ , its poles implicitly make a choice of one of these equivalent contours γ . For problems associated with real functions on real intervals, one will hardly notice this effect since symmetry will make γ real too, as in Figures 22.1 and 22.2. In cases like Figure 22.3, however, the rational approximation is genuinely choosing the contour as well as the nodes and weights. More examples can be found in (Horning and Trefethen (submitted)).

23. Cauchy, Wiener-Hopf, Riemann-Hilbert

Many problems in complex analysis involve jumps of analytic functions across contours. AAA approximation usually has something to contribute, and in this section we will illustrate the possibilities by a Cauchy transform, a Wiener-Hopf problem and a Riemann-Hilbert problem.

The starting point for many problems of this kind is the Cauchy integral

$$f(z) = \frac{1}{2\pi i} \int_{\Gamma} \frac{h(t)}{t-z} dt,$$
 (23.1)

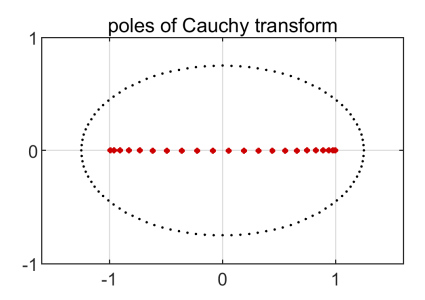
which appeared as (22.6) in the last section. Here Γ is a smooth bounded contour that may be open or closed, and we assume h is Hölder continuous. The formula implies that f is analytic for $z \in \mathbb{C} \cup \{\infty\} \setminus \Gamma$, with $f(\infty) = 0$. If Γ is a closed contour, then it divides the plane into two components, on which f will normally take different analytic branches with Γ as a branch cut between them. If Γ is open, then $\mathbb{C} \cup \{\infty\} \setminus \Gamma$ is connected, and f is a single-valued analytic function with Γ as an internal branch cut, typically with logarithmic singularities at the endpoints.

A key mathematical result associated with (23.1) goes by the name of the Sokhotski-Plemelj formulas. The first of these formulas asserts that f(z) jumps by h(t) as z crosses Γ at a point $t \in \Gamma$ (not an endpoint). This is written as

$$h(t) = f_{+}(t) - f_{-}(t),$$
 (23.2)

where f_+ denotes f as defined by (23.1) on the left of Γ and f_- is the same on the right. ("Left" and "right" are defined with respect to the orientation of Γ .) The other Sokhotski-Plemelj formula states that for $t \in \Gamma$, we have

$$f(t) = \frac{1}{2}(f_{+}(t) + f_{-}(t)), \tag{23.3}$$



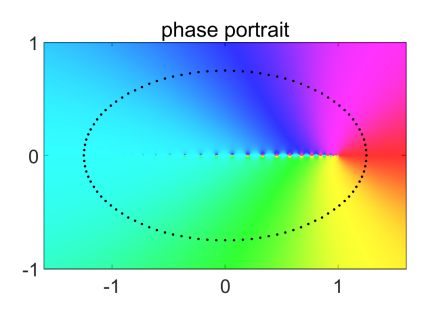


Figure 23.1. The Cauchy transform of $h(t) = e^{3t}$ on $\Gamma = [-1, 1]$ is computed by evaluating the integral (23.1) at 100 points on an ellipse by adaptive quadrature and then approximating the result by a AAA rational function. The approximation has degree 22, with little asymmetry in the pole positions (10 poles in [-1,0], 12 poles in [0,1]) but a strong asymmetry in their strengths as revealed by the phase portrait.

where f(t) is defined for $t \in \Gamma$ by the *principal value* of (23.1). A careful and detailed reference on these topics is (Henrici (1986)).

As discussed in the last section, the map from h to f defined by (23.1) is called the Cauchy transform. The application of AAA approximation to the numerical computation of Cauchy transforms was proposed in (Horning and Trefethen (submitted)). Figures 22.1–22.3 presented examples from that paper involving AAA approximation of Cauchy transforms that are known analytically: $\log((z+1)/(z-1))$ outside an interval or 0 and 1 on two sides of a closed curve (both divided by $2\pi i$). But AAA can also treat problems that are fully numerical, and section 5 of (Horning and Trefethen (submitted)) illustrates these too. Suppose, for example, we want a rational approximation to the Cauchy transform of $h(t) = e^{3t}$ on $\Gamma = [-1,1]$. The following lines evaluate (23.1) at 100 points on a Bernstein ellipse surrounding [-1,1] using the Matlab adaptive quadrature code quadgk and then compute a AAA approximation to the usual 13-digit relative accuracy. The result is shown in Figure 23.1.

We noted above that the Cauchy transform f takes the value $f(\infty) = 0$. When f is approximated by a rational function r by standard AAA, the algorithm does not enforce this constraint, though the analytic structure of the problem is likely to make it hold approximately: in the example of Figure 23.1, we have $|r(\infty)| < 10^{-15}$. The possibility of computing approximants

that are constrained to be zero at ∞ is discussed at the end of section 32. As a practical matter, so long as the aim is near-best as opposed to truly best approximation, one can often approximate a function without a condition at ∞ and then subtract the constant $r(\infty)$ from the result.

Many applications of (23.1) involve situations where Γ is a real interval, in which case h is often assumed to be real too. Often h(t)dt is replaced by a nonnegative measure $d\mu(t)$ that can include point masses. (At such points (23.2) and (23.3) will not make sense.) With $\Gamma = (-\infty, 0]$ this leads to Stieltjes functions, and with $\Gamma = [a, b]$ one gets Markov functions. Finite intervals arise in quadrature problems, as discussed in the last section. In these cases the Cauchy transform is normalised differently and renamed the Stieltjes or Markov-Stieltjes transform.

A context in which infinite intervals in (23.1) arise is in certain problems of Wiener-Hopf factorisation. In the simplest scalar additive Wiener-Hopf problem, one has a function h(t) defined for $t \in \mathbb{R}$ and the aim is to write it as a sum $h(t) = f_+(t) + f_-(t)$ of functions analytic in the upper and lower half-planes \mathbb{C}_+ and \mathbb{C}_- , respectively. We assume $h(t) \to 0$ as $|t| \to \infty$. According to (23.2), this problem is solved by (23.1) with the adjustment that we need to flip the sign of f_- . In a multiplicative Wiener-Hopf problem, it is the same except that one wants a representation as a product $h(t) = g_+(t)g_-(t)$. If h(t) > 0 for all $t \in \mathbb{R}$, then the multiplicative Wiener-Hopf problem for h reduces to the additive Wiener-Hopf problem for h reduces to the additive Wiener-Hopf problem for h

Starting in 2021, we have explored AAA approximation for a few Wiener-Hopf problems, but there is no publication as yet. We illustrate the idea here by computing the additive Wiener-Hopf decomposition of $h(t) = e^{-|t|}$ on \mathbb{R} . First we set up a grid, exponentially clustered at t=0 in view of the singularity there, and apply AAA to approximate h on the grid by a rational function r to accuracy 10^{-10} . What we need at this stage are the poles of r, which are plotted in Figure 23.2, and the corresponding residues. (We discard a couple of poles that AAA returns on the real line, which are Froissart doublets with negligible residues.)

```
h = @(t) exp(-abs(t));
T = logspace(-10,10,200)'; T = [T; -T];
[~,pol,res] = aaa(h(T),T,'tol',1e-10);
jj = find(imag(pol)==0); pol(jj) = []; res(jj) = [];
```

We then need to split r into its components analytic in \mathbb{C}_+ and \mathbb{C}_- . We do this by reconstructing it from its poles and residues in each half-plane:

```
p = pol.';
ii = (imag(p)>0); p1 = p(ii); p2 = p(~ii);
res1 = res(ii).'; res2 = res(~ii).';
f1 = @(z) reshape(sum(res1./(z(:)-p1),2),size(z));
f2 = @(z) reshape(sum(res2./(z(:)-p2),2),size(z));
```

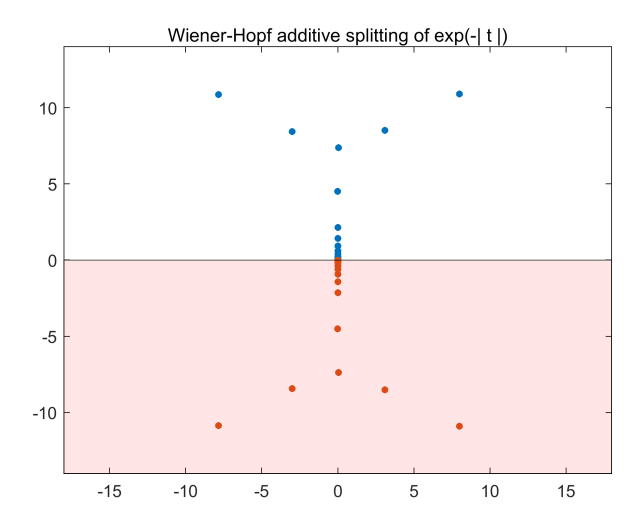


Figure 23.2. Poles of a AAA rational approximation to $h(t) = e^{-|t|}$ for $t \in \mathbb{R}$. To decompose h approximately into $f_+ + f_-$, the contributions from the poles above and below the real axis are separated. Here there are 41 poles in each half-plane and the combination gives ten-digit accuracy.

A check of accuracy shows a maximal error $|h(t_j) - (f_+(t_j) + f_-(t_j))|$ of $2.1 \cdot 10^{-10}$ over the sample grid. The computation takes about 0.1 s on our laptop.

It is interesting to try to explain the forked structure of the distribution of poles in Figure 23.2. In the terminology of the final paragraph of section 12, we believe this figure shows a mix of branch cut poles along the imaginary axis near t=0 and approximation poles further out.

We are Wiener-Hopf amateurs, but among the experts there is awareness of rational approximation as a useful tool (Kisil (2013)). A survey of constructive aspects of Wiener-Hopf problems can be found in (Kisil, Abrahams, Mishuris and Rogosin (2021)), and AAA approximation is used to treat a Wiener-Hopf problem on the unit circle in (Nethercote, Kisil and Assier (2023)). Whether rational approximations can be used to treat matrix-valued Wiener-Hopf problems is unknown.

Wiener-Hopf problems are a special case of $Riemann-Hilbert \ problems$, in which arbitrary linear jump conditions are applied across a contour $\Gamma \subset \mathbb{C}$ that is generally not just the real line or unit circle. As early as 2020, Costa proposed in the final sentence of Costa (2020) that AAA should be effective for solving certain Riemann-Hilbert problems, but so far as we know, not much has yet been done in this direction. As encouragement to further work we will show just one example. Suppose we want to find functions f_+ and f_- analytic inside and outside the 3-lobed curve Γ of Figure 23.3,

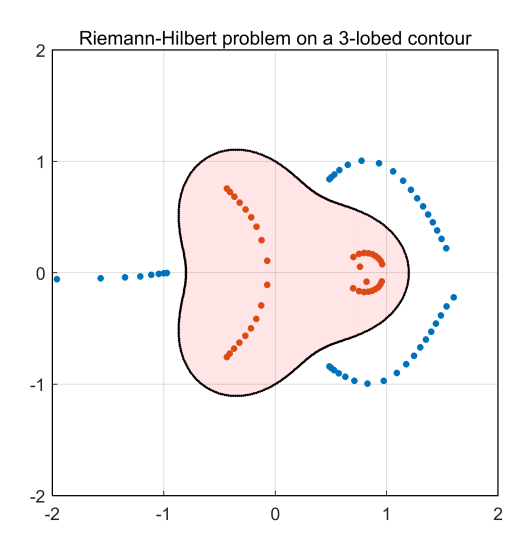


Figure 23.3. Poles for a rational approximation to solve a Riemann-Hilbert problem involving splitting of the function (23.4) on a 3-lobed contour. Piecing together rational approximations to f_+ and f_- from the poles outside and inside, respectively, solves the problem to 6 digits of accuracy.

respectively, that satisfy the jump condition

$$f_{+}(t) - f_{-}(t) = g(t) = \cos(\exp(3\operatorname{Re}(t)))$$
 (23.4)

on Γ with the normalisation $f_{-}(\infty) = 0$. We carry out AAA approximation as usual, but instead of outputting poles and residues as in the last example we just take the poles, because the residues will have to be computed separately as we shall explain. The poles are plotted in Figure 23.3.

```
Z = exp(2i*pi*(1:400)'/400);
Z = Z.*(1+.2*cos(3*angle(Z)));
g = @(z) cos(exp(3*real(z)));
[~,pol] = aaa(g(Z),Z); pol = pol.';
```

To compute residues, we solve a least-squares problem. This is what the code aaa.m does too, internally (see footnote 4), but there, a constant term is included in the least-squares fit. Here, we must omit the constant term to end up with a fit with $r(\infty) = 0$:

```
A = 1./(Z-pol); c = A\backslash g(Z); res = c.';
```

Now we split r into two pieces r_+ and r_- as before. The accuracy is $6.8 \cdot 10^{-7}$ in this example.

```
inpoly = @(z,w) inpolygon(real(z),imag(z),real(w),imag(w));
ii = inpoly(pol,Z);
```

```
fp = @(z) reshape(sum(res(~ii)./(z(:)-pol(~ii)),2),size(z));
fm = @(z) reshape(-sum(res(ii)./(z(:)-pol(ii)),2),size(z));
err = norm(fp(Z)-fm(Z)-g(Z),inf)
```

24. Laplace problems and AAA least-squares

We are now at a transition point of this paper. The last 21 sections have explored problems in which data are given that we wish to approximate by a rational function. For the next four sections, data are given that we wish to approximate by the *real part* of a rational function. This is an entirely different problem, and the breakthrough came with a paper published by Stefano Costa in 2020 (Costa (2020)).

It will take a couple of pages to explain. We start with the observation that the real part of an analytic function is harmonic, i.e., a solution to the Laplace equation $\Delta u=0$. In the other direction, given a harmonic function u(z) in a planar domain Ω , is it the real part of an analytic function f(z)=u(z)+iv(z)? The answer is yes if Ω is simply-connected, and the harmonic conjugate v is uniquely determined up to an arbitrary additive constant. If Ω is multiply connected, then one only needs to generalise the result slightly by allowing f to have a logarithmic term in each hole. This is the logarithmic conjugation theorem, originating perhaps in (Walsh (1929)), which we reproduce in the words of (Axler (1986)) since this basic result is not as well known as it should be. Its consequence is that the methods to be discussed here and in the next three sections generalise readily to multiply-connected geometries.

Theorem 24.1. Logarithmic Conjugation Theorem. Suppose Ω is a finitely connected region, with K_1, \ldots, K_N denoting the bounded components of the complement of Ω . For each j, let a_j be a point in K_j . If u is a real valued harmonic function on Ω , then there exist an analytic function f on Ω and real numbers c_1, \ldots, c_N such that

$$u(z) = \text{Re} f(z) + c_1 \log |z - a_1| + \dots + c_N \log |z - a_N|$$
 (24.1)

for every $z \in \Omega$.

It is also known that analytic functions can be approximated by polynomials. Specifically, if f is analytic in the closure of a simply-connected bounded domain, then it can be approximated by polynomials with exponential convergence as a function of degree n, and if the domain has holes, then the same is true so long as additional polynomials are included involving reciprocal powers at an arbitrary point in each hole. This is Runge's theorem (Runge (1885)).

For simplicity we will confine the remaining discussion to the simply-connected case of a Dirichlet problem on a Jordan domain Ω bounded by a

contour Γ . The aim is to find a function u satisfying

$$\Delta u(z) = 0, \ z \in \Omega, \quad u(z) = h(z), \ z \in \Gamma, \tag{24.2}$$

where h is a given real continuous function. A unique solution exists, as can be proved by transplanting the problem to the unit disk by the Riemann mapping theorem and applying the Poisson integral formula. Variations such as Neumann or mixed boundary conditions are easily treated by the same methods we shall describe.

In view of the results summarised above, it is not surprising that an old idea for solving (24.2) is to represent u, to sufficient accuracy, as the real part of a polynomial or a rational function that is pole-free in Ω . Thanks to the maximum principle for harmonic functions, one only needs to approximate on Γ , and the result will be accurate throughout Ω . This vision was pursued by Joseph Walsh and his student John Curtiss (Walsh (1929), Curtiss (1962)). Numerical analysis and computers were not advanced enough for their attempts to be relevant computationally, but in the polynomial case, such methods are now eminently practical if coefficients are determined by least-squares fitting (Trefethen (2018)). For complicated domains, it is important to use a well-conditioned basis, as can be computed by Vandermonde with Arnoldi orthogonalisation (Brubeck et al. (2021)).

The approximation to u is not a polynomial: it is the real part of a polynomial. To fit the boundary function h by means of a polynomial of degree n, therefore, one does not have n+1 real parameters to determine, but 2n+1 real parameters corresponding to real and imaginary parts. If m sample points $\{z_j\}$ are distributed along Γ , this will lead to an $m \times (2n+1)$ matrix whose columns correspond to 1 and to the real and imaginary parts of the powers $z_j, z_j^2, \ldots, z_j^n$. This is in the monomial basis; on an interval one would use Chebyshev polynomials, and on a general domain the basis would be constructed by Vandermonde with Arnoldi orthogonalisation.

All of this is excellent except that polynomials fail in two cases, as mentioned in the final paragraph of section 3 and discussed at length in (Trefethen (2024)). First, if u has a singularity on Γ , which will usually be the case if Γ has a corner or h itself is singular, then the polynomial convergence rate falls from exponential to algebraic, and obtaining more than 2 or 3 digits of accuracy typically becomes difficult. Of course, polynomials also have trouble when there are singularities near Γ but not exactly on it. Rational approximations, by contrast, can achieve root-exponential convergence despite the presence of branch point singularities (Newman (1964), Gopal and Trefethen (2019c)). Second, if Ω is nonconvex, as illustrated in the example of Figure 12.5, then polynomials may converge exponentially in asymptotic theory but at a rate so low that in practice their convergence is again just algebraic. The asymptotic convergence rate scales as $\exp(-\pi L)$, where L is the aspect ratio of a nonconvex indentation of Ω (Trefethen 2024,

sec. 7). For example, in a Laplace problem on an inverted ellipse of parameter $\rho=1.2$ (reciprocal of a Bernstein ellipse), the polynomial degree will have to be increased asymptotically by about 430,000 for each additional digit of accuracy (Trefethen 2024, Table 1). Rational approximations, by contrast, can converge very fast because they can place poles in the inlets, as in Figure 12.5 and Table 12.1.

Thus there are potentially huge advantages if rational functions rather than polynomials are used to solve Laplace problems. Before AAA, the main paper we are aware of that explores this possibility is (Hochman, Leviatan and White (2013)), which presents very impressive results confirming the power of rational functions. The challenge is, how to compute them? This is not rational approximation of the kind accomplished by AAA, because only the real part of f is known. Or to put it another way, AAA can approximate the real function h(z) on Γ , but the resulting approximation will be real on Γ , to the approximation tolerance, and it will achieve this by having poles inside Γ as well as outside, making it useless for solving the Laplace problem.

So one is left with the problem of where to put poles outside Γ for a good approximation, which Hochman, et al. interpret as an example of the Method of Fundamental Solutions (MFS) (Doicu, Eremin and Wriedt (2000), Fairweather and Karageorghis (1998)). (Their extensive introduction, with many references, is very much worth reading.) They propose an iterative process of pole-adjustment which is successful in a number of examples, but lacks the easy speed and reliability of AAA.

During 2016–2020, we had the AAA algorithm but could not see a way to use it to approximate real harmonic functions as opposed to complex analytic ones. Instead, in this period the second author and Gopal devised the lightning Laplace method for solution of Laplace problems dominated by corner singularities, in which poles are clustered exponentially at preassigned positions near each corner in the manner established as effective by theory and experiment (Gopal and Trefethen (2019c), Trefethen et al. (2021)). The poles are placed in an a priori fashion, independently of the right-hand-side h, making this essentially a linear method that reduces to matrix least-squares problems. (See Figure 27.1 for an illustration of lightning pole clustering.) It easily solves Laplace problems of this kind to high accuracy, and software is available at (Trefethen (2020a)). In (Gopal and Trefethen (2019c)), theorems are developed establishing that exponentially clustered poles, together with a low-degree polynomial, can resolve general

⁹ This does not seem to have been Walsh's perspective. He considered rational functions more because they are a natural extension of polynomials, and because they are needed for regions with holes, than because of their superior approximation properties, which he may not have been very aware of—perhaps unsurprisingly in that pre-numerical era.

Laplace problems with any finite number of branch point singularities with root-exponential convergence.

The challenge, however, was to find a AAA-style method to work automatically on arbitrary regions, and the new idea came in a paper posted on arXiv in 2020 by Stefano Costa (Costa (2020)). Costa's original AAA-least squares (AAALS) method, described also in (Costa and Trefethen (2023)), is as follows. (In a moment we will modify it by changing poles to double poles and then optionally compressing the final result by a further AAA approximation.)

- 1 Use AAA to approximate h by a complex rational function r on Γ ;
- 2 Compute the poles of r, and discard those inside Γ ;
- 3 Use linear least-squares to fit h by the remaining poles outside Γ .

If r has n poles $\{\pi_k\}$ outside Γ and there are m sample points $\{z_j\}$ on Γ , the least-squares fit will involve a matrix of dimension $m \times (2n+1)$, with one column corresponding to the constant 1 and the others corresponding to $\text{Re}(1/(z_j-\pi_k))$ and $\text{Im}(1/(z_j-\pi_k))$. For better numerical stability when poles cluster near the boundary Γ , it is better to rescale the columns via $\text{Re}(d_k/(z_j-\pi_k))$ and $\text{Im}(d_k/(z_j-\pi_k))$, where $d_k=\min_j|z_j-\pi_k|$. As mentioned above, sometimes a few columns are added to the matrix corresponding to a low-degree polynomial, whether expressed in a monomial, Chebyshev, or Vandermonde with Arnoldi basis. For an analysis of the sometimes surprisingly great power of low-degree polynomial additions to rational function approximations, see (Herremans, Huybrechs and Trefethen (2024)).

Like the lightning Laplace method, the AAALS method produces a solution to a Laplace problem in the form of the real part of a single rational function, typically evaluable on a laptop in a matter of microseconds per point. The function is globally analytic throughout Ω , so there are no derivative discontinuities of the sort one would find with finite elements or with integral representations evaluated adaptively. Another appealing feature of these methods is that the harmonic conjugate, being just the imaginary part of the same rational function, is available for free. In applications, the harmonic conjugate is usually of physical interest, representing flow lines of heat, charge, ideal fluid, or probability orthogonal to the equipotential lines of the original Laplace problem.

Let us illustrate how AAA works for a simple problem, shown in Figure 24.1. We define the domain and the boundary function like this:

```
t = 2*pi*(1:500)'/500;
r = 1 + sin(4*t)/4;
Z = r.*exp(1i*t);
h = @(z) exp(real(z));
```

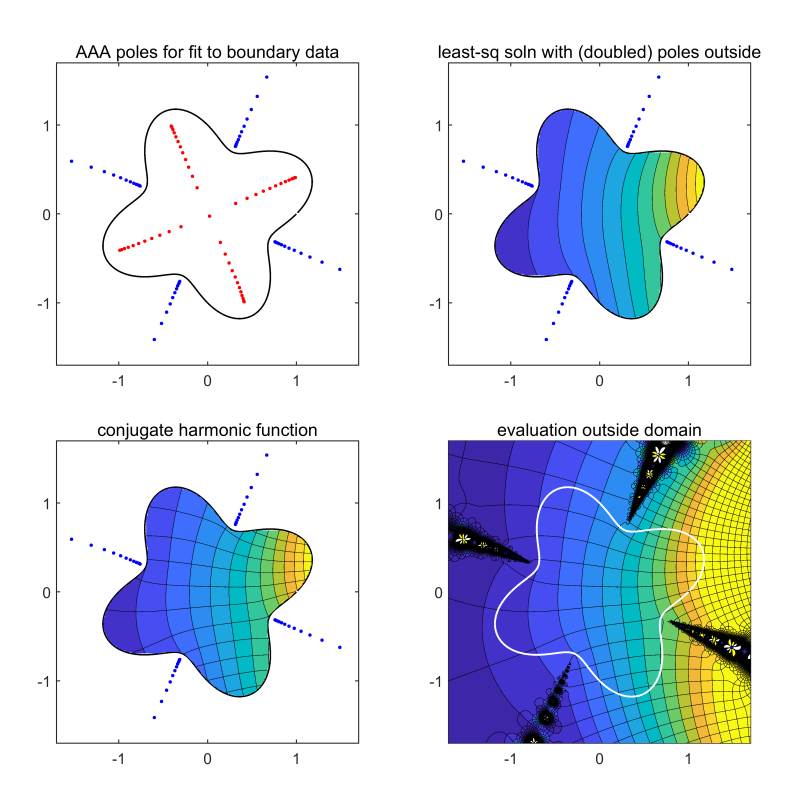


Figure 24.1. Illustration of AAA-least squares (AAALS) for a Laplace Dirichlet problem on a smooth nonconvex domain Ω with boundary data $h(z) = \exp(\text{Re}(z))$. First h is approximated by a complex rational function r with poles inside and outside Ω . The poles inside are discarded, and the poles outside are taken as the locations of 2nd-order poles for a least-squares fit to h by the real part of a rational function of degree 114. In this example 12-digit global accuracy is achieved in about 1/4 second on a laptop; we estimate the value at the centre as $u(0) \approx 1.2157681370405$. The same accuracy with a polynomial fit would require a degree in the thousands, which would increase to millions for slightly deeper indentations.

A complex rational AAA fit is then computed to the boundary data, which turns out to have degree 105:

```
[r,pol] = aaa(h(Z),Z,'mmax',300);
```

This rational function has 48 poles inside Ω and 57 outside. The inner poles are discarded and the outer ones are retained for a least-squares fit.

```
inpoly = @(z,w) inpolygon(real(z),imag(z),real(w),imag(w));
ii = inpoly(pol,Z); p = pol(~ii).';
```

From here, if we proceed as described above, we will fit h(z) by the real

part of a rational function of degree 57, and the maximum absolute error (measured a posteriori on a finer grid) will be $6.6 \cdot 10^{-8}$. This improves to $5.0 \cdot 10^{-13}$, however, if we use a modification of the original AAALS method in which instead of simple poles, we fit with double poles, following a rationale to be explained in a moment along with a potential further improvement. The code looks as follows. We find a vector c of fitting coefficients by solving a 500×230 matrix least-squares problem. This vector is then used to construct function handles for the approximate solution u, its harmonic conjugate v, and the analytic combination f = u + iv.

A curious fine point is that the matrix A is of dimensions 500×230 , not 500×229 , as one of its columns (the 116th) is the imaginary part of 1, namely 0. Thus A has infinite condition number, raising questions about the associated least-squares problem. As it happens, the Matlab backslash operation ignores such columns (Moler 2004, sec. 5.7), so we have not found it necessary to remove them explicitly from our matrices.

The third panel of Figure 24.1 shows level curves of the conjugate function v(z), making an orthogonal net in the problem domain as always with Laplace problems. The fourth panel extends the colours and contour lines of the rational approximation $\operatorname{Re}(r(z))$ outside the domain. This is not the same as an analytic continuation of u(z) itself, which would be multivalued, but one sees that u(z) must have branch points in the four indentations. A plot like this highlights the difference between solving PDEs by rational approximation and by integral equations. With integral equations—a highly advanced subject computationally—the name of the game is to compute the unique single- and/or double-layer density functions on the boundary Γ that generate the solution in the interior (Kress (1989)). This necessitates accurate representation of the density functions followed by accurate calculation of an integral whenever the solution is to be evaluated in Ω . With rational functions, the solution is represented by poles outside the boundary rather than charge distributions along the boundary. The poles and residues are numerically non-unique, and evaluation of u(z) for $z \in \Omega$ is just a matter of adding them up. Rational approximation methods for PDEs are thus a variant of the Method of Fundamental Solutions (MFS) (Doicu et al. (2000), Fairweather and Karageorghis (1998)) in which the singularity locations are chosen with exceptional efficiency, which ordinarily is such a big challenge

for these methods that it is probably the main reason why they have not been more widely used (Barnett and Betcke (2008)).

No theory has yet been developed for AAALS beyond a couple of theorems in (Costa and Trefethen (2023)) applying just on a disk or a half-plane together with counterexamples there showing that the method does not always work. However, here is our understanding of why it usually works in practice. In typical Laplace problems involving boundaries with corners or indentations, most of the difficulty is geometry-driven rather than data-driven in the sense that the singularities of the solution being computed, when analytically continued outside Ω , are essentially those of the Schwarz function for Ω , as discussed in section 11; see (Trefethen (2024)). (Indeed, the results come out much the same if aaa(h(Z),Z) above is changed to aaa(conj(Z),Z).) The poles chosen by the AAALS method are thus adapted to the function that needs to be approximated.

An important challenge for the next few years is to make this rigorous and develop a true theory of AAALS solution of Laplace problems.

We can now explain our understanding of why it may be advantageous to use poles of order 2 instead of 1 in the least-squares fit, while emphasising that solid understanding of how AAALS works and how to optimise it is not yet available. One might imagine that this compensates for the fact that about half the poles have been thrown away, those inside Γ , but we believe the actual logic is different. In fact, we think a more accurate view may be that the doubling of the poles compensates for the "factor of 2" discussed in section 12 in connection with the transition from (12.2) to (12.3) and the green and yellow dots in the figures of that section. From ordinary potential theory involving the function (12.2), one gets a certain accuracy that is on the order of half that of the AAA approximation $r \approx h$ on Γ . There would exist some very slightly perturbed choice of poles, corresponding to a best harmonic approximation of u, for which this accuracy could be doubled. However, the AAA-LS rational approximation does not provide this appropriate perturbation of the poles. Instead, we explicitly double the number of poles, yielding an approximation with more or less the accuracy associated with an optimal approximation of degree n—but it is actually a rational function of degree 2n.

Thus AAA-LS with pole doubling tends to provide a solution of degree 2n whose accuracy may approximate that of an optimal solution of degree n. We can optionally exploit this connection by taking the computed solution, together with its computed harmonic conjugate so that we have a computed analytic function, and then re-approximating it by AAA, perhaps with the tolerance slightly loosened. (This idea is due to Stefano Costa.) For the present example we can do this with the code

```
f2 = aaa(f(Z),Z,'tol',1e-12);
```

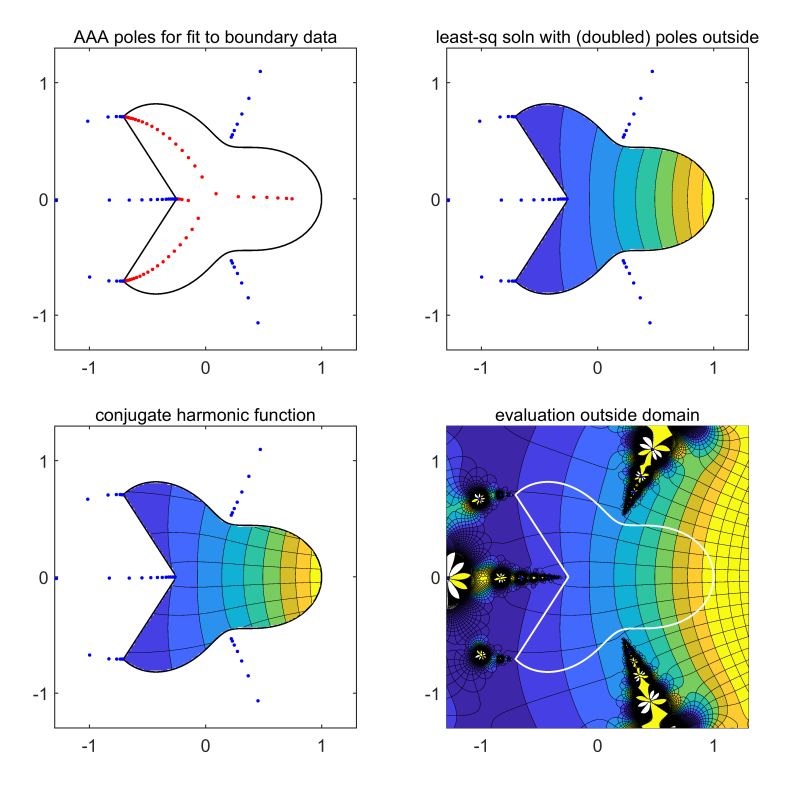


Figure 24.2. Repetition of Figure 24.1 for a harder problem with both corner singularities and nonconvexity. The global accuracy is about 7 digits, and the value at the centre is $u(0) \approx 1.081415507437$.

```
u2 = 0(z) real(f(z)); v2 = 0(z) imag(f(z));
```

The result is an approximation with about the same accuracy as before but degree now 54 instead of 115.

We close this section with another figure like Figure 24.1, but for a more difficult domain mixing both corners and inlets, as defined by this code:

```
s = tanh(linspace(-12,12,1000)');
r = 1 - .5*sin(pi*s).^2;
z = -.25 + (exp(-3i*pi/4)+.25)*(s+1)/2;
Z = [z; exp((3i/4)*pi*s).*r; flipud(conj(z))];
```

The tanh(linspace(...)) construction clusters sample points exponentially near corners. In view of the corner singularities, the AAA relative tolerance is loosened to 10^{-8} , and the absolute accuracy of the solution u comes out as about $5 \cdot 10^{-8}$. The computation takes 3 s because the boundary grid has 3000 points. This could probably be speeded up by switching to the continuum AAA algorithm (section 30).

Since its introduction, the AAALS method has been applied by a number of authors to quite a few problems involving interior, exterior, and coupled domains, as well as for variations on the Laplace equation as we will mention in the upcoming sections. For example, see (Costa, Costamagna and Di Barba (2024), Harris, Palmer and McDonald (2025), Harris and Mc-Donald (2025b)), where problems with matching conditions across interfaces are treated. A doubly-connected geometry is treated in (Harris and McDonald (2025a); another can be found in Figure 25.3. A particularly simple variation concerns Poisson problems with simple right-hand sides, such as $\Delta u = C$ for a constant C. Here, one can subtract off a known function like $u = C(x^2 + y^2)/4$ with the desired Laplacian (Harris and McDonald (2023)), and what remains is a Laplace problem. Computing Green's functions can follow the same pattern with subtraction of a point singularity $\log |z-z_0|$, a method we shall exploit in the next section. Much the same mathematics enables AAALS to compute Hele-Shaw fluid flows as well as solutions to other moving boundary problems associated with Laplace potentials (Baddoo and Hinton (2025)).

25. Conformal mapping

Conformal mapping problems can be reduced to Laplace problems, and the AAALS method of the last section is a good way of solving them. Before illustrating this, however, we discuss a more distinctive application of rational approximation to conformal mapping. This is the matter of compactly representing a map once it has been computed, as well as its inverse, an idea put forward in (Gopal and Trefethen (2019b)).

Numerical conformal mapping is an established topic in numerical analysis; for high-level and detailed surveys, respectively, see (Trefethen (to appear)) (5 pages) and (Wegmann (2005)) (127 pages), and see also (Henrici (1986)). Many different methods appear in this field, based often on integral equations and equally often on other ideas. In the case of conformal mapping of polygons, one can take advantage of the Schwarz-Christoffel formula, whose numerical realisation is available in Driscoll's widely-used SC Toolbox in Matlab (Driscoll (2005)).

Almost every conformal mapping method maps a priori in one direction or the other: from the problem domain to the canonical domain (say, the unit disk), or from the canonical domain to the problem domain. Traditionally, one first solves the mapping problem in the given direction, typically obtaining the boundary correspondence function (BCF), the homeomorphism that maps one boundary to the other. Then one applies an auxiliary method for inverting the map, perhaps by iteration. The new observation of (Gopal and Trefethen (2019b)) was that, regardless of how the BCF may have been computed, both the a priori map and its inverse can often be represented most

efficiently by rational functions. If Z is a vector discretising one boundary and F is the corresponding vector obtained by applying the BCF to Z, then the computation of efficient representations of the conformal map and its inverse may be as simple as

```
f = aaa(F,Z); finv = aaa(Z,F);
```

at least for smooth domains. This is an example of AAA computation of inverse functions as discussed in section 7. (In mapping a domain with corners, it will probably be necessary to loosen the tolerance for reasons of ill-conditioning as well as efficiency, and additionally, one must be careful to cluster sample points near the corners and their preimages, or to let the clustering be taken care of automatically by the continuum AAA algorithm of section 30.)

For example, the following code defines the smooth cross-shaped domain shown in the top row of Figure 25.1 and then invokes the conformal command of Chebfun, which computes the BCF of a domain onto the unit disk by means of a discretisation of the Kerzman-Stein integral equation (Kerzman and Trummer (1986)):

```
C = chebfun('exp(pi*1i*t)*(1+.4*cos(4*pi*t))','trig');
C = real(C) + .7i*imag(C);
tol = 1e-10;
[f,finv] = conformal(C,'plots','tol',tol);
```

The figure shows conformally equivalent nets of orthogonal contours in the two domains. As a sample value we have $f(1) \approx 0.984313068276404$, accurate we believe to these 15 digits. What is notable about this figure for our purposes, however, are the poles plotted as red dots outside each boundary, whose numbers are indicated in the titles. The conformal code has called AAA twice and found that the map can be represented to the prescribed tolerance by a rational function of degree 74 in the direction from the cross to the disk, and by another rational function of degree 54 in the direction from the disk to the cross. Each of these maps can be evaluated on our laptop in less than 1 μ s per point, and since the representations utilise global rational functions, no numerical discontinuities will appear even if one or more derivatives are taken. Note that although the smooth cross contour is analytic, its nonconvexity is such that poles of f come as close as 0.024 to the boundary; likewise the poles of f^{-1} come as close as 0.0008 to the unit circle. It follows that polynomial representations of these maps would require degrees in the tens of thousands to get a few digits of accuracy (Trefethen (2024)). Conformal mappers refer to such distortions as the "crowding phenomenon," which makes certain numerical methods terribly inefficient but is circumvented by the strategic placement of poles of

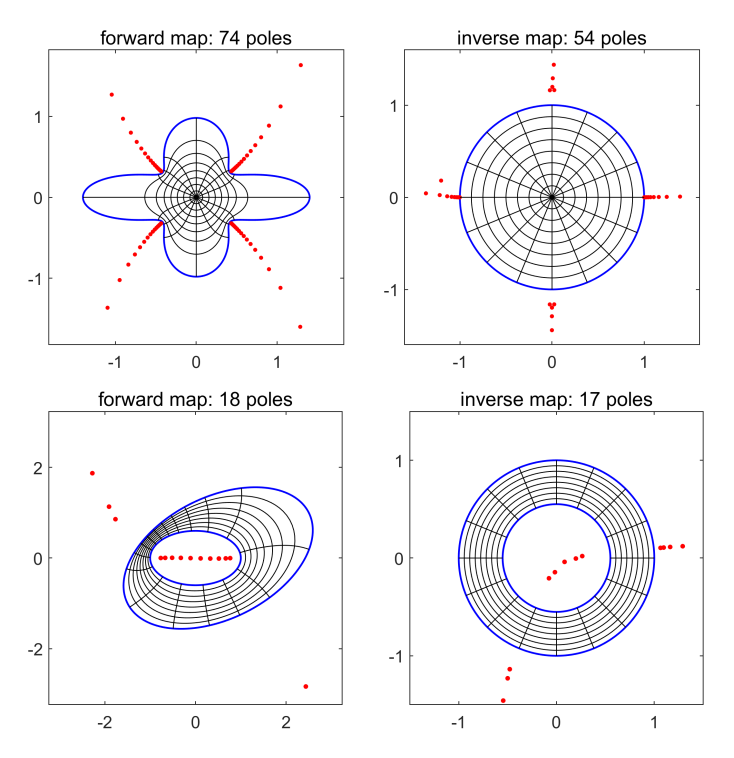


Figure 25.1. First row: conformal map computed by Chebfun conformal from a smooth cross-shaped domain to a disk, and its inverse. Each map is represented to 9-digit accuracy by a rational function obtained by AAA, and can be evaluated in about $0.5~\mu s$ per point. Second row: doubly-connected conformal map computed by Chebfun conformal2 and its inverse. Each map is represented to 7-digit accuracy by a rational function obtained by AAA, and can be evaluated in about $0.1~\mu s$ per point.

near-best rational approximations. See (Wegmann (2005)) and (Gopal and Trefethen 2019b, Thms. 2–5).

The second row of Figure 25.1 shows the same kind of image, but for a doubly-connected domain mapped with the Chebfun conformal2 command (based on series expansions as in (Trefethen (2018))) by this code:

```
circle = chebfun('exp(1i*pi*z)', 'trig');
ellipse2 = real(circle) + .6i*imag(circle);
ellipse1 = (2+1i)*ellipse2 + .5;
[f,finv,rho] = conformal2(ellipse1,ellipse2,'plots');
```

For a doubly-connected domain like this, the circular annulus image has a uniquely determined ratio of inner to outer radii, known as the *conformal modulus* of the domain. Although conformal2 with its default tolerance

has pointwise accuracy of just about 10^{-7} for this problem, numerical explorations suggest that the computed modulus $\rho \approx 0.55098544815237$ is accurate to 15 digits.

We now turn to the other connection of rational approximation with conformal mapping, the use of AAALS to compute a map by solving a Laplace problem, an idea that was first suggested in (Costa (2020)) and is discussed more extensively in (Trefethen (2020b)). We start with the basic case of the conformal map f of a Jordan domain Ω containing the origin to the unit disk, with f(0)=0 and f'(0)>0. Following an old idea presented for example in (Henrici 1986, Theorem 16.5a), we note that $g(z)=\log(f(z)/z)$ is a nonzero analytic function on Ω with real part $-\log|z|$ on the boundary Γ . If we write g(z)=u(z)+iv(z), where u and v are harmonic functions, then u is the solution of the Laplace Dirichlet problem

$$\Delta u = 0, \ z \in \Omega, \quad u(z) = -\log|z|, \ z \in \Gamma$$
 (25.1)

and v is its harmonic conjugate in Ω with v(0) = 0. This implies

$$f(z) = ze^{u(z)+iv(z)},$$
 (25.2)

so a solution to (25.1) solves the conformal mapping problem. Note that, following a remark at the end of the last section, $u(z) + \log |z|$ is the Green's function of Ω with respect to the point z = 0, so f is essentially the exponential of the Green's function.

For example, the following code computes the map of the upper row of Figure 25.1 to about 15 digits of accuracy in half a second on our laptop, which is about ten times faster than the Chebfun conformal code that was used to generate that figure. First we apply AAA to approximate $-\log|z|$ on a 600-point discretisation of the boundary.

```
C = chebfun('exp(pi*1i*t)*(1+.4*cos(4*pi*t))','trig');
C = real(C) + .7i*imag(C);
Z = C(-1 + 2*(1:600)'/600);
U = -log(abs(Z));
[r,pol] = aaa(U,Z,'mmax',300,'tol',1e-10);
```

Then we discard the poles in the domain and use AAALS as in the last section to solve the Laplace problem. The computed map f gives the same value $f(1) \approx 0.984313068276404$ as before.

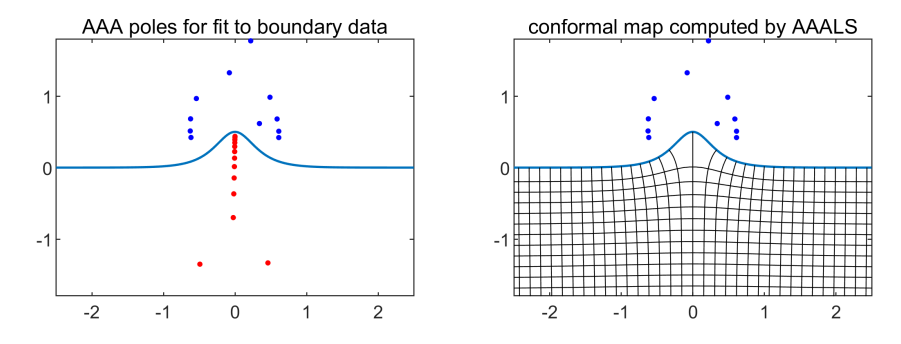


Figure 25.2. Conformal map onto a half-plane computed by AAALS.

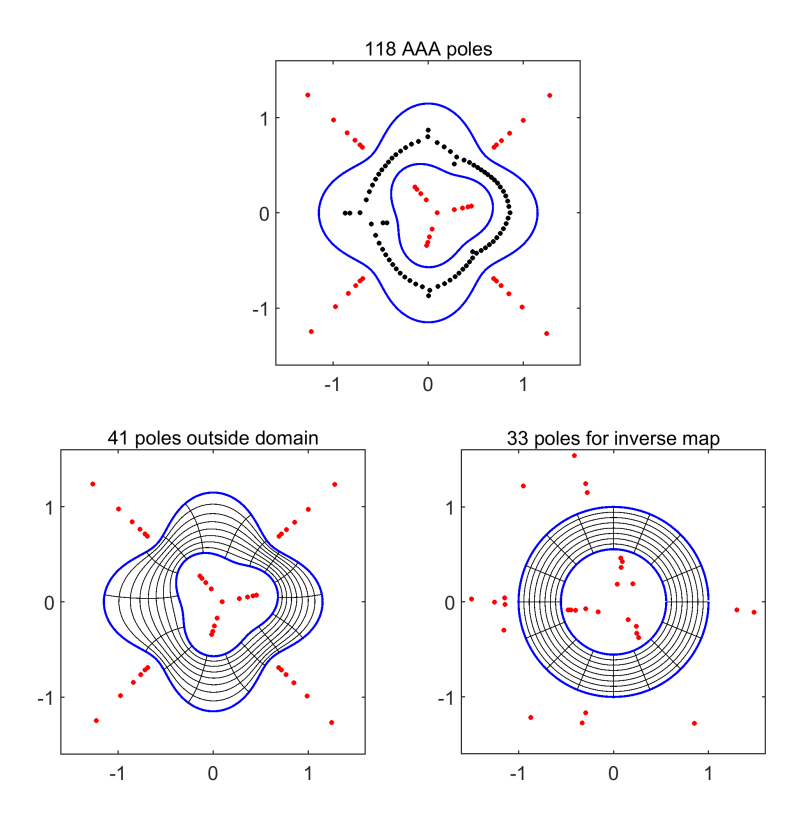


Figure 25.3. Doubly-connected conformal map computed by AAALS.

```
g = Q(z) g1(z) - 1i*imag(g1(0));

f = Q(z) z.*exp(g(z));
```

For other conformal mapping configurations, other Laplace problems become relevant. For example, Figure 25.2 shows the conformal map to the

lower half-plane of an infinite region under a curve. Without spelling out the mathematics, we list a code, below. The value f(0) comes out as $f(0) \approx -0.20646984i$.

A doubly-connected example is shown in Figure 25.3, corresponding to the code below. Again we do not explain the mathematics; see (Trefethen (2020b)). The conformal modulus comes out as $\rho \approx 0.5544210$. For higher-connectivity conformal mapping with AAA, see (McKee and Burns (2025)).

```
z = exp(2i*pi*(1:400)'/400);
c1 = z.*abs(1+.15*z.^4); c2 = .1+(.5+.1i)*z.*abs(1+.15*z.^3);
Z = [c1; c2];
[r,pol] = aaa(conj(Z),Z,'tol',1e-8,'mmax',300);
ii = inpoly(pol,c1) & ~inpoly(pol,c2); p = pol(~ii).';
H = -log(abs(Z));
rvec = [zeros(np,1); ones(np,1)];
H(np+1:2*np) = H(np+1:2*np) + 1;
A = [Z.^0 real(1./(Z-p)) imag(1./(Z-p)) rvec];
c = A\H;
logr = 1 - c(end); rho = exp(logr), c(end) = [];
u = @(z) [ ones(size(z)) real(1./(z-p)) imag(1./(z-p))]*c;
v = @(z) [zeros(size(z)) imag(1./(z-p)) -real(1./(z-p))]*c;
f = @(z) z.*exp(u(z)+1i*v(z));
```

26. Helmholtz equation and scattering

As we have mentioned, the AAALS method of section 24 can be interpreted as an application of the Method of Fundamental Solutions (MFS) (Doicu et al. (2000), Fairweather and Karageorghis (1998)) in which the locations of the singularities are chosen by rational approximation. This is a crucial improvement to the MFS, since otherwise, effective placement of singularities for problems with corners or nonconvex geometry is difficult (Barnett and Betcke (2008), Trefethen (2024), Liu (2000)).

Even before AAA was employed for the calculations, the idea had arisen

of generalising Laplace equation ideas by using rational approximations to place singularities for problems involving the Helmholtz equation,

$$\Delta u + \kappa^2 u = 0, \tag{26.1}$$

which is the basic equation of acoustics and scattering theory (seen already in (16.1)). This lightning-Helmholtz method was proposed in (Gopal and Trefethen (2019a)) in the context of "lightning" rational approximations, in which poles are positioned near corners according to an a priori exponential clustering formula rather than determined implicitly by approximation (Trefethen et al. (2021)). For further developments see (Gopal (2021), Ginn (2023)). What's different with the MFS for the Helmholtz equation is the nature of the fundamental solutions. For the Laplace equation, these are poles $1/(z-t_k)$ or their monopole counterparts $\log |z-t_k|$, both of which are solutions of the equation except at the singular point t_k .¹⁰ For the Helmholtz equation, the corresponding fundamental solutions are the complex functions

$$H_0(\kappa|z-t_k|) \tag{26.2}$$

and

$$H_1(\kappa|z-t_k|)\operatorname{Re}\left(\frac{z-t_k}{|z-t_k|}\right), \quad H_1(\kappa|z-t_k|)\operatorname{Im}\left(\frac{z-t_k}{|z-t_k|}\right),$$
 (26.3)

where H_0 and H_1 are Hankel functions of the first kind (Doicu *et al.* (2000), Rokhlin (1990)).

For general domains as opposed to domains dominated by corner singularities, one would like to upgrade the lightning-Helmholtz method to a AAA-Helmholtz method. Unpublished experiments by ourselves and Stefano Costa since August 2023 have shown that such a method can work, but there is no published literature as yet, and certainly no theory. To illustrate the method, let us repeat Figure 24.1 but now for (26.1) rather than the Laplace equation. Instead of a Dirichlet problem in the interior of the daisy, we consider a scattering problem in the exterior in which we want to calculate the time-harmonic response to a plane wave with wave number $\kappa=20$ incident from the left. Since the computational domain is the exterior, singularities will be placed in the interior. Each singularity corresponds to an outgoing circular wave for the given κ (the Sommerfeld radiation condition, imposed by employing H_0 and H_1 as above instead of their complex conjugates), and the boundary condition is that the sum of the contributions of these outward-radiating fundamental solutions must

AAA works with "dipoles," i.e., complex poles $1/(z-t_k)$. Although dipoles and monopoles $\log |z-t_k|$ are mathematically almost equivalent, since a dipole can be approximated by a pair of monopoles, so far as we know, no numerically effective algorithm has been found for approximation by monopoles.

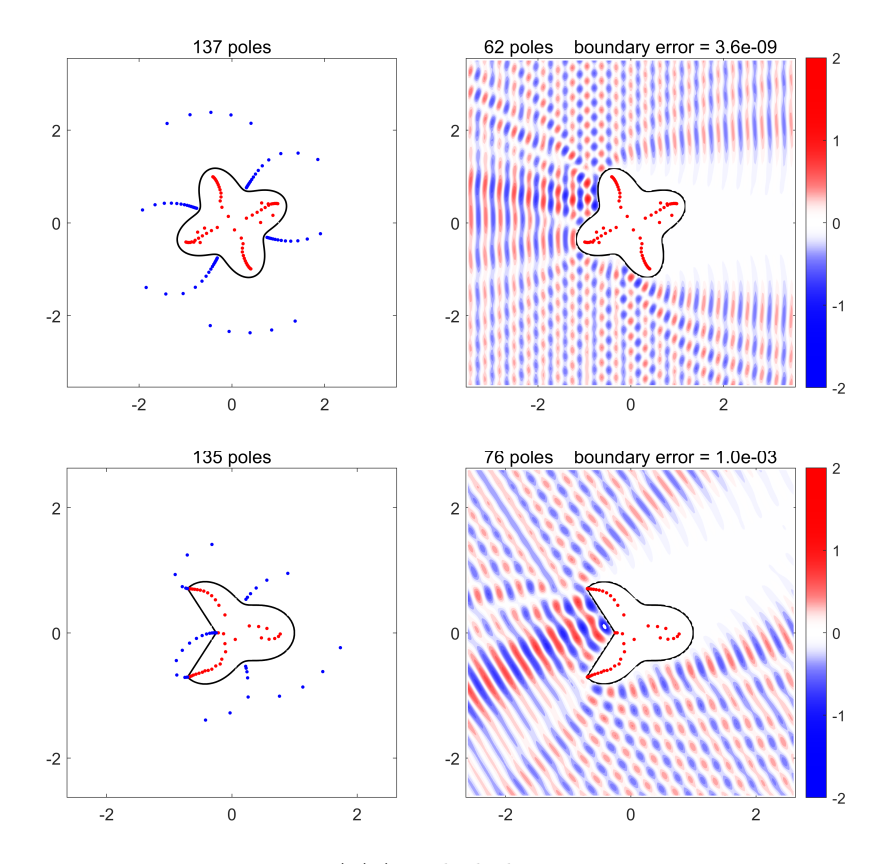


Figure 26.1. Upper row: a AAA-Helmholtz scattering computation with k=20 for the domain of Figure 24.1; the real part of the complex solution u(z) is plotted. Lower row: a similar calculation for the domain of Figure 24.2. Here the incident wave has been rotated to an angle aligned with one of the straight boundary segments, causing strong reflection in that direction—amplitudes $\approx \pm 2$ associated with constructive interference.

cancel the incident wave on the boundary (the so-called sound-soft boundary condition). This is the same principle as with the integral equation of section 16.

The opening lines of an illustrative calculation are mostly the same as before, apart from the different boundary condition:

```
t = 2*pi*(1:600)'/600;
r = 1 + sin(4*t)/4;
Z = r.*exp(1i*t);
K = 20; h = @(z) -exp(1i*real(K*z));
[r,pol] = aaa(real(h(Z)),Z,'mmax',300);
ii = inpoly(pol,Z); p = pol(ii).';
```

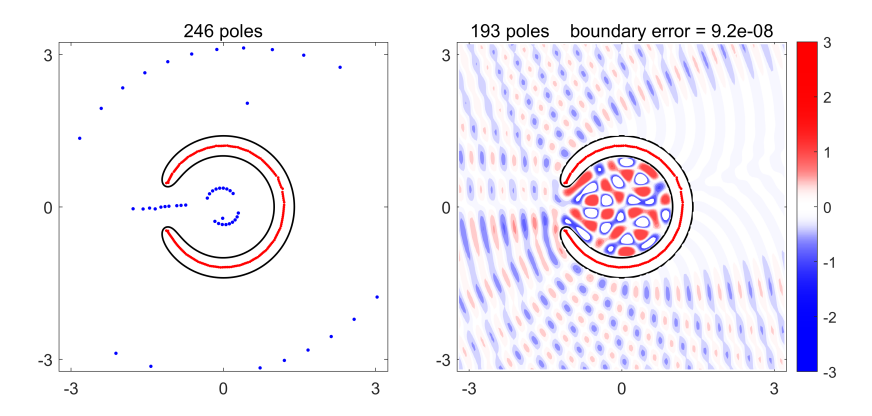


Figure 26.2. Another AAA-Helmholtz scattering computation involving a corral. The wave number has been picked to be close to a resonance for this shape, which is why the amplitudes are bigger inside the corral than outside. Compare Figure 16.1.

To complete the calculation, we employ H_0 and H_1 as indicated in (26.2)–(26.3). This example runs in about 1 s on our laptop, producing results accurate to 9 digits as shown in the first row of Figure 26.1. The second row shows a comparable experiment for a scatterer in the shape of the domain of Figure 24.2, but now the accuracy is less. Figure 26.2 shows a third experiment, now for a "corral" with an incident wave at a near-resonant frequency in the sense of section 16.

```
H0 = @(z) besselh(0,z); H1 = @(z) besselh(1,z);
P = H0(K*abs(Z-p));
Q1 = H1(K*abs(Z-p)); Q2 = (Z-p)./abs(Z-p);
A = [P Q1.*real(Q2) Q1.*imag(Q2)];
c = A\h(Z);
u = @(z) reshape([H0(K*abs(z(:)-p)) ...
H1(K*abs(z(:)-p)).*real(z(:)-p)./abs(z(:)-p) ...
H1(K*abs(z(:)-p)).*imag(z(:)-p)./abs(z(:)-p)]*c,size(z));
```

As mentioned above, there is no literature on the AAA-Helmholtz method and no solid understanding of why it works, how well it works, and how it can be made better. Can rapid convergence under certain assumptions be proved? To get more digits of accuracy, should one add low-degree series of Hankel functions, or use singularities of doubled order as we did in section 24 (involving H_2 as well as H_1), or use a AAA forcing function with artificially increased frequency, or some combination of these ideas, or something else? How competitive can this method ultimately be against the standard, highly-developed technologies of integral equations? Comprehensive research is needed to provide answers to these and other questions. For

the moment, what we can say is that the method certainly looks promising, and unpublished experiments by Costa show that it can handle considerably higher frequencies than those in the examples presented here.

27. Biharmonic problems and Stokes flow

The biharmonic equation is a fourth-order PDE, the square of the Laplace equation:

$$\Delta^2 u(z) = 0, \ z \in \Omega. \tag{27.1}$$

Two boundary conditions are normally required, which, depending on the application, would typically involve u as well as its first or second normal derivative, or perhaps both components of the gradient. The best-known applications are in 2D elasticity, where u is the transverse deflection, and in 2D viscosity-dominated fluid mechanics, known as $Stokes\ flow$, where u is the stream function (Goodier (1934)).

Since 1898, it has been known that 2D biharmonic problems can be reduced to pairs of Laplace problems. In addition to the original method of Goursat, there are also alternative reductions due to Alamansi and to Krakowski and Charnes; see (Brubeck and Trefethen (2022)) for details. In the latter paper, which was written before AAALS was developed, Stokes problems are solved by rational functions with the Goursat reduction using the lightning method mentioned in section 24.1. An example is reproduced in Figure 27.1, showing resolution to 10 digits of accuracy of a challenging driven-cavity flow by rational functions with 147 poles (17 of them off-scale in this figure). The authors report that this computation took half a second on a laptop for 10-digit accuracy all the way up to the corners.

The Goursat reduction to Laplace problems can also be employed with the AAALS method, and the leading figure here has been Yidan Xue, who, by combining both lightning and AAA methods for placing poles, has solved a varied set of problems with corners and curved boundaries as well as multiple connectivity. Xue deals with both steady and time-dependent flows, including in periodic geometries (Xue et al. (2024), Xue (2025a)); his software is available at (Xue (2025b)). Figure 27.2 shows an example of another driven cavity problem solved with AAA. The bottom boundary is now curved, illustrating how AAA places poles very differently near corners and near smooth segments. Many more examples of Stokes flows computed with lightning and AAA poles can be found in Xue's papers. In addition to his published work, he has also explored further aspects of rational function solutions of Stokes flows, including the use of continuum AAA (see section 30) and the treatment of unbounded domains.

There is another and possibly superior AAA-related approach to Stokes problems that might be considered, which so far has apparently not yet been tried. In the last section we solved Helmholtz problems by the Method of

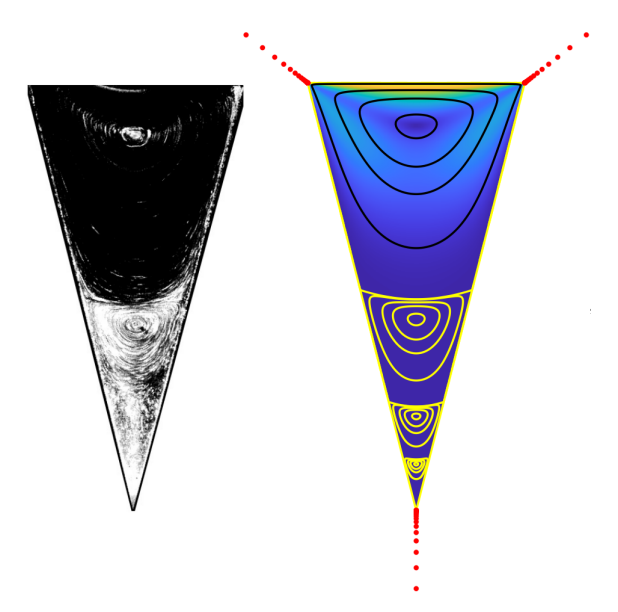


Figure 27.1. Figure from (Brubeck and Trefethen (2022)) showing Stokes flow in a triangular driven cavity computed by the lightning Stokes method. No-slip boundary conditions are applied everywhere, with the top boundary moving at constant speed and the remainder of the boundary stationary. The red dots are poles placed near each corner according to the lightning a priori clustering formula. The yellow contours mark the first three of an infinite series of counter-rotating Moffatt eddies, each with amplitude about 830 times less than the one above. On the left, a laboratory experiment in the same configuration from Taneda in 1979 reproduced in the Album of Fluid Motion (Van Dyke (1982)).

Fundamental Solutions, using AAA to choose singularity locations but then taking the actual singularities to be Hankel functions, not poles of a rational function. A similar approach could be followed for the biharmonic equation, whose fundamental solutions are known as *stokeslets* (monopoles) and *stresslets* and *rotlets* (dipoles) (Pålsson and Tornberg (2020), Pozrikidis (1992, 2002), Zhao, Lauga and Koens (2019)). The success of the AAA-Helmholtz method suggests that a AAA-Stokes method based on this principle may also be successful, and perhaps it may be simpler than the use of the Goursat representation.

So far as we know, rational approximations have not yet been used to solve biharmonic problems arising in elasticity.

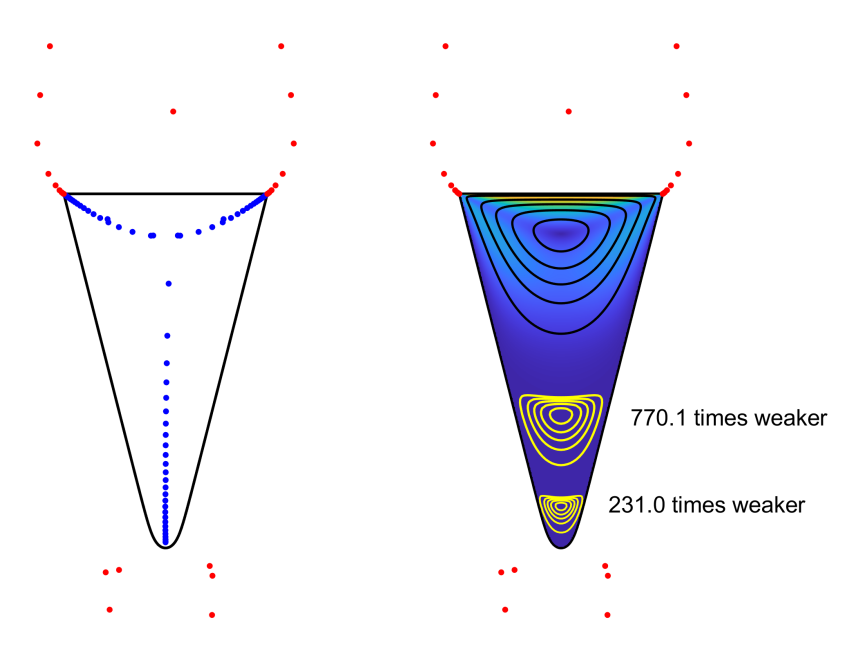


Figure 27.2. Stokes flow in another triangular driven cavity with a curved bottom computed by the AAALS Stokes method, following (Xue, Waters and Trefethen (2024)). As in section 24, the left image shows all the AAA poles and the right one shows the poles outside the problem domain together with the computed solution. The poles placed by AAA are again clustered near the corners, but no longer lie on straight lines. The poles near the bottom are few, but still important for representing the solution to high accuracy. There are now two Moffatt eddies instead of an infinite sequence.

28. The Hilbert transform

If $f_+ = u + iv$ is an analytic function in the upper half-plane \mathbb{C}_+ , the *Hilbert transform* is the map from u on \mathbb{R} to v on \mathbb{R} . Thus a computation of the Hilbert transform of a function u solves the Laplace Dirichlet problem in \mathbb{C}_+ with boundary data u, since once you have $f_+ = u + iv$ on \mathbb{R} , you can extend it to \mathbb{C}_+ by a Cauchy integral or a rational approximation. The Hilbert transform is also equivalent to what is known as the *Dirichlet-to-Neumann* map for the upper half-plane.¹¹

Since the Hilbert transform solves a Laplace problem, one might expect that to compute it with AAA, it will be necessary to use AAALS as in the last four sections. Indeed, this was the route followed in (Costa and Tre-

Differentiating v gives dv/dt for $t \in \mathbb{R}$, and by the Cauchy-Riemann conditions, this is equal to the downward-pointing normal derivative u_n of u on \mathbb{R} . Thus, once you've got v, you've got u_n .

fethen (2023)), where the effectiveness of this method even for functions u and v with singularities was demonstrated. However, AAALS is not actually necessary here. Because of the real symmetry in the Hilbert transform, it can be computed simply by additive Wiener-Hopf decomposition, which section 23 showed is a matter of AAA, not AAALS.

Before explaining and illustrating the method, we record how the Hilbert transform can be derived as a special case of the Cauchy transform, which was defined in section 23 as the map

$$f(z) = \frac{1}{2\pi i} \int_{\Gamma} \frac{h(t)}{t - z} dt$$
 (28.1)

from functions h on a contour Γ to functions f in $\mathbb{C} \cup \{\infty\} \setminus \Gamma$. We defined f_+ and f_- to be the branches of f to the left and the right of Γ near a point $t \in \Gamma$. Then according to the Sokhotski-Plemelj formulas (23.2)–(23.3), h is equal to the jump in f across the contour,

$$h(t) = f_{+}(t) - f_{-}(t), (28.2)$$

and if we evaluate f on the contour we get

$$f(t) = \frac{1}{2}(f_{+}(t) + f_{-}(t)), \quad t \in \Gamma,$$
 (28.3)

where f(t) is defined by taking the integral (28.1) in the principal value sense. The Hilbert transform is the special case of these relationships in the setting where $\Gamma = \mathbb{R}$ and h is real with $\lim_{|t| \to \infty} h(t) = 0$. Conventionally (28.1) is multiplied by -2i, so that (28.3) becomes

$$v(s) = \frac{1}{\pi} \operatorname{PV} \int_{-\infty}^{\infty} \frac{u(t)}{s-t} dt, \quad s \in \mathbb{R}$$
 (28.4)

as a map from u to v. (The minus sign in the factor -2i has been incorporated by switching the denominator from t-s to s-t.) We can explain as follows why (28.1) is multiplied by -2i. If $f_+(z) = u(z) + iv(z)$ is analytic in the closed upper half-plane $\overline{\mathbb{C}_+}$ and we define $f_-(z) = 0$ in the closed lower half-plane $\overline{\mathbb{C}_-}$, then by (28.2), f_+ is the Cauchy integral (28.1) in \mathbb{C}_+ of $h(t) = f_+(t)$ on \mathbb{R} , whereas by (28.3), the principal value on \mathbb{R} is $f(t) = f_+(t)/2$. Thus the principal value Cauchy integral maps u(t) + iv(t) to $\frac{1}{2}u(t) + \frac{i}{2}v(t)$ on \mathbb{R} . Therefore -2i times this integral maps u(t) + iv(t) to -iu(t) + v(t) on \mathbb{R} . Taking real parts, we see that -2i times the integral maps u to v, and this is (28.4).

Since the harmonic conjugate of $\cos(kt)$ is $\sin(kt)$ and the harmonic conjugate of $\sin(kt)$ is $-\cos(kt)$, it follows that the Hilbert transform acts on a Fourier transform or series by mapping the Fourier coefficient $\hat{u}(k)$ to $-\text{sign}(k)i\hat{u}(k)$. (From here, or by considering harmonic conjugates directly, one sees that the square of the Hilbert transform is the negative of the identity.) Many numerical methods for the Hilbert transform have been based

on Fourier series. For example, this is the approach used by the hilbert command in the MATLAB Signal Processing Toolbox. A different method based on expansion in rational functions with pre-assigned poles was proposed in (Weideman (1995)). For some other approaches see (Bilato, Maj and Brambilla (2014)) and (Zhou, Yang, Liu and Yang (2009)).

But let us return to AAA. Given a real function u(t) for $t \in \mathbb{R}$, section 23 showed that AAA approximation can provide a rational Wiener-Hopf splitting

$$u(t) \approx r(t) = r_{+}(t) + r_{-}(t).$$
 (28.5)

(We assume that u goes to 0 at ∞ and likewise r_+ and r_- .) By the Schwarz reflection principle, $r(\bar{z}) = \overline{r(z)}$ for all $z \in \mathbb{C}$, implying that the poles and residues of r_+ are the conjugates of those of r_- . It follows that r_+ and r_- have equal real parts for $t \in \mathbb{R}$ and opposite imaginary parts. Therefore

$$v(s) \approx 2\operatorname{Im}(r_{+}(s)). \tag{28.6}$$

Together, (28.5) and (28.6) constitute a numerical method for computation of the Hilbert transform.

To illustrate, we return to the function $u(t) = e^{-|t|}$ as in Figure 23.2, an example that was treated in (Weideman (1995)). The exact solution is known analytically:

$$u(t) = e^{-|t|}, \quad v(s) = \frac{\operatorname{sign}(s)}{\pi} [e^{|s|} E_1(|s|) + e^{-|s|} E_1(|s|)],$$
 (28.7)

where E_1 and E_i are the exponential integrals computed in MATLAB by expirt and ei. Both u and v have branch point singularities at the origin, a context in which the rational representations of AAA show their power. For a computation with tolerance 10^{-10} based on (28.6), we compute f1 and f2 exactly as on p. 97 and then just execute

$$v = O(s) 2*imag(f2(s));$$

The result, shown in Figure 28.1, differs from the exact solution (28.7) by a maximum of $9.6 \cdot 10^{-10}$ for $t \in \mathbb{R}$.

Let us comment further on AAA vs. AAALS and on the Dirichlet-to-Neumann map on \mathbb{R} vs. on a general closed contour Γ . (Here \mathbb{R} stands for any line or circle, since these are equivalent by a Möbius transformation. The Hilbert transform on the unit circle is discussed at length in (Henrici (1986)).) As we have just shown, the symmetry of \mathbb{R} enables the Dirichlet-to-Neumann map to be computed directly by approximation, without the need for an additional least-squares step. In the paper (Costa and Trefethen (2023)), this special symmetry is mirrored in the fact that Theorems 6.1 and 6.2 only apply on lines and circles. For a more general domain, AAALS is needed. One might observe that a more general domain can be reduced to a half-plane or a disk by a conformal map, so why is the Hilbert transform

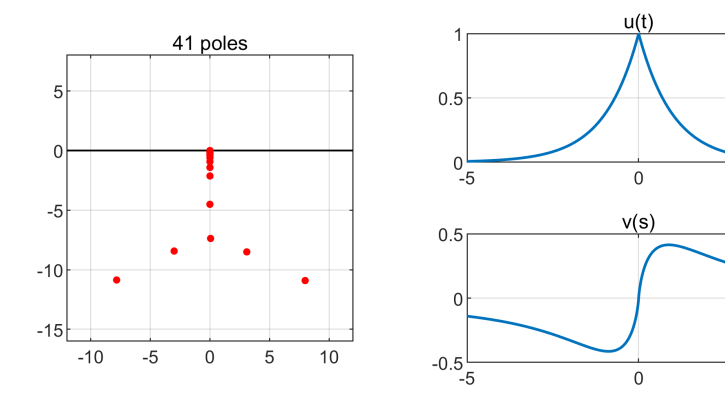


Figure 28.1. Numerical computation of the Hilbert transform (28.7) of $u(t) = e^{-|t|}$ by AAA (not AAALS). The same Wiener-Hopf splitting is used as in Figure 23.2, and the solution v(s) is then given by (28.6). A solution matching the exact result with accuracy 10^{-9} is found in 0.06 s on a laptop.

setting not equivalent to the general case? The answer is that while this is true theoretically, it is not relevant computationally since the conformal map itself amounts to a Laplace problem that must be solved somehow, as discussed in section 25.

29. AAA-Lawson for best approximation

This completes our survey of applications of AAA approximation. Here and in the next four sections, we will return to fundamentals and briefly describe five extensions of the standard AAA algorithm as presented in section 2.

AAA reliably produces near-best approximations of a given degree n, but it cannot produce actual best approximations—"best" in the sense of minimising the ∞ norm of the error $\|r(Z) - F\|$ in the notation of section 2. The reason is that AAA represents r by the barycentric formula (2.1), which forces r to interpolate the data vector F at the support points $\{t_k\}$ (assuming the weights β_k are nonzero). This constraint precludes the representation of a best approximation, since in general a best approximation on a discrete set need not interpolate the data anywhere. 12

¹² In theory, best approximations on continua exist but need not be unique, and on discrete sets or other sets with isolated points, they need not exist (Istace and Thiran (1993)). (The case of real approximation on a real interval is special: here we have both existence and uniqueness, and the Remez algorithm for computations.) However, nonuniqueness and nonexistence seem rarely to be issues in practice, at least for an algorithm like AAA-Lawson that does not attempt to enforce a characterisation of optimality.

From the beginning of work on AAA, therefore, the idea has been pursued of generalising (2.1) to an "alpha-beta barycentric representation,"

$$r(z) = \frac{N(z)}{D(z)} = \sum_{k=0}^{n} \frac{\alpha_k}{z - t_k} / \sum_{k=0}^{n} \frac{\beta_k}{z - t_k} .$$
 (29.1)

This differs from (2.1) in having arbitrary constants $\{\alpha_k\}$ rather than interpolation data $\{f_k\beta_k\}$ in the numerator. For any choice of support points $\{t_k\}$, any rational function of degree n can be represented in the form (29.1), and thus best approximations should be in reach if an algorithm can be found for computing $\{\alpha_k\}$ and $\{\beta_k\}$. If r^* is a best approximation to F on Z, and the points $\{t_k\}$ are fixed arbitrarily, then there will be a choice of $\{\alpha_k\}$ and $\{\beta_k\}$ for which r in (29.1) is equal to r^* ; the choice is unique up to a normalisation constant if r^* is of degree n but not n-1 (Nakatsukasa and Trefethen 2020, Thm. 3.1). Arbitrary choices of $\{t_k\}$ will be numerically awful, but the choices made by AAA iteration are generally excellent.

The algorithm that has been explored from the beginning, AAA-Lawson, first runs AAA as usual and then switches to the formulation (29.1) with the support points $\{t_k\}$ chosen by AAA, aiming to find $\{\alpha_k\}$ and $\{\beta_k\}$ by a process known as iteratively reweighted least-squares. This algorithm was introduced in (Nakatsukasa et al. (2018)) and (Filip et al. (2018)) and became fully practical with various improvements introduced in (Nakatsukasa and Trefethen (2020)). As mentioned in (20.2), the idea is to solve the weighted least-squares problem

$$\min_{\gamma, \|\gamma\|_2 = 1} \sum_{j=1}^{m} w_j \left(f_j \sum_{k=0}^{n} \frac{\beta_k}{z_j - t_k} - \sum_{k=0}^{n} \frac{\alpha_k}{z_j - t_k} \right)^2, \tag{29.2}$$

where γ denotes the concatenation of the weight vectors α and β , and then adjust the weights iteratively by the formula

$$w_j^{\text{(new)}} = w_j |e_j|.$$
 (29.3)

The prime on the summation sign in (29.2) reflects special treatment when z_j is one of the support points t_k ; see (Nakatsukasa and Trefethen (2020)) for details. For linear approximation problems, the Lawson iteration was introduced by Lawson in 1961 (Lawson (1961)), and convergence was proved by Rice (real) and Ellacott and Williams (complex); see (Nakatsukasa and Trefethen (2020)) for references. The AAA-Lawson iteration is nonlinear, however, and there is no theory proving that it will converge. Indeed, it does not always converge.

To illustrate AAA-Lawson approximation, we begin with the example of Figure 3.3, approximation of the gamma function $\Gamma(z)$ on the circle |z| = 1.5. Both sides of Figure 29.1 plot error curves defined as the image of the circle under $e(z) = \Gamma(z) - r(z)$, with AAA near-best approximation on the left

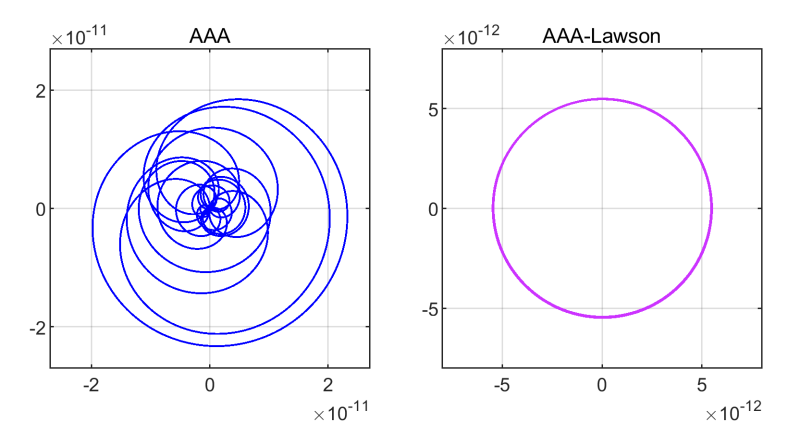


Figure 29.1. Repetition of Figure 3.3, but with the degree n of the AAA approximation of $\Gamma(z)$ on the circle |z|=1.5 reduced from 12 to 11 to stay well above the level of rounding errors. On the left, the error curve for AAA near-best approximation passes through the origin n+1=12 times, at each of the support points. On the right, the error curve for AAA-Lawson best approximation is a near-circle of winding number 2n-3=19. Note the different scales on the two sides, reflecting the pattern that best approximations typically have errors smaller than those of AAA approximations by a factor less than 10.

and AAA-Lawson best approximation on the right. In Figure 3.3 the error curve was erratic because it was close to the level of rounding error, but here, the degree has been reduced from 12 to 11 and we get a clean result. The computation of the curve on the left is effected by the commands

```
Z = 1.5*exp(2i*pi*(1:100)'/100);
r = aaa(g(Z),Z,'degree',11,'lawson',0);
E = g(Z) - r(Z);
```

with g being the complex gamma function routine from (Godfrey (2025)). (Actually a finer grid than just 100 points is used for plotting.) For the curve on the right, the 'lawson',0 flag has been removed so that the iteration (29.2)–(29.3) is applied for the default number of 20 steps. The computations on a laptop take about 4 and 10 ms, respectively. The error curve is a near-circle of winding number 2n-3=19, as we can verify with the commands

```
theta = unwrap(angle(E));
windingnumber = (theta(end)-theta(1))/(2*pi)
```

If $\Gamma(z)$ were analytic inside the circle, the winding number would be 2n+1, but the two poles inside reduce it by 4, as explained in the footnote on p. 14.

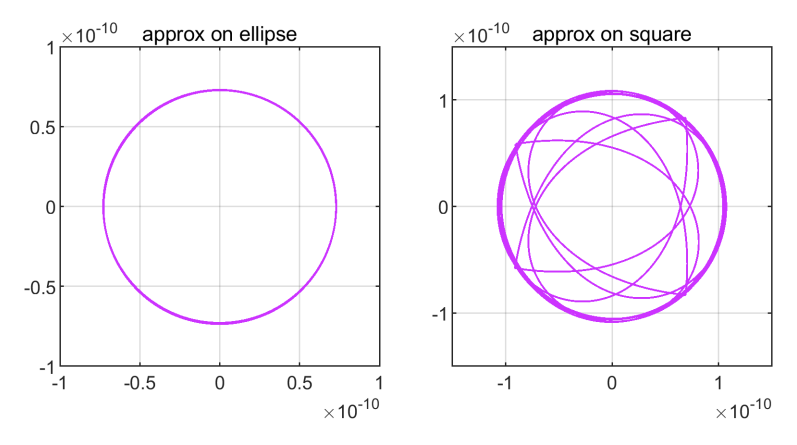


Figure 29.2. Error curves for two more degree 11 AAA-Lawson approximations of $\Gamma(z)$. On the left, the domain is the ellipse with extreme points $\operatorname{Re} z = \pm 1.5$ and $\operatorname{Im} z = \pm 2$ and the error curve is very nearly circular. On the right, the domain is the square $-1.5 \leq \operatorname{Re} z$, $\operatorname{Im} z \leq 1.5$, and the four corners are visible in the error curve. The windings numbers are 18 on the left and 19 on the right.

The near-circularity phenomenon exemplified in the right panel of Figure 29.1 was explained in (Trefethen (1981)), and it applies not just for approximation on a disk but also on other smooth approximation domains. On domains with corners, the error function e(z) will have to preserve the corner angles since it is locally a conformal map, but the rest of the error curve will tend to come close to a circle. To illustrate these effects, Figure 29.2 repeats the degree 11 best approximation of Figure 29.1 but for approximation on a 3×4 ellipse and on a square of side length 3. The winding number is 19 again on the square, but just 18 on the ellipse for reasons we have not investigated.

Before AAA-Lawson, no method was available for computing complex rational best approximations that was effective enough to play a role in scientific computing. With AAA-Lawson, most problems are now easy, and many more examples can be found in (Nakatsukasa and Trefethen (2020)), including cases with disconnected approximation domains. AAA-Lawson is less important for real approximations on intervals, on the other hand, since the Remez algorithm has been around for many years, with robust barycentric implementations in (Ionita (2013)) and Chebfun minimax (Filip et al. (2018)). Still, it may sometimes be advantageous for real problems, and an example of a real AAA-Lawson computation appears in Figure 30.1.

As described in (Nakatsukasa and Trefethen (2020)), AAA-Lawson converges often but not always, and with the 'damping' variation described in section 20, its success rate improves but is still not 100%. As a particularly

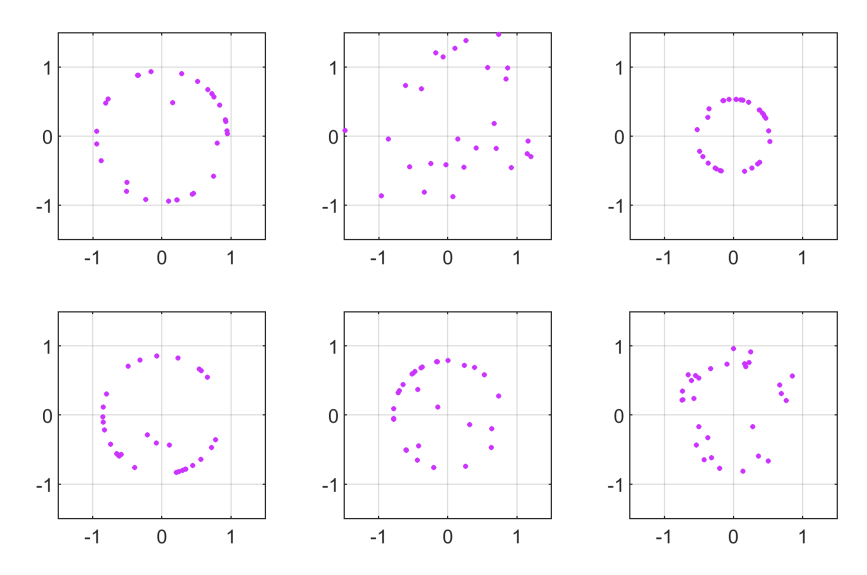


Figure 29.3. The error "curve" (discrete dots) for six trials of degree 10 AAA-Lawson best approximation of complex random data in 30 roots of unity. The first, third, fourth and fifth images appear to have achieved optimality, whereas the second one is not converging. The sixth image is close but is also not converging. More research is needed to find a AAA-Lawson algorithm that always succeeds.

challenging problem of a fundamentally discrete rather than continuous nature, what if we try to fit random complex data in 30 roots of unity by an optimal rational function of degree 10? Six trials generated by the code

```
rng(0)
Z = exp(2i*pi*(1:30)'/30);
for k = 1:6
   F = randn(30,1) + 1i*randn(30,1);
   r = aaa(F,Z,'degree',10,'lawson',500,'damping',.5);
   subplot(2,3,k), plot(r(Z)-F,'.')
end
```

lead to the images shown in Figure 29.3. Four of the six trials appear successful, but the failure rate rapidly grows if the problem size is increased.

If a variant of AAA-Lawson with guaranteed convergence could be found, would we recommend that best approximation should replace near-best as the default? Of course it would depend on the details of the new algorithm, but our guess is that we would not, for two reasons. One is that even an algorithm with provable convergence in exact arithmetic may prove fragile in floating point for approximations close to machine precision. The other is that the cost of AAA-Lawson is considerable: an increase in computing

time over standard AAA typically by at least a factor of 2 (see Figure 1.1 of (Nakatsukasa and Trefethen (2020))) and sometimes by much more, when many Lawson steps are needed. Note that inevitably, a best-approximation algorithm like AAA-Lawson must sample the function at more points than a near-best algorithm like AAA, since it depends on accurate information near extrema.

30. Continuum AAA

Some approximation problems are intrinsically discrete: one may genuinely have m points $\{z_k\}$ with m associated data values $\{f_k\}$ to approximate. Most problems, however, involve continuous data on continuous domains. Throughout this survey, and throughout most of the work by us and our collaborators, we have addressed such situations by discretising the domains a priori without worrying too much about the discretisation details. Since the computational effort only grows linearly with the number of points, not much is lost if, say, 1000 points are used in a setting that might have been treated successfully with 300. Admittedly, such constant factors can get aggravating in problems with expensive function evaluations.

There is a context where discretisation challenges become more extreme, however, and that is when there are singularities on or near the boundary of the approximation region. If poles are going to cluster near a point z_0 , then it is crucial that sample points cluster there too, or one will end up with a discrete approximation that fails to fit the continuous problem. We are experienced at choosing grids with exponential clustering near known singularity locations, as in the computation for Figure 24.2 for example, but this is hardly an ideal way to proceed in cases with several singularities or singularities at unknown locations. Here the cost of discretising "by hand" may be much worse than a constant factor, and with this in mind, a continuum AAA algorithm was introduced in (Driscoll et al. (2024)) and has been subsequently explored and extended by Driscoll (Driscoll (submitted)). We have already illustrated some continuum AAA results in Figure 13.1.

The idea of continuum AAA is to work with a discrete sample grid that is extended adaptively as the AAA iteration proceeds. Throughout the iteration, there are at least three equispaced sample points between each pair of support points (somewhat more in the early steps). This means that the Loewner matrices have only about three times as many rows as columns, and the total number of function evaluations (including at the support points) is about four times the degree. At each greedy step, a new support point is chosen where the error is largest, and then new sample points are added on either side of the new sample point to maintain the 3-to-1 ratio. This leads to an algorithm that with good though not perfect

reliability distributes sample and support points where they are needed, including clustering them near singularities.

A helpful corollary of approximation on a continuum is that one must specify that continuum. This means that when a AAA approximation is computed, one can compute its poles and find out if any of them lie where they shouldn't. Such "bad poles" render an approximation useless, ¹³ and the continuum AAA algorithm simply proceeds to the next greedy step, where with luck there will be no bad poles. Usually—though not always—one eventually reaches an approximation to the required tolerance that is known to be free of bad poles.

The codes introduced in (Driscoll et al. (2024)) are aaax for approximation on [-1,1], aaaz for approximation on the unit circle or the unit disk and aaai for approximation on the imaginary axis or the right half-plane. (The difference between the circle and the disk lies in which poles are rejected as bad ones; likewise the difference between the imaginary axis and the half-plane.) Many examples can be found in (Driscoll et al. (2024)) and (Driscoll and Zhou (2025), Driscoll (submitted)), and here we will just show one to give the idea. To approximate $\log(1 + 1000(x - \frac{1}{2})^2)$ by a degree 25 rational function on [-1,1], one can execute

```
aaax(@(x) log(1+1000*(x-.5).^2),25);
```

This produces the upper two plots of Figure 30.1, showing a near-best approximation with error about 10^{-10} computed with 26 support points and just 75 additional sample points. For a true best approximation of the same degree, one can specify that 60 AAA-Lawson iterations should be taken with the command

```
aaax(@(x) log((1+1000*(x-.5).^2)),25,60);
```

This gives the third plot, with error six times smaller, showing the characteristic equioscillation between 2n+2=52 extrema. The error curve shows that much of the action is near $x=0.5.^{14}$ To get good equioscillation over the whole continuum, aaax by default works with a grid five times finer.

Although this article has almost exclusively dealt with discrete AAA approximation, this is partly due to our limited experience. It is likely that many of the applications presented here could have been carried out successfully in continuum mode, often with a computational speedup. Good candidates would be Figures 11.3, 19.1, 24.2 and 26.1. We expect that continuum versions of AAA will be increasingly prominent in the years ahead.

¹³ Useless in principle, at any rate, making the approximation error ∞ in the ∞-norm. In practice, bad poles often have residues near machine epsilon—numerical Froissart doublets—in which case their effects are so localised that they may be harmless after all.

¹⁴ A reminder of the point of rational approximations: polynomials can't do this.

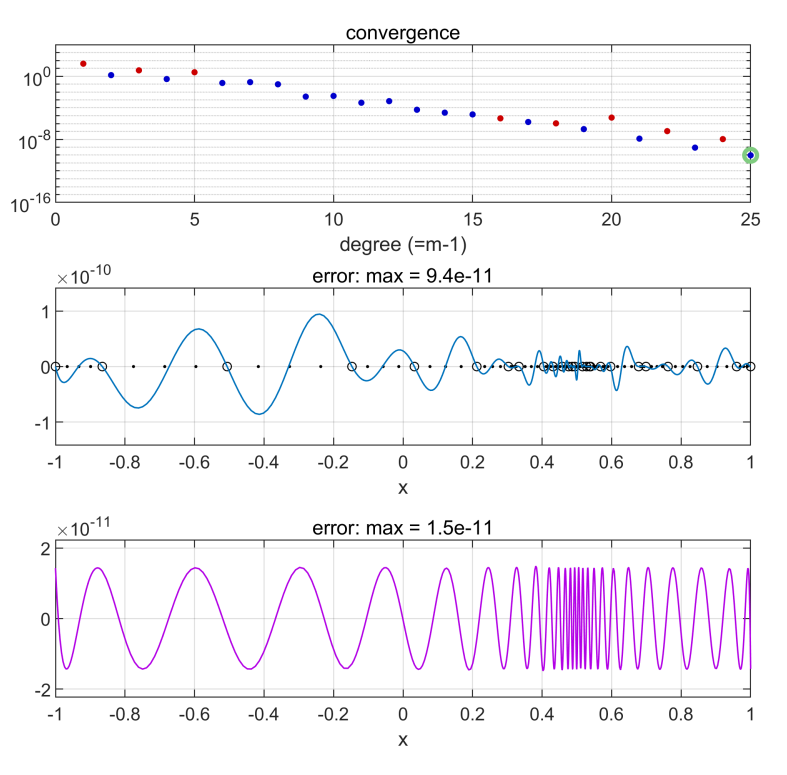


Figure 30.1. Continuum AAA near-best rational approximation of $f(x) = \log(1+1000(x-\frac{1}{2})^2)$ on [-1,1]. The convergence curve in the first image shows red dots at degrees with "bad poles" in [-1,1] and blue dots at degrees without such poles. The second plot shows the final degree 25 AAA error curve, with adaptively determined support points marked by circles and other sample points by dots. The final plot shows the error curve for a best approximation of the same degree computed by continuum AAA-Lawson.

31. Periodic AAA

Often a geometry is periodic, and one would like to apply an appropriate analogue of rational approximation. With 2π -periodicity, for example, one would like to replace algebraic rational functions p(z)/q(z) by trigonometric rational functions $p(\theta)/q(\theta)$, where p and q are trigonometric polynomials. The approximation is then not rational but meromorphic.

There are two approaches to such problems. One can derive trigonometric variants of the usual algebraic formulas and algorithms and work explicitly in the variable θ . Or one can make the change of variables $z=e^{i\theta}$ and recover the usual algebraic case on the unit circle. The choice between these two approaches long predates AAA. For example, in section 14 we mentioned the idea of Fourier-Padé approximation (Baker, Jr. and Graves-

Morris (1999)) and commented that some authors call this simply Padé approximation, probably because what they do in practice is change variables and then use standard Padé.

To date, there have been three main publications concerned with periodic AAA approximation. One of these, a paper by Xue mentioned in section 27, follows the transplantation approach and calls $\mathtt{aaa.m}$ (Xue (2025a)). The other two, working in the θ variable, are by Wilber et al. (Wilber et al. (2022)), who wrote a code called PronyAAA, and Peter Baddoo¹⁵ (Baddoo (2021)), who provided the code $\mathtt{aaatrig}$ in Chebfun (Baddoo (2021)). These projects required a generalisation of the algebraic barycentric formula (2.1) to a trigonometric barycentric formula, and on this topic there is a literature going back to Salzer, Henrici and Berrut (Salzer (1960), Henrici (1979), Berrut (1984)). We will not give details, which are complicated by a distinction that must be observed between the cases of an odd or an even number of support points. This distinction also arises in the more elementary context of computation with trigonometric polynomials, as in Fourier spectral methods for ODEs and PDEs and the "trig" mode in Chebfun (Wright, Javed, Montanelli and Trefethen (2015), Austin (2023)).

To illustrate periodic AAA approximation, consider the 2π -periodic function

$$f(\theta) = e^{\sin(\theta)} \sqrt{1.01 + \cos(\theta)}, \tag{31.1}$$

which has branch points at about $\pi \pm 0.14i$ and its translates by multiples of 2π . The code

```
f = @(t) exp(sin(t)).*sqrt(1.01+cos(t));
T = 2*pi*(1:300)/300;
[r,pol] = aaatrig(f(T),T);
```

calls aaatrig to compute a periodic rational approximant, and the results are shown in Figure 31.1. The function handle \mathbf{r} maintains real symmetry, giving exactly real values for real arguments, but the vector \mathbf{pol} of poles deviates from conjugate pairs at the level of about 10^{-8} as a transformation to an algebraic eigenvalue problem has been used in the computation.

Which is the better approach to periodic AAA approximation, explicitly periodic in θ or transformed to the unit circle with z? We do not have a definitive answer to this question, but it is interesting to note that in mathematics more generally, nobody would recommend eliminating Fourier series by transplanting every problem to Laurent series on the unit circle. If we

Peter Baddoo grew up in Britain, with roots also in Ghana, and studied and worked at Oxford, Cambridge, Imperial College and MIT. He was one of the brightest and most appealing people we have ever encountered, and it was devastating news when we learned in 2023 that he had died as the result of a heart abnormality after a basketball game at MIT. He was 29 years old.

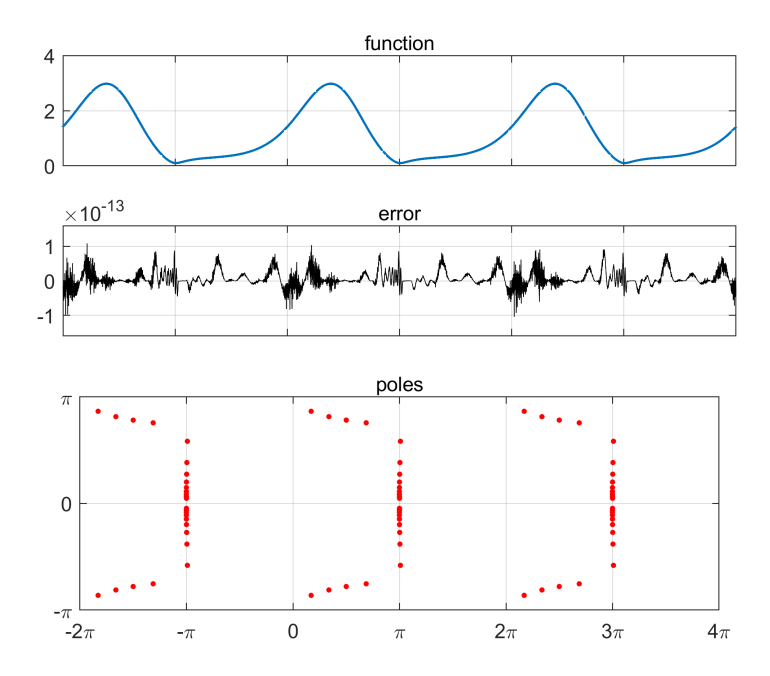


Figure 31.1. Periodic AAA approximation of (31.1) computed by aaatrig. Three periods are shown.

ask ourselves why not, perhaps the first answer is that such a transplantation converts real problems to complex ones, which adds computational and conceptual complexity. On a computer, transplantation also breaks the symmetry across the real axis, for whereas the set of complex floating numbers is invariant under complex conjugation $\theta \mapsto \bar{\theta}$, it is not invariant under reflection in the unit circle $z \mapsto \bar{z}^{-1}$. A practical consequence in the AAA context is that a periodic approximation to a periodic real function may not come out exactly real, if it is computed via transplantation to the unit circle, nor will its poles necessarily lie in exactly conjugate pairs.

That said, there is no denying the simplicity of computing periodic AAA approximations by transplantation. Essentially the same results as in Figure 31.1 are produced in this fashion by the following code calling aaa, not aaatrig. The indented lines effect the transformations between θ and z.

```
f = @(t) exp(sin(t)).*sqrt(1.01+cos(t));
    g = @(z) f(log(z)/1i);
T = 2*pi*(1:300)/300;
    Z = exp(1i*T);
[r0,pol] = aaa(g(Z),Z);
    r = @(t) r0(exp(1i*t)); pol = log(pol)/1i;
```

32. Type (m, n) AAA

A rational function is said to be of $type\ (m,n)$ if it can be written as a quotient p/q where p is a polynomial of degree at most m and q is a polynomial of degree at most n. It is of $exact\ type\ (\mu,\nu)$ if it is of type (μ,ν) and these numbers are as small as possible. Thus $z/(1+z)^2$ is of exact type (1,2), for example, and it is of type (m,n) for any $m \ge 1$ and $n \ge 2$. A constant is of exact type (0,0), except that the special case of the zero constant is said to be of exact type $(-\infty,0)$. A rational function of exact type (μ,ν) has a zero of order $\nu - \mu$ at ∞ if $\mu \le \nu$ and a pole of order $\mu - \nu$ if $\mu \ge \nu$. In the extended complex plane $\mathbb{C} \cup \{\infty\}$ (the Riemann sphere), a rational function of exact type (μ,ν) has exactly $\max\{\mu,\nu\}$ poles and also $\max\{\mu,\nu\}$ zeros in total, counted with multiplicity.

Note that according to these definitions, type (n, n) is the same as degree n, and we denote the space of rational functions of degree n by \mathcal{R}_n .

In approximation theory, it is common for theorists to consider all values of m and n; we denote the corresponding spaces of rational functions by \mathcal{R}_{mn} . The Padé table of a function f, for example, is the array of all of its Padé approximants of types (m, n) for $m \geq 0$ and $n \geq 0$, each defined by matching the Taylor series of f as far as possible. A notable property of the Padé table is that degeneracies may occur in which several pairs (m, n)have the same approximant—for example, this always happens if f is odd or even—and such degeneracies always occupy exactly square blocks of the table (except in the special case of an identically zero Padé approximant). Similarly, the Walsh table of a function f is the array of its best ∞ -norm approximants on a given real or complex domain E for m, n > 0. If f and its rational approximants are real and E is a real interval, then the equioscillation theorem implies that degeneracies in the Walsh table also fill square blocks, with the same exception for the identically zero approximation. These approximations can be computed even in quite challenging cases by the Chebfun minimax command, which is based on the Remez algorithm implemented with a barycentric representation (Filip et al. (2018)). For robust computation of Padé approximations, see (Gonnet, Güttel and Trefethen (2013)). All these matters are described in (Trefethen (2019a)).

In approximation practice, on the other hand, usually the interest is in type (n,n) or sometimes (n-1,n) approximations. (These classes are coupled in some procedures for generating continued fractions, which follow a staircase sequence $(0,0),(0,1),(1,1),(1,2),\ldots$ or $(0,0),(1,0),(1,1),(2,1),\ldots$ (Henrici (1977), Salazar Celis (2024)).) This is one reason why the standard AAA algorithm, and its Chebfun implementation aaa.m, treat just the case of type (n,n). Nevertheless, a method for extending AAA to type (m,n)

¹⁶ This is the "mathematician's definition" of Padé approximation (Trefethen (2019a)). The "physicist's definition" (Baker, Jr. and Graves-Morris (1999)) is slightly different.

was proposed in section 9 of the original AAA paper (Nakatsukasa *et al.* (2018)).

Consider the barycentric representation (2.1) that AAA is based upon. As is shown in Theorem 2.1 of (Nakatsukasa et al. (2018)), this representation covers not just rational functions of exact type (n,n) but all rational functions of type (n,n). This statement applies for any fixed set of support points $\{t_k\}$ —having a good choice matters numerically but not algebraically—and it applies even if attention is restricted to weights $\{\beta_k\}$ that are all nonzero. Thus, algebraically at least, it should be possible to retain the form (2.1) for computing type (m, n) approximations with m < n; for m > n we would increase the limit on the sum to m. The method for doing this proposed in (Nakatsukasa et al. (2018)) is to restrict the weight vector $\{\beta_k\}$ to lie in a subspace where the numerator degree is constrained to be less than the denominator degree if m < n, and the reverse if m > n. This is a condition of linear algebra that can be imposed by modifications of the computation that we shall not go into. These computations implicitly work with polynomials, and for numerical stability, it is important that a good basis for the polynomials is utilised. This can be achieved by employing Vandermonde with Arnoldi orthogonalisation as described in (Brubeck et al. (2021)). All these elements are combined successfully in Chebfun minimax (Filip et al. (2018)), but to this date they have not yet been implemented in a general-purpose AAA code. Therefore, unusually, we shall conclude this discussion without a numerical illustration.

* * *

However, a related matter must be brought up; we focus on the case (n-1,n) because of its practical interest. To say that r is of type (n-1,n) rather than (n,n) is not the same as saying that it takes the value 0 at ∞ . For example, r(z) = (z+1)/(z-1) is of type (1,2), but $r(\infty) = 1$. In an application, one must be clear which of the two is wanted, and if it is $r(\infty) = 0$, then a new algorithm will be needed from the one mentioned above.

The condition $r(\infty) = 0$ is important in model order reduction (section 19), where the interest is usually in approximations that tend to zero on the imaginary axis. In the MathWorks RF Toolbox (MathWorks Inc. (2020)), there is a flag TendsToZero that the user can set to impose this condition. In the Control System and System Identification toolboxes, similarly, one can specify a value at ∞ that may be zero or nonzero. Mathematically, interpolation conditions like these are quite special, as $z = \infty$ is just one point among many of $\mathbb{C} \cup \{\infty\}$. Whereas one could in principle impose a condition at $z = \infty$ in any rational approximation problem, it is only likely to serve much purpose in a problem involving approximation on a domain that extends to ∞ , like the imaginary axis.

Best ∞ -norm approximation with $r(\infty) = 0$ may be problematic, for it is ill-posed. (More generally, best approximation of exact type (μ, ν) as opposed to type (m, n) is ill-posed.) We can show this with the example of approximation of $f(x) = 2xe^{1-x}$ for $x \in [0, \infty)$. This function takes the extreme values 0 at x = 0 and ∞ and 2 at x = 1, so by the equioscillation theorem, r(x) = 1 is its unique best approximant of type (1, 1), with error ||f-r|| = 1. Now suppose we ask for a best approximant of type (1, 1) with $r(\infty) = 0$. By uniqueness of best approximations, such a function will have to have ||f-r|| > 1. It can come arbitrarily close to ||f-r|| = 1, as we see by considering $r(x) = 1/(1+\varepsilon x)$ as $\varepsilon \to 0$, but the limit cannot be attained.

Fortunately, the ill-posed cases are non-generic, and approximation with $r(\infty) = 0$ often makes sense. A method for computing such approximants is to replace the usual barycentric formula (2.1) by

$$r(z) = \sum_{k=1}^{n} \frac{f_k \beta_k}{z - t_k} / \left(1 + \sum_{k=1}^{n} \frac{\beta_k}{z - t_k} \right)$$
 (32.1)

and adjust the AAA iteration accordingly. The big change is that it is no longer appropriate to impose the normalisation (2.4) on the weights $\{\beta_k\}$, so instead of an SVD, we get a least-squares problem at each step. The fact that $\{\beta_k\}$ may be arbitrarily large, diverging to ∞ in special cases, reflects the risk of ill-conditioning and in the limit ill-posedness. Nevertheless (32.1) is often an effective basis for AAA approximation with $r(\infty) = 0$, and this variant of the barycentric formula has been used by a number of authors going back at least to (Ionita 2013, sec. 1.5.2).

For approximation with more than one zero at ∞ , Dave Darrow (private communication) has proposed a similar algorithm with the constant 1 of (32.1) replaced by a monic polynomial of degree $\nu - \mu - 1$. Presumably in general it would be desirable to use Vandermonde with Arnoldi orthogonalisation to represent that polynomial, but we have no experience with this.

33. Vector-valued AAA

Instead of a single function f(z), in some applications one has several functions $\{f_j(z)\}$ that one would like to fit by rational functions $\{r_j\}$ all with the same poles. This could happen in an engineering context, for example, when various signals are available that ultimately derive from the same dynamical process, as in a MOR or ROM problem of the kind discussed in section 19. We also encountered such a situation in sections 16–18, where a linear or nonlinear resolvent $A(z)^{-1}$ is scalarised by conversion to $u^*A(z)^{-1}v$, with u and v taken as arbitrary vectors, and the results may be more accurate if these are replaced by matrices with several independent columns. If u

and v have p and m columns, respectively, as in (19.2), then we have a vector-valued approximation of dimension pm to construct.

Rational fits of this kind, with shared poles, have not only arisen in the context of AAA. An interesting example is (Wright and Fornberg (2017)), which presents an algorithm for shared-pole rational approximation for applications to radial basis functions (RBFs). In their application, an RBF $f_{\varepsilon}(\vec{x})$ depends analytically on the shape parameter ε , and values $\varepsilon \approx 0$ are impossible to determine by direct evaluation but are accessible via rational approximation based on data at larger values of ε . By using several values of \vec{x} to construct a fit, the authors obtain a more reliable and accurate answer than if they used just one value of \vec{x} .

For AAA, generalisations of the basic algorithm to handle vector-valued data include "FastAAA" (Hochman (2017)), the MathWorks rational code (MathWorks Inc. (2020)), and "setAAA" (Lietaert et al. (2022)) (first posted on arXiv in 2018; software is available at (Meerbergen (2022)). The idea is simple, as expressed in the words of Hochman:

We replace the Löwner matrix... by a block-Löwner analogue. Its size is now $p(N-n) \times n$.

(In the notation of the present paper around (2.6), this becomes $p(m-n-1) \times (n+1)$.) In other words, one fits all the functions simultaneously, and the AAA least-squares problem at each step minimises a residual based on all of them. The result is an approximation with a single set of support points and barycentric weights and hence a single set of poles, but with p different function values interpolated at each each support point. Since the number of rows of the Loewner matrix is multiplied by p but the number of columns is not, the work scales just linearly with p. In applications involving scalarisation vectors u and v as described above, for example, one can increase accuracy and robustness by replacing these vectors by tall-skinny matrices with 3 or 4 columns, say, and thereby increase the computational cost by just a factor on the order of 9 or 16.

For an idea of what dimensions may be relevant in applications, it is interesting to look at the SLICOT collection of model problems for MOR/ROM mentioned in section 19 (Chahlaoui and Van Dooren (2002)). Of the 56 problems, 19 involve scalars and 37 involve vectors. Most of these 37 have dimensionality just 2 or 3, with only one problem having dimensionality bigger than 7 (namely 20). Thus all of these problems would be readily accessible to vector-valued AAA. On the other hand, the SLICOT collection dates to 2002, and much larger problems are also of interest nowadays.

In this section we have discussed vector-value approximations, making no distinction between vectors and matrices since the approximations in question treat components individually though with shared poles. FastAAA, setAAA and the MathWorks RF Toolbox all operate in this mode. In (Gosea

and Güttel (2021)), a different approach called blockAAA is introduced, which deals intrinscially with matrix-valued approximations. This can be advantageous in MIMO applications, and the method is implemented in the MathWorks Control System and System Identification toolboxes.

34. Discussion

Rational approximations are changing numerical analysis, and more broadly, applied mathematics. The change was sparked by AAA, which has been the tool used in this review, but other methods may also prove competitive. As mentioned in the introduction, the greedy Thiele Continued Fractions (TCF) method is impressive (Salazar Celis (2024), Driscoll and Zhou (2025), Driscoll (submitted)). It is faster than AAA, and while it does not take advantage of least-squares fitting, it may perhaps prove to be equally reliable. One limitation of TCF is that, so far at least, it does not have a variant analogous to AAA-Lawson for upgrading near-best to best approximations.

We have discussed many applications, but there are potentially many more, for rational functions have a role to play in almost all areas of computational continuous mathematics. One topic we are particularly curious about is the theory and computation of *composite* rational approximations, as discussed in the final paragraph of section 20. As argued in (Trefethen (March 2022b)), almost everything one can do numerically on a computer comes down to piecewise composite rational approximations, and the machine learning revolution has been driven by composite approximations—not necessarily rational, although as shown in (Boullé, Nakatsukasa and Townsend (2020)), they may be.

For AAA, TCF and potentially other methods, an important question is to what extent continuum variants as in section 30 should replace the discrete approximations we have emphasised here. Most applications—in fact, every example considered in this paper apart from that of Figure 29.3—ultimately concern continuous domains, and Driscoll has shown that continuum AAA is extremely effective. With more experience, it is possible that it will emerge that continuum rational approximation algorithms should be the default.

Many research questions have arisen in this survey, including the following.

- 1. Section 2: How might AAA linear algebra be modified to speed up $O(n^4)$ to $O(n^3)$ in a numerically stable fashion?
- 2. Section 2: Can theorems be developed to explain the rapid convergence of AAA to near-best approximations? (Question 13 below may play into this investigation.)
- 3. Section 2: What are the prospects for developing an AAA-style algorithm that avoids producing poles in unwanted regions of \mathbb{R} or \mathbb{C} ? A

- method based on semidefinite programming has been put forward in (Bradde, Grivet-Talocia, Aumann and Gosea (2025)). See also question 19.
- 4. Sections 2 and 8: Can methods be developed to help AAA stop at the right moment if noise is encountered, or to otherwise reduce the impact of noise? For polynomial approximations, a method is proposed in (Matsuda and Nakatsukasa (2025)).
- 5. Sections 2 and 4: Should AAA be modified to measure errors in the Riemann sphere metric $|w w'|/\sqrt{(1+|w|^2)(1+|w'|^2)}$ rather than the complex plane metric |w w'|? This might improve performance in problems with poles near the approximation domain, and it might make polefinding and zerofinding more nearly equivalent.
- 6. Section 6: How can rational approximations be used to identify branch point structure for functions with several branch points, as in Figures 11.2, 11.3, and 14.2?
- 7. Section 6: Can a AAA-style algorithm be developed for reciprocallog approximations (Baddoo and Trefethen (2022), Nakatsukasa and Trefethen (2021))? This would have the potential of speeding up root-exponential to exponential convergence, and also of offering new methods for dealing with functions near branch points and on Riemann surfaces, and for approximation on domains with slits.
- 8. Section 8: What theorem might be proved to explain the success of rational approximations in interpolating equispaced data?
- 9. Section 10: What's going on with the "one-wavelength principle" in analytic continuation?
- 10. Section 11: How can the branch structure of Schwarz functions be computed numerically? See question 6.
- 11. Section 12: Can a Hermite integral theory for rational approximations be developed based on zeros of r(z) instead of poles, or based on both zeros and poles? See question 5 above.
- 12. Section 13: How can adaptive rational approximations be used on the fly to solve ODEs and PDEs whose solutions have singularities or near-singularities? The vision here is to create a kind of "Ratfun" in analogy to Chebfun.
- 13. Section 20: How can the 'sign' variant of AAA be modified into a bulletproof procedure that might replace the current default selection of the smallest singular vector of the Loewner matrix?
- 14. Section 23: Can AAA be useful for solving more advanced Riemann-Hilbert problems? Very little has been attempted so far.
- 15. Sections 24–27: What theoretical support can be developed for the AAALS method, and for its extensions from the Laplace equation to other PDEs such as the Helmholtz and biharmonic equations?

- 16. Section 27: Can AAA placement of stokeslets be the basis of a new MFS method for solving biharmonic problems?
- 17. Sections 24–27: Can AAALS-style methods be developed based on monopoles $\log |z t_k|$ rather than dipoles $1/(z t_k)$?
- 18. Section 29: Can the AAA-Lawson algorithm be improved to give guaranteed convergence, at least in exact arithmetic? Presumably this will require a reconsideration of the 'damping' option discussed in section 20.
- 19. Section 30: Can the continuum AAA algorithm be modified to avoid "bad poles" more unfailingly, such as arise in many problems especially with real functions on real intervals?
- 20. Section 32: Can type (m, n) AAA approximation be realised in a fashion as robust numerically as what we have for type (n, n)?

These questions are all important, but let us distinguish two further questions which perhaps are even more so. One is, what can be done in multiple dimensions? At present, neither multivariate rational approximation per se nor applications to PDEs in more than two dimensions have tools comparable to univariate AAA (see section 15). Is this restriction to a single variable—or to the plane—unbreakable?

Secondly, now that greedy algorithms are changing rational approximation so profoundly, what about analogous algorithms for other problems that might seem to have a similar flavor? In particular, how about fitting a function f(x) near-optimally by a linear combination of Gaussians, or radial basis functions, of unknown widths and centres? If there were a AAA-style algorithm for such problems, applications would be found everywhere. So far, we have been stymied by the lack of a barycentric representation for Gaussians or RBFs, but is there an idea here we haven't spotted?

Acknowledgments

Every section of this paper has been read and reread by a number of our colleagues during the writing process, and the combined help from all of these people has added up to a major contribution. We would like to thank Anthony Austin, Alex Barnett, Jean-Paul Berrut, Felix Binkowski, Jake Bowhay, Oscar Bruno, Sven Burger, Keaton Burns, Anil Damle, Dave Darrow, Tom DeLillo, Mark Embree, Marco Fasondini, Eamonn Gaffney, Abi Gopal, Victor Gosea, Serkan Gugercin, Stefan Güttel, Sam Harris, Astrid Herremans, Sam Hocking, Andrew Horning, Daan Huybrechs, Cosmin Ionita, Anastasia Kisil, Andrei Martinez-Finkelshtein, Robb McDonald, Kyle McKee, Karl Meerbergen, Andrea Moiola, Hadrien Montanelli, Mark Reichelt, Oliver Salazar Celis, Manuel Santana, Olivier Sète, Nian Shao, Shuai Shao, Anna-Karin Tornberg, Alex Townsend, Tom Trogdon, Michael Tsuk, Kieran Vlahakis, André Weideman, Nicholas West, Heather Wilber,

Grady Wright, Tony Xu, Fei Xue, Yidan Xue and Maxim Yattselev. A few errors in a late draft of the paper were also caught by an AI system: by the Refine software created by Yann Calvó López and Ben Golub.

In addition to these wonderfully helpful friends and colleagues, we wish to single out two others whose contributions to the AAA enterprise have been particularly extensive and are visible in many sections of this article. One is Stefano Costa, the originator of the AAALS method and the first to propose that it could be applied not just to Laplace problems on simple domains but also to PDEs with interfaces, conformal mapping, Riemann-Hilbert problems and other applications. As we have worked on AAALS in the past five years, many of the best ideas for improvements and understanding of the method have come from Costa. The other is Toby Driscoll, who was already a close colleague of ours through Schwarz-Christoffel mapping, the Chebfun project and the book *Exploring ODEs*. For AAA, Driscoll has been a leader in Julia implementations, high-precision analytic continuation, exploration of the alternative method of Thiele continued fractions, and the development and implementation of the continuum AAA algorithm.

References

- B. Adcock and D. Huybrechs (2019), Frames and numerical approximation, SIAM Rev. 61, 443–473.
- B. Alpert, L. Greengard and T. Hagstrom (2000), Rapid evaluation of nonreflecting boundary kernels for time-domain wave propagation, SIAM J. Numer. Anal. 37, 1138–1164.
- A. C. Antoulas and B. D. Q. Anderson (1986), On the scalar rational interpolation problem, *IMA J. Math. Control Inform.* **3**, 61–88.
- A. C. Antoulas, C. A. Beattie and S. Gugercin (2020), Interpolatory Methods for Model Reduction, SIAM.
- J. Asakura, T. Sakurai, H. Tadano, T. Ikegami and K. Kimura (2009), A numerical method for nonlinear eigenvalue problems using contour integrals, JSIAM Letters 1, 52–55.
- Q. Aumann, P. Benner, I. V. Gosea, J. Saak and J. Vettermann (2023), A tangential interpolation framework for the AAA algorithm, PAMM 23, e202300183.
- A. P. Austin (2023), On trigonometric interpolation in an even number of points, Electr. Trans. Numer. Anal. 58, 271–288.
- A. P. Austin and L. N. Trefethen (2015), Computing eigenvalues of real symmetric matrices with rational filters in real arithmetic, SIAM J. Sci. Comput. 37, A1365–A1387.
- A. P. Austin, P. Kravanja and L. N. Trefethen (2014), Numerical algorithms based on analytic function values at roots of unity, SIAM J. Numer. Anal. 52, 1795– 1821
- A. P. Austin, M. Krishnamoorthy, S. Leyffer, S. Mrenna, J. Müller and H. Schulz (2021), Practical algorithms for multivariate rational approximation, *Computer Phys. Commun.* 261, 107663.
- S. Axler (1986), Harmonic functions from a complex analysis viewpoint, *Amer. Math. Monthly* **93**, 246–258.
- P. J. Baddoo (2021), The AAAtrig algorithm for rational approximation of periodic functions, SIAM J. Sci. Comput. 43, A3372–A3392.
- P. J. Baddoo and E. M. Hinton (2025), Computing fluid–fluid interface evolution in Hele-Shaw cells using rational approximation, *Proc. Roy. Soc. A* **481**, 20250011.
- P. J. Baddoo and L. N. Trefethen (2022), Log-lightning computation of capacity and Green's function, *Maple Trans.* 1, 1.
- Z. Bai and J. Demmel (1998), Using the matrix sign function to compute invariant subspaces, SIAM J. Matrix Anal. Applies. 19(1), 205–225.
- Z. Bai, J. Demmel and M. Gu (1997), An inverse free parallel spectral divide and conquer algorithm for nonhermitian eigenproblems, *Numer. Math.* 76, 279–308.
- G. A. Baker, Jr. (1961), Application of the Padé approximant method to the investigation of some magnetic properties of the Ising model, *Phys. Rev.* 124, 768–774.
- G. A. Baker, Jr. and P. Graves-Morris (1999), Padé Approximants, Cambridge U. Press.
- G. A. Baker, Jr. and C. Xie (2011), Singularities in the complex physical plane for deep water waves, J. Fluid Mech. 685, 83–116.
- R. Baltensperger and J.-P. Berrut (2001), The linear rational collocation method, J. Comput. Appl. Math. 134, 243–258.

- J. Banks, J. Garza-Vargas, A. Kulkarni and N. Srivastava (2023), Pseudospectral shattering, the sign function, and diagonalization in nearly matrix multiplication time, Found. Comp. Math. 23, 1959–2047.
- A. H. Barnett and T. Betcke (2008), Stability and convergence of the method of fundamental solutions for Helmholtz problems on analytic domains, J. Comput. Phys. 227, 7003–7026.
- Z. Battles and L. N. Trefethen (2004), An extension of MATLAB to continuous functions and operators, SIAM J. Sci. Comput. 25, 1743–1770.
- C. Beattie and S. Gugercin (2012), Realization-independent \mathcal{H}_2 -approximation, in 2012 IEEE 51st IEEE Conference on Decision and Control (CDC), IEEE, pp. 4953–4958.
- P. Benner, S. Güğercin and K. Willcox (2015), A survey of projection-based model reduction methods for parametric dynamical systems, SIAM Rev. 57, 483–531.
- M. Berljafa and S. Güttel (2017), The RKFIT algorithm for nonlinear rational approximation, SIAM J. Sci. Comput. 39, A2049–A2071.
- J.-P. Berrut (1984), Baryzentrische Formeln zur trigonometrischen Interpolation (I), Z. angew. Math. Phys. 35, 91–105.
- J.-P. Berrut and R. Baltensperger (2001), The linear rational pseudospectral method for boundary value problems, *BIT Numer. Math.* 41, 868–879.
- J.-P. Berrut and H. D. Mittelmann (2002), Linear rational interpolation and its application in approximation and boundary value problems, *Rocky Mountain J. Math.* 32, 527–544.
- J.-P. Berrut and H. D. Mittelmann (2004), Adaptive point shifts in rational approximations with optimized denominator, *J. Comput. Appl. Math.* **164–165**, 81–92.
- D. Bessis and J.-D. Fournier (1990), Complex singularities and the Riemann surface for the Burgers equation, in *Nonlinear physics (Shanghai, 1989)*, Springer, Berlin, pp. 252–257.
- T. Betcke, N. J. Higham, V. Mehrmann, C. Schröder and F. Tisseur (2013), NLEVP: A collection of nonlinear eigenvalue problems, ACM Trans. Math. Softw. 39, 1–28.
- F. Betz, M. Hammerschmidt, L. Zschiedrich, S. Burger and F. Binkowski (2024), Efficient rational approximation of optical response functions with the AAA algorithm, *Laser Photonics Rev.* 18, 2400584.
- W.-J. Beyn (2012), An integral method for solving nonlinear eigenvalue problems, *Lin. Alg. Applics.* **436**, 3839–3863.
- R. Bilato, O. Maj and M. Brambilla (2014), An algorithm for fast Hilbert transform of real functions, *Adv. Comput. Math.* **40**, 1159–1168.
- F. Binkowski, F. Betz, M. Hammerschmidt, L. Zschiedrich and S. Burger (2025), Resonance modes in microstructured photonic waveguides: efficient and accurate computation based on AAA rational approximation, *Nanophotonics* 14, 1665– 1671.
- N. Boullé, A. Herremans and D. Huybrechs (2024), Multivariate rational approximation of functions with curves of singularities, SIAM J. Sci. Comput. 46, A3401–A3426.
- N. Boullé, Y. Nakatsukasa and A. Townsend (2020), Rational neural networks, *Adv. Neural Info. Proc. Syst.* **33**, 14243–14253.

- J. Bowhay, Y. Nakatsukasa and I. Zaid (2025), Computing the zeros of a holomorphic function using quadrature-based subdivision and rational approximation of the logarithmic derivative, arXiv preprint arXiv:2509.15936.
- J. P. Boyd (2002), A comparison of numerical algorithms for Fourier extension of the first, second, and third kinds, *J. Comput. Phys.* **178**, 118–160.
- J. P. Boyd (2014), Solving Transcendental Equations: the Chebyshev Polynomial Proxy and Other Numerical Rootfinders, Perturbation Series, and Oracles, SIAM.
- T. Bradde, S. Grivet-Talocia, Q. Aumann and I.-V. Gosea (2025), A modified AAA algorithm for learning stable reduced-order models from data, *J. Sci. Comput.* **103**, 14.
- M. C. Brennan, M. Embree and S. Gugercin (2023), Contour integral methods for nonlinear eigenvalue problems: A systems theoretic approach, SIAM Rev. 65, 439–470.
- P. D. Brubeck and L. N. Trefethen (2022), Lightning Stokes solver, SIAM J. Sci. Comput. 44, A1205–A1226.
- P. D. Brubeck, Y. Nakatsukasa and L. N. Trefethen (2021), Vandermonde with Arnoldi, SIAM Rev. 63, 405–415.
- O. P. Bruno and S. K. Lintner (2012), A high-order integral solver for scalar problems of diffraction by screens and apertures in three-dimensional space, J. Comput. Phys. 252, 250–274.
- O. P. Bruno and J. Paul (2022), Two-dimensional Fourier continuation and applications, SIAM J. Sci. Comput. 44, A964–A992.
- O. P. Bruno and M. A. Santana (2025), Efficient time-domain scattering synthesis via frequency-domain singularity subtraction, arXiv preprint arXiv:2505.06189.
- O. P. Bruno, M. A. Santana and L. N. Trefethen (submitted), Evaluation of resonances: adaptivity and AAA rational approximation of randomly scalarized boundary integral resolvents, SIAM J. Sci. Comput.
- R. E. Caffisch and O. F. Orellana (1989), Singular solutions and ill-posedness for the evolution of vortex sheets, *SIAM J. Math. Anal.* **20**, 293–307.
- R. E. Caflisch, F. Gargano, M. Sammartino and V. Sciacca (2015), Complex singularities and PDEs, *Riv. Matem. Univ. Parma* **6**, 69–133.
- R. E. Caflisch, F. Gargano, M. Sammartino and V. Sciacca (2022), Complex singularity analysis for vortex layer flows, *J. Fluid Mech.* **932**, A21.
- Y. Chahlaoui and P. Van Dooren (2002), A collection of benchmark examples for model reduction of linear time invariant dynamical systems, Technical report, Manchester Institute for Mathematical Sciences.
- W. J. Cody (1975), The FUNPACK package of special function subroutines, ACM Trans. Math. Softw. 1, 13–25.
- W. J. Cody (1993), Algorithm 715: SPECFUN—a portable FORTRAN package of special function routines and test drivers, ACM Trans. Math. Softw. 19, 22–32.
- R. M. Corless (2004), Generalized companion matrices in the Lagrange basis, in *Proceedings EACA*, Citeseer, pp. 317–322.
- S. Costa (2020), Solving Laplace problems with the AAA algorithm, arXiv preprint arXiv:2001.09439v1.
- S. Costa (2022), 'Rootfinding with the AAA algorithm', chebfun.org/examples/ roots/AAAZeros.html.

- S. Costa and L. Trefethen (2023), AAA-least squares rational approximation and solution of Laplace problems, in *European Congress of Mathematics* (H. Hujdurović et al., ed.), pp. 511–534.
- S. Costa, E. Costamagna and P. Di Barba (2024), Modelling permanent magnet excited uniform fields with rational approximations, *COMPEL The International Journal for Computation and Mathematics in Electrical and Electronic Engineering* **43**, 604–619.
- S. C. Crew and P. H. Trinh (2016), New singularities for Stokes waves, 798, 256–283.
- J. H. Curtiss (1962), Interpolation by harmonic polynomials, J. SIAM 10, 709–736.
- P. J. Davis (1974), The Schwarz Function and its Applications, Math. Assoc. Amer.
- P. J. Davis and H. Pollak (1958), On the analytic continuation of mapping functions, *Trans. AMS* 87, 198–225.
- E. Deckers, S. Jonckheere and K. Meerbergen (2022), Time integration of finite element models with nonlinear frequency dependencies, arXiv preprint arXiv:2206.09617.
- G. Deng and C. Lustri (2023), Exponential asymptotics of woodpile chain nanoptera using numerical analytic continuation, *Studies Appl. Math.* **150**, 520–557.
- A. Doicu, Y. Eremin and T. Wriedt (2000), Acoustic and Electromagnetic Scattering Analysis Using Discrete Sources, Elsevier.
- T. A. Driscoll (2005), 'Schwarz-Christoffel Toolbox in Matlab', https://github.com/tobydriscoll/sc-toolbox.
- T. A. Driscoll (submitted), RationalFunctionApproximation.jl: Rational approximation on discrete and continuous domains, in *The Proceedings of the JuliaCon Conferences*, 2025.
- T. A. Driscoll and Y. Zhou (2025), Greedy Thiele continued-fraction approximation on continuum domains in the complex plane, arXiv preprint arXiv:2510.07295.
- T. A. Driscoll, F. Bornemann and L. N. Trefethen (2008), The chebop system for automatic solution of differential equations, *BIT Numerical Mathematics* **48**, 701–723.
- T. A. Driscoll, N. Hale and L. N. Trefethen (2014), *Chebfun Guide*, Pafnuty Publications, Oxford.
- T. A. Driscoll, Y. Nakatsukasa and L. N. Trefethen (2024), AAA rational approximation on a continuum, SIAM J. Sci. Comput. 46, A929–A952.
- S. Dyatlov and M. Zworski (2019), Mathematical Theory of Scattering Resonances, Amer. Math. Soc.
- S. Ellacott and J. Williams (1976), Rational Chebyshev approximation in the complex plane, SIAM J. Numer. Anal. 13, 310–323.
- C. L. Epstein, F. Fryklund and S. Jiang (2025), An accurate and efficient scheme for function extension on smooth domains, SIAM J. Numer. Anal. 63, 1427–1453.
- G. Fairweather and A. Karageorghis (1998), The method of fundamental solutions for elliptic boundary value problems, *Adv. Comput. Math.* **9**, 69–95.
- S.-I. Filip, Y. Nakatsukasa, L. N. Trefethen and B. Beckermann (2018), Rational minimax approximation via adaptive barycentric representations, SIAM J. Sci. Comput. 40, A2427–A2455.

- B. Fornberg and C. Piret (2022), Complex Variables and Analytic Functions: An Illustrated Introduction, SIAM.
- F. Fryklund, E. Lehto and A.-K. Tornberg (2018), Partition of unity extension of functions on complex domains, *J. Comput. Phys.* **375**, 57–79.
- W. Gautschi (2004), Orthogonal Polynomials: Computation and Approximation, Oxford U. Press.
- E. Gawlik and Y. Nakatsukasa (2021), Approximating the pth root by composite rational functions, J. Approx. Theory 226, 105577.
- H. Ginn (2023), Lightning Helmholtz solver, arXiv preprint arXiv:2310.016665v1.
- P. Godfrey (2025), 'gamma.m', www.mathworks.com/matlabcentral/fileexchange/3572-gamma.
- S. Goedecker (1999), Linear scaling electronic structure methods, *Rev. Mod. Phys.* **71**, 1085–1123.
- A. A. Gonchar (1969), Zolotarev problems connected with rational functions, Math. USSR Sb. 7, 623–635.
- A. A. Gonchar (1975), On convergence of Padé approximants for some classes of meromorphic functions, *Math. USSR Sb.* **26**, 555–575.
- A. A. Gonchar and G. López Lagomasino (1978), On Markov's theorem for multipoint Padé approximants, *Math. USSR Sb.* **34**, 449–459.
- P. Gonnet, S. Güttel and L. N. Trefethen (2013), Robust Padé approximation via SVD, SIAM Rev. 55, 101–117.
- I. J. Good (1961), The colleague matrix, a Chebyshev analogue of the companion matrix, Quart. J. Math. 12, 61–68.
- J. N. Goodier (1934), An analogy between the slow motions of a viscous fluid in two dimensions, and systems of plane stress, *Philos. Mag.* 17, 554–576.
- A. Gopal (2021), High-order numerical methods for scattering problems, PhD thesis, University of Oxford.
- A. Gopal and L. N. Trefethen (2019a), New Laplace and Helmholtz solvers, *Proc. Nat. Acad. Sci. USA* **116**, 10223.
- A. Gopal and L. N. Trefethen (2019b), Representation of conformal maps by rational functions, *Numer. Math.* **142**, 359–382.
- A. Gopal and L. N. Trefethen (2019c), Solving Laplace problems with corner singularities via rational functions, SIAM J. Numer. Anal. 57, 2074–2094.
- I. V. Gosea and S. Güğercin (2022), Data-driven modeling of linear dynamical systems with quadratic output in the AAA framework, J Sci. Comput. 91, 16.
- I. V. Gosea and S. Güttel (2021), Algorithms for the rational approximation of matrix-valued functions, SIAM J. Sci. Comput. 43, A3033–A3054.
- A. Greenbaum and L. N. Trefethen (1994), GMRES/CR and Arnoldi/Lanczos as matrix approximation problems, SIAM J. Sci. Comp. 15, 359–368.
- S. Gugercin, A. C. Antoulas and C. Beattie (2008), H_2 model reduction for large-scale linear dynamical systems, $SIAM\ J.\ Matrix\ Anal.\ Appl.\ 30$, 609–638.
- B. Gustafsson (2001), Lectures on Balayage, Technical report, U. of Joensuu.
- B. Gustavsen and A. Semlyen (1999), Rational approximation of frequency domain responses by vector fitting, *IEEE Trans. Power Deliv.* **14**, 1052–1061.
- S. Güttel and F. Tisseur (2017), The nonlinear eigenvalue problem, *Acta Numer*. **26**, 1–94.

- S. Güttel, G. M. Negri Porzio and F. Tisseur (2022), Robust rational approximations of nonlinear eigenvalue problems, SIAM J. Sci. Comput. 44, A2439–A2463.
- S. Güttel, E. Polizzi, P. T. P. Tang and G. Viaud (2015), Zolotarev quadrature rules and load balancing for the FEAST eigensolver, SIAM J. Sci. Comput. 37, A2100–A2122.
- A. J. Guttmann (2015), Analysis of series expansions for non-algebraic singularities, J. Phys. A.: Math. Theor. 48, 045209.
- N. Hale and T. W. Tee (2009), Conformal maps to multiply slit domains and applications, SIAM J. Sci. Comput. 31, 3195–3215.
- N. Hale and L. N. Trefethen (2008), New quadrature formulas from conformal maps, SIAM J. Numer. Anal. 46, 930–948.
- N. Hale, N. J. Higham and L. N. Trefethen (2008), Computing A^{α} , $\log(A)$, and related matrix functions by contour integrals, SIAM J. Numer. Anal. **46**, 2505–2523.
- S. J. Harris and N. R. McDonald (2023), Penguin huddling: a continuum model, *Acta Appl. Math.* **185**, 7.
- S. J. Harris and N. R. McDonald (2025a), Modelling wildfire spread and spotfire merger using conformal mapping and AAA-least squares methods, *Environ. Model. Softw.* **185**, 106303.
- S. J. Harris and N. R. McDonald (2025b), Vortex equilibria using least-squares methods, *Theor. Comput. Fluid Dyn.* **39**, 1–17.
- S. J. Harris, R. A. Palmer and N. R. McDonald (2025), Modeling floral and arthropod electrostatics using a two-domain AAA-least squares algorithm, SIAM J. Appl. Math. 85, 916–944.
- P. W. Hemker (1977), 'A numerical study of stiff two-point boundary problems'.
- P. Henrici (1977), Applied and Computational Complex Analysis: Special Functions, Integral Transforms, Asymptotics, Continued Fractions, Vol. 2, Wiley.
- P. Henrici (1979), Barycentric formulas for interpolating trigonometric polynomials and their conjugates, *Numer. Math.* **33**, 225–234.
- P. Henrici (1986), Applied and Computational Complex Analysis: Discrete Fourier Analysis, Cauchy Integrals, Construction of Conformal Maps, Univalent Functions, Vol. 3, Wiley.
- A. Herremans, D. Huybrechs and L. N. Trefethen (2024), Resolution of singularities by rational functions, SIAM J. Numer. Anal. 61, 2580–2600.
- N. J. Higham (2004), The numerical stability of barycentric Lagrange interpolation, *IMA J. Numer. Anal.* **24**, 547–556.
- N. J. Higham (2008), Functions of Matrices: Theory and Computation, SIAM.
- A. Hochman (2017), FastAAA: A fast rational-function fitter, in 2017 IEEE 26th Conference on Electrical Performance of Electronic Packaging and Systems (EPEPS), IEEE, pp. 1–3.
- A. Hochman, Y. Leviatan and J. K. White (2013), On the use of rational-function fitting methods for the solution of 2d laplace boundary-value problems, *J. Comput. Phys.* **238**, 337–358.
- A. Horning and Y. Nakatsukasa (2022), Twice is enough for dangerous eigenvalues, SIAM J. Matrix Anal. Applics. 43, 63–93.
- A. Horning and L. N. Trefethen (submitted), Quadrature formulas from rational approximations, *IMA J. Numer. Anal.*

- D. Huybrechs and L. N. Trefethen (2023), AAA interpolation of equispaced data, BIT Numer. Math. 63, 21.
- A. C. Ionita (2013), Lagrange rational interpolation and its applications to approximation of large-scale dynamical systems, PhD thesis, Rice University.
- M.-P. Istace and J.-P. Thiran (1993), On computing best complex rational approximants, Numerical Algorithms 5, 299–308.
- M.-P. Istace and J.-P. Thiran (1995), On the third and fourth Zolotarev problems in the complex plane, SIAM J. Numer. Anal. 32, 249–259.
- J. Jonas and B. Bamieh (2024), An adaptation of the AAA-interpolation algorithm for model reduction of MIMO systems, in 2024 American Control Conference (ACC), IEEE, pp. 2740–2745.
- J.-P. Kahane (1985), Some Random Series of Functions, 2nd ed., Cambridge U. Press.
- C. S. Kenney and A. J. Laub (2002), The matrix sign function, *IEEE transactions* on Automatic Control 40(8), 1330–1348.
- N. Kerzman and M. R. Trummer (1986), Numerical conformal mapping via the Szegő kernel, J. Comput. Appl. Math. 14, 111–123.
- S. Kim, A. Krasnok and A. Alù (2025), Complex frequency excitations in photonics and wave physics, *Science* **387**, eado4128.
- A. V. Kisil (2013), A constructive method for an approximate solution to scalar Wiener-Hopf equations, Proc. Roy. Soc. A 469, 20120721.
- A. V. Kisil, I. D. Abrahams, G. Mishuris and S. V. Rogosin (2021), The Wiener–Hopf technique, its generalizations and applications: constructive and approximate methods, *Proc. Roy. Soc. A* 477, 20210533.
- R. Kress (1989), Linear Integral Equations, Springer.
- M. D. Kruskal (1974), The Korteweg-de Vries equation and related evolution equations, in Nonlinear wave motion (Proc. AMS-SIAM Summer Sem., Clarkson Coll. Tech., Potsdam, N.Y., 1972), Lectures in Appl. Math., Vol. 15, Amer. Math. Soc., Providence, RI, pp. 61–83.
- A. B. J. Kuijlaars (2006), Convergence analysis of Krylov subspace iterations with methods from potential theory, SIAM Rev. 48, 3–40.
- H. J. Landau (1986), Extrapolating a band-limited function from its samples taken in a finite interval, *IEEE Trans. Inf. Thy.* **IT-32**, 464–470.
- E. Larsson, V. Shcherbakov and A. Heryudono (2017), A least squares radial basis function partition of unity method for solving PDEs, SIAM J. Sci. Comput. 39, A2538–A2563.
- P. W. Lawrence (2013), Eigenvalue Methods for Interpolation Bases, PhD thesis, University of Western Ontario.
- C. L. Lawson (1961), Contributions to the Theory of Linear Least Maximum Approximation, PhD thesis, UCLA.
- J.-Y. Lee and L. Greengard (1997), A fast adaptive numerical method for stiff two-point boundary value problems, SIAM J. Sci. Comput. 18, 403–429.
- P. Lietaert, K. Meerbergen, J. Pérez and B. Vandereycken (2022), Automatic rational approximation and linearization of nonlinear eigenvalue problems, IMA J. Numer. Anal. 42, 1087–1115.
- Y. Liu (2000), The Numerical Solution of Frequency-Domain Acoustic and Electromagnetic Periodic Scattering Problems, PhD thesis, Dartmouth College.

- S. Loisel and P. Maxwell (2018), Path-following method to determine the field of values of a matrix with high accuracy, SIAM J. Matrix Anal. Applies. 39, 1726–1749.
- P. M. Lushnikov, S. A. Dyachenko and D. A. Silantyev (2017), New conformal mapping for adaptive resolving of the complex singularities of Stokes wave, *Proc. Roy. Soc. A* 473, 20170198.
- C. J. Lustri and S. J. Chapman (2013), Steady gravity waves due to a submerged source, J. Fluid Mech. 732, 660–686.
- D. S. Mackey, N. Mackey, C. Mehl and V. Mehrmann (2006), Vector spaces of linearizations for matrix polynomials, SIAM J. Matrix Anal. Applics. 28, 971– 1004.
- D. MacMillen (2024), BaryRational.jl. github.com/macd/BaryRational.jl.

MathWorks Inc. (2020), 'RF Toolbox', https://www.mathworks.com.

- T. Matsuda and Y. Nakatsukasa (2025), Polynomial approximation of noisy functions, *Numer. Math.* **157**, 1285–1311.
- S. W. McCue, C. J. Lustri, D. J. VandenHeuvel, J. Zhang, J. R. King and S. J. Chapman (2025), Small-time asymptotics and the emergence of complex singularities for the KdV equation, arXiv preprint arXiv:2509.07397.
- K. McKee and K. Burns (2025), Steady advection-diffusion in multiply-connected potential flows, arXiv preprint arXiv:2509.09444.
- K. Meerbergen (2022), https://people.cs.kuleuven.be/karl.meerbergen/files/aaa/autoCORK.zip.
- V. Mehrmann and H. Voss (2004), Nonlinear eigenvalue problems: A challenge for modern eigenvalue methods, *GAMM-Mitteilungen* **27**, 121–152.
- K. Miller (1970), Stabilized numerical analytic prolongation with poles, SIAM J. Appl. Math. 18, 356–363.
- W. Mitchell (2025), Two intriguing variants of the AAA algorithm for rational approximation, arXiv preprint arXiv:2508.11169.
- C. B. Moler (2004), Numerical Computing with MATLAB, SIAM.
- C. B. Moler and G. W. Stewart (1973), An algorithm for generalized matrix eigenvalue problems, SIAM J. Numer. Anal. 10, 241–256.
- J.-M. Muller (2016), Elementary Functions: Algorithms and Implementation, 3rd ed., Birkhäuser.
- Y. Nakatsukasa and R. W. Freund (2016), Computing fundamental matrix decompositions accurately via the matrix sign function in two iterations: The power of Zolotarev's functions, *SIAM Rev.* **58**, 461–493.
- Y. Nakatsukasa and L. N. Trefethen (2020), An algorithm for real and complex rational minimax approximation, SIAM J. Sci. Comput. 42, A3157–A3179.
- Y. Nakatsukasa and L. N. Trefethen (2021), Reciprocal-log approximation and planar PDE solvers, SIAM J. Numer. Anal. **59**, 2801–2822.
- Y. Nakatsukasa, O. Sète and L. N. Trefethen (2018), The AAA algorithm for rational approximation, SIAM J. Sci. Comput. 40, A1494–A1522.
- M. A. Nethercote, A. V. Kisil and R. C. Assier (2023), Diffraction of acoustic waves by multiple semi-infinite arrays, J. Acoust. Soc. America 154(3), 1493–1504.
- M. A. Nethercote, A. V. Kisil and R. C. Assier (2024), Acoustic wave diffraction by a quadrant of sound-soft scatterers, arXiv preprint arXiv:2410.23647.
- D. J. Newman (1964), Rational approximation to |x|, Michigan Math. J. 11, 11–14.

- A. V. Oppenheim and R. W. Schafer (2001), Discrete-Time Signal Processing, Pearson.
- M. R. Osborne and G. A. Watson (1969), An algorithm for minimax approximation in the nonlinear case, *Comput. J.* **12**, 63–68.
- S. Pålsson and A.-K. Tornberg (2020), An integral equation method for closely interacting surfactant-covered droplets in wall-confined stokes flow, Int. J. Numer. Meth. Fluids 92, 1975–2008.
- T. Park and Y. Nakatsukasa (2023), A fast randomized algorithm for computing an approximate null space, *BIT Numer. Math.* **63**, 36.
- R. Platte, L. N. Trefethen and A. B. J. Kuijlaars (2011), Impossibility of fast stable approximation of analytic functions from equispaced samples, SIAM Rev. 53, 308–318.
- E. Polizzi (2009), Density-matrix-based algorithm for solving eigenvalue problems, *Phys. Rev. B* **79**, 115112–1–115112–6.
- C. Pozrikidis (1992), Boundary Integral and Singularity Methods for Linearized Viscous Flow, Cambridge U. Press.
- C. Pozrikidis (2002), A Practical Guide to Boundary Element Methods with the Software Library BEMLIB, CRC Press.
- E. A. Rakhmanov (2016), The Gonchar-Stahl ρ^2 theorem and associated directions in the theory of rational approximations of analytic functions, *Sbornik: Mathematics* **207**, 1236.
- A. C. Rodriguez, L. Balicki and S. Gugercin (2023), The p-AAA algorithm for data-driven modeling of parametric dynamical systems, SIAM J. Sci. Comput. 45, A1332–A1358.
- V. Rokhlin (1990), Rapid solution of integral equations of scattering theory in two dimensions, J. Comput. Phys. 86, 414–439.
- C. Runge (1885), Zur Theorie der eindeutigen analytischen Functionen, Acta Math. 6, 229–244.
- C. Runge (1901), Uber empirische Funktionen und die Interpolation zwischen äquidistanten Ordinaten, Z. Math. Phys. 46, 224–243.
- E. B. Saff and R. S. Varga (1978), On the zeros and poles of Padé approximants to e^z . III, Numer. Math. 30, 241–266.
- T. Sakurai and H. Sugiura (2003), A projection method for generalized eigenvalue problems using numerical integration, *J. Comput. Appl. Math.* **159**, 119–128.
- O. Salazar Celis (2024), Numerical continued fraction interpolation, *Ukrainian Math. J.* 76, 568–580.
- H. E. Salzer (1960), New formulas for trigonometric interpolation, J. Math. Phys. 39, 83–96.
- C. K. Sanathanan and J. Koerner (1963), Transfer function synthesis as a ratio of two complex polynomials, *IEEE Trans. Aut. Contr.* 8, 56–58.
- C. Schneider and W. Werner (1986), Some new aspects of rational interpolation, Math. Comput. 47, 285–299.
- H. Schwarz (1870), Über die Integration der partiellen Differentialgleichung $\frac{\partial^2 u}{\partial x^2} + \frac{\partial^2 u}{\partial y^2} = 0$ unter vorgeschriebenen Grenz- und Unstetigkeitsbedingungen, *Monatsber. Königl. Akad. Berlin* pp. 767–795.
- H. Shapiro (1992), The Schwarz Function and its Generalization to Higher Dimensions, Wiley.

- M. Siegel and R. E. Caffisch (2009), Calculation of complex singular solutions to the 3D incompressible Euler equations, *Physica D* **238**, 2368–2379.
- V. Simoncini (2016), Computational methods for linear matrix equations, SIAM Rev. 58, 377–441.
- H. Stahl (1989), On the convergence of generalized Padé approximants, Constr. Approx. 5, 221–240.
- H. Stahl (1997), The convergence of Padé approximants to functions with branch points, J. Approx. Theory **91**, 139–204.
- H. Stahl (1998), Spurious poles in Padé approximation, J. Comput. Appl. Math. 99, 511–527.
- G. Starke (1992), Near-circularity for the rational Zolotarev problem in the complex plane, *J. Approx. Theory* **70**, 115–130.
- C. Sulem, P. L. Sulem and H. Frisch (1983), Tracing complex singularities with spectral methods, *J. Comput. Phys.* **50**, 138–161.
- M. Tabor and J. Weiss (1981), Analytic structure of the Lorenz system, *Phys. Rev.* A 24, 2157–2167.
- P. T. P. Tang and E. Polizzi (2014), FEAST as a subspace iteration eigensolver accelerated by approximate spectral projection, SIAM J. Matrix Anal. Applies. Math. 35, 354–390.
- S. Tanveer (1993a), Evolution of Hele-Shaw interface for small surface tension, *Phil. Trans. Roy. Soc. A* **343**, 155–204.
- S. Tanveer (1993b), Singularities in the classical Rayleigh-Taylor flow: formation and subsequent motion, *Proc. Roy. Soc. A* 441, 501–525.
- T. W. Tee and L. N. Trefethen (2006), A rational spectral collocation method with adaptively transformed Chebyshev grid points, SIAM J. Sci. Comput. 28, 1798–1811.
- F. Tisseur and K. Meerbergen (2001), The quadratic eigenvalue problem, SIAM Rev. 43, 235–286.
- L. N. Trefethen (1981), Rational Cheybyshev approximation on the unit disk, *Numer. Math.* **37**, 297–320.
- L. N. Trefethen (2016), Inverse Yogiisms, Notices of the AMS 61, 1281–1285.
- L. N. Trefethen (2018), Series solution of Laplace problems, ANZIAM J. 60, 1–26.
- L. N. Trefethen (2019a), Approximation Theory and Approximation Practice, Extended Edition, SIAM, Philadelphia, PA.
- L. N. Trefethen (2019b), 'Why is the field of values so nonsmooth?', chebfun.org/examples/linalg/NonsmoothFOV.html.
- L. N. Trefethen (2020a), 'Lightning Laplace solver', http://people.maths.ox.ac.uk/trefethen/laplace.
- L. N. Trefethen (2020b), Numerical conformal mapping with rational functions, Comput. Meth. Func. Thy. 20, 369–387.
- L. N. Trefethen (2020c), Quantifying the ill-conditioning of analytic continuation, BIT Numer. Math. **60**, 901–915.
- L. N. Trefethen (2022a), Exactness of quadrature formulas, SIAM Rev. 64, 132–150
- L. N. Trefethen (2023), Numerical analytic continuation, *Jpn. J. Ind. Appl. Math.* **40**, 1587–1636.

- L. N. Trefethen (2024), Polynomial and rational convergence rates for Laplace problems on planar domains, *Proc. Roy. Soc. A* **480**, 20240178.
- L. N. Trefethen (2025a), Numerical computation of the Schwarz function, Constr. Approx.
- L. N. Trefethen (2025b), Rational approximation, Notices of the AMS 72, 78–81.
- L. N. Trefethen (2025c), Unbounded growth of band-limited functions, *Notices of the AMS* **72**, 666–669.
- L. N. Trefethen (March 2022b), Is everything a rational function?, *LMS Newsletter* p. 25.
- L. N. Trefethen (to appear), Numerical conformal mapping, Notices of the AMS.
- L. N. Trefethen and J. A. C. Weideman (2014), The exponentially convergent trapezoidal rule, SIAM Rev. 56, 385–458.
- L. N. Trefethen and H. D. Wilber (2025), Computation of Zolotarev rational functions, SIAM J. Sci. Comput. 47, A2205–A2220.
- L. N. Trefethen, A. Birkisson and T. A. Driscoll (2018), Exploring ODEs, SIAM.
- L. N. Trefethen, Y. Nakatsukasa and J. A. C. Weideman (2021), Exponential node clustering at singularities for rational approximation, quadrature, and PDEs, *Numer. Math.* 147, 227–254.
- L. N. Trefethen, J. A. C. Weideman and T. Schmelzer (2006), Talbot quadratures and rational approximations, BIT Numer. Math. 46, 653–670.
- M. Van Barel and P. Kravanja (2016), Nonlinear eigenvalue problems and contour integrals, *J. Comput. Appl. Math.* **292**, 526–540.
- M. Van Dyke (1982), An Album of Fluid Motion, Parabolic Press.
- D. VandenHeuvel, C. Lustri, J. King, I. Turner and S. McCue (2023), Burgers' equation in the complex plane, *Physica D* 448, 133686.
- R. S. Varga, A. Ruttan and A. D. Carpenter (1993), Numerical results on best uniform rational approximation of |x| on [-1,1], *Mathematics USSR-Sbornik* **74**, 271–290.
- P. Virtanen *et al.* (2020), SciPy 1.0: Fundamental algorithms for scientific computing in Python, *Nat. Methods* **17**, 261–272.
- D. Viswanath and S. Sahutoglu (2010), Complex singularities and the Lorenz attractor, SIAM Rev. 52, 294–314.
- J. L. Walsh (1929), The approximation of harmonic functions by harmonic polynomials and harmonic rational functions, *Bull. Amer. Math. Soc.* **35**, 499–544.
- J. L. Walsh (1969), Interpolation and Approximation by Rational Functions in the Complex Domain, 5th edition, American Mathematical Society, Providence, RI.
- R. Wegmann (2005), Methods for numerical conformal mapping, in *Handbook of Complex Analysis: Geometric Function Theory*, v. 2 (R. Kühnau, ed.), Vol. 2, Elsevier, pp. 351–477.
- J. A. C. Weideman (1995), Computing the Hilbert transform on the real line, Math. Comput. 64, 745–762.
- J. A. C. Weideman (2003), Computing the dynamics of complex singularities of nonlinear PDEs, SIAM J. Appl. Dynam. Syst. 2, 171–186.
- J. A. C. Weideman (2022), Dynamics of complex singularities of nonlinear PDEs: analysis and computation, in *Recent Advances in Industrial and Applied Mathematics* (T. Chyacón Rebollo, ed.), Springer, Cham, pp. 227–247.

- H. D. Wilber (2021), Computing Numerically with Rational Functions, PhD thesis, Cornell University.
- H. D. Wilber, A. Damle and A. Townsend (2022), Data-driven algorithms for signal processing with trigonometric rational functions, SIAM J. Sci. Comput. 44, C185–C209.
- G. B. Wright and B. Fornberg (2017), Stable computations with flat radial basis functions using vector-valued rational approximations, *J. Comput. Phys.* **331**, 137–156.
- G. B. Wright, M. Javed, H. Montanelli and L. N. Trefethen (2015), Extension of Chebfun to periodic functions, SIAM J. Sci. Comput. 37, C554–C573.
- K. Xu (2012), 'Arc length in the complex plane', chebfun.org/examples/complex/ComplexArcLength.html.
- Y. Xue (2025a), Computing Stokes flows in periodic channels via rational approximation, *Proc. Roy. Soc. A* p. 20240676.
- Y. Xue (2025b), 'LARS', https://github.com/YidanXue/LARS.
- Y. Xue, S. L. Waters and L. N. Trefethen (2024), Computation of two-dimensional Stokes flows via lightning and AAA rational approximation, SIAM J. Sci. Comput. 46, A1214–A1234.
- B. Zhao, E. Lauga and L. Koens (2019), Method of regularized stokeslets: Flow analysis and improvement of convergence, *Phys. Rev. Fluids* 4, 084104.
- C. Zhou, L. Yang, Y. Liu and Z. Yang (2009), A novel method for computing the Hilbert transform with Haar multiresolution approximation, J. Comput. Appl. Math. 223, 585–597.
- E. I. Zolotarev (1877), Application of elliptic functions to questions of functions deviating least and most from zero, Zap. Imp. Akad. Nauk. St. Petersburg.